Peptide-based Molecular Constructs for Cellular Targeting and Small Molecule Delivery

A thesis submitted in partial fulfillment of the requirements for the degree of

DOCTOR OF PHILOSOPHY

by

RUCHIKA GOYAL

Department of Biosciences and Bioengineering
Indian Institute of Technology Guwahati
Guwahati-781039, India

February 2020

Peptide-based Molecular Constructs for Cellular Targeting and Small Molecule Delivery

A thesis submitted in partial fulfillment of the requirements for the degree of

DOCTOR OF PHILOSOPHY

by

RUCHIKA GOYAL

Department of Biosciences and Bioengineering
Indian Institute of Technology Guwahati
Guwahati-781039, India

February 2020

Dedicated

to

THE INVENTORS OF RAMACHANDRAN MAP

G. N. Ramachandran

C. Ramakrishnan

V. Sasisekharan

A Tribute to G. N. Ramachandran

A sparkling speck of cosmos,

A wizard of mathematics,

A bright biophysicist

and

A man who

ignited the inquisitive minds, inspired the generations,

opened the new dimensions, gave wings to-

Syaad Nyaan Philosophy to Boolean Vector Matrix Formulation,

Pauling alpha-helix to Collagen triple helix,

Chemical bonds to Mathematical equations,

The joy of Phi-Psi to the Pleasure of Protein Science...!!!

-- Ruchika

Indian Institute of Technology Guwahati

Department of Biosciences and Bioengineering

DECLARATION

I do hereby declare that the research findings of this thesis are the result of research work carried out by me in the Department of Biosciences and Bioengineering, Indian Institute of Technology Guwahati, Guwahati, India, under the joint supervision of Prof. Vibin Ramakrishnan and Prof. Vishal Trivedi.

As per the general norms of reporting research findings, I take full responsibility for the data represented. Acknowledgments have been made wherever the research findings of other researchers have been cited in this thesis.

Date: 26-02-2020

Ruchika Goyal

Indian Institute of Technology Guwahati

Department of Biosciences and Bioengineering

CERTIFICATE

It is certified that the work described in this thesis entitled "Peptide-based Molecular Constructs for Cellular Targeting and Small Molecule Delivery" by Ms. Ruchika Goyal for the award of degree of Doctor of Philosophy is an authentic record of the results obtained from the research work carried out under our joint supervision in the Department of Biosciences and Bioengineering, Indian Institute of Technology Guwahati, India, and this work has not been submitted elsewhere for the award of any other degree.

Prof. Vibin Ramakrishnan (Supervisor)

26.2.2020

Prof. Vishal Trivedi (Co-Supervisor)

Acknowledgments

"Gratitude makes sense of our past, brings peace for today,

and creates a vision for tomorrow"

The presented work was performed at Molecular Informatics and Design lab at Indian Institute of Technology Guwahati and is a result of several collaborations. This would not have been possible without the intellectual and technical support of many people. At the outset, my sincere gratitude goes to my supervisor Prof. Vibin Ramakrishnan for giving me this opportunity to work on this fascinating and thought-provoking topic. He ignited the idea, stimulated my imagination, supported and guided me through the highs and lows of the study, and, most importantly, taught me many essential life lessons. His articulate work plans made the most complicated things look very simple many times. I always believed that – "Research is like a roller-coaster ride; it is always exciting but is full of surprises." My Professor made this ride feel decidedly less tiring and more exciting. I place on record the time and efforts Prof. Vibin put in to mold me into a better person in general and a focused researcher in particular.

I am immensely thankful to my co-supervisor, Prof. Vishal Trivedi, for his guidance and support throughout the last five years. His comments, critical reviews, and suggestions have always been very helpful in meeting the cutting-edge expectations of scientific research. I am particularly indebted to him for allowing me to use his laboratory space and services whenever required.

I would like to thank my doctoral committee Dr. Nitin Chaudhary, Dr. Sachin Kumar, and Dr. B. Anand for the insightful comments, constructive criticism, and encouragement during the progress seminars. I thank Dr. Anupam Sarma for collaborating with us to carry out the clinical studies.

My profound gratitude goes to Dr. T. R. Santhoshkumar for his guidance, insightful comments, and support during my studies at Rajiv Gandhi Centre for Biotechnology, Thiruvananthapuram. I especially thank his team members for their unconditional support and cherishable memories.

I thank all the former and current lab members of Molecular Informatics and Design lab, Biophysical Chemistry lab, and Malaria Research group – 'You all have contributed to the presented work in one way or other and have been the best colleagues one could wish for.' Thanks for being part of joyful laughter, exciting trips, and endless memories.

My profound thanks go to my friends who have actively or passively supported me through this journey. I would like to specially mention: Trishna, Shruti, Peeyushi, Monika, Aditi, Mukul, Divyesh, Deepti, Sunil, Ekta, Deepika, Prerna, Princi and a few others, for almost incredible support and being the constant source of encouragement.

Finally, I thank my parents, my brother, and my entire family, who have stood as my pillars of support in the hardest of times. They made sure that I had the necessary emotional stability and supported me every day all throughout my journey. They believed in me and never let me lose my focus towards work. I am ever grateful for their enormous love and patience.

"Little drops of water make the mighty ocean," I would like to thank the Almighty God for making me a channel to contribute a bit in the enormous ocean of knowledge.

--Ruchika

Table of Contents

List of figures ... xi

List of Tables ... xix

Abbreviations ... xxi

Abstract ... xxv

1. INTRODUCTION ... 1

2. PEPTIDE-BASED DRUG DELIVERY SYSTEMS ... 7

2.1. PEPTIDES IN TARGETED DRUG DELIVERY ... 9

2.2. STRATEGIES FOR PEPTIDE-BASED DRUG DESIGN ... 9

2.2.1. Torsion angle and Peptide Backbone Alterations ... 10

2.2.2. Peptidomimetics with Unnatural amino acids ... 11

2.2.3. Macrocyclization of peptides ... 13

2.3. PEPTIDES AS CARRIERS FOR DRUG DELIVERY ... 14

2.3.1. Targeting Peptides ... 14

2.3.2. Cell Penetrating Peptides (CPPs) ... 21

2.4. FUTURE OF PEPTIDE-BASED DRUG DELIVERY SYSTEMS ... 24

3. OBJECTIVES AND RESEARCH DESIGN ... 27

3.1. OBJECTIVES ... 29

3.2. RESEARCH DESIGN DIRECTIVES TO GENERATE DRUG DELIVERY VECTORS ... 29

4. GEOMETRY ENCODED FUNCTIONAL PROGRAMMING OF DRUG DELIVERY VEHICLES ... 33

4.1 INTRODUCTION ... 35

4.2. MATERIALS AND METHODS ... 37

4.2.1. Molecular Modeling. ... 37

4.2.2. Electrostatic Profiling of Peptides. ... 37

4.2.3. Peptide Synthesis and Characterization. ... 37

4.2.4. Circular Dichroism (CD) Spectroscopy. 39
4.2.5. Fourier Transform Infrared (FTIR) Spectroscopy. 39
4.2.6. Cell Culture. 39
4.2.7. Flow cytometry for comparative peptide uptake. 40
4.2.8. Fluorescence imaging to confirm cellular uptake. 40
4.2.9. TMRM Cytotoxicity Assay. 40
4.2.10. Cell death by apoptosis 41
4.2.11. Hemolytic activity. 42
4.2.12. Biocompatibility of peptides. 42
4.2.13. Comparative Histopathological Staining of peptides. 42
4.2.14. Statistical analysis. 42
4.3. RESULTS AND DISCUSSION 43
4.3.1. Geometry encoded functional programming 43
4.3.2. Peptide Synthesis and Characterization 43
4.3.3. Secondary Structure Characterization 46
4.3.4. Cellular uptake of peptides by flow cytometry 47
4.3.5. Cellular uptake of peptides by confocal imaging 48
4.3.6. Cytotoxicity of designed peptides 51
4.3.7. Activation of Caspase-3 by ratiometric fluorescence-based assay 53
4.3.8. Biocompatibility of peptides 53
4.3.9. Hemotoxicity of peptides 54
4.3.10. Comparative histopathological peptide staining 55
4.4. CONCLUSION 58
5. PEPTIDE-BASED DELIVERY VECTORS WITH PRE-DEFINED GEOMETRICAL LOCKS 59
5.1. INTRODUCTION 61

5.2. MATERIALS AND METHODS 62
5.2.1. Right Angle Scattering of designed peptides. 62
5.2.2. Thioflavin T (ThT) Fluorescence assay. 62
5.2.3. Field emission scanning electron microscopy (FESEM). 62
5.3. RESULTS 63
5.3.1. Design of D-Proline Induced Geometrical Locks 63
5.3.2. Electrostatic Fingerprinting of designed delivery vectors 63
5.3.3. Peptide Synthesis and Characterization 64
5.3.4. Cellular Uptake of the designed peptide-based delivery vectors 65
5.3.5. Cytotoxicity assessment 68
5.3.6. Caspase-3 activation 68
5.3.7. Biocompatibility of peptides 69
5.3.8. Hemotoxicity of peptides 70
5.3.9. Verification of peptide aggregation propensity 71
5.4. DISCUSSION 73
5.5. CONCLUSION 75
6. GENERATION OF A COMPLETE TUMOR TARGETING MOLECULAR CONSTRUCT 77
6.1. INTRODUCTION 79
6.2. MATERIALS AND METHODS 80
6.2.1. Mechanism of uptake. 80
6.2.2. MTT Cell Viability assay. 81
6.2.3. Annexin V- Propidium iodide (PI) staining. 81
6.2.4. Penetration in 3D tumorospheres. 81
6.3. RESULTS AND DISCUSSION 82
6.3.1. Design Strategy and Peptide Synthesis 82
6.3.2. Electrostatic Fingerprinting 82

6.3.3. Secondary Structure Characterization 83
6.3.4. Cellular uptake of designed peptides 84
6.3.5. Mechanism of cellular uptake 87
6.3.6. Biocompatibility of designed peptides 88
6.3.7. Cytotoxicity of the designed peptides 90
6.3.8. Hemotoxicity of designed peptides 92
6.3.9. Penetration in 3D tumorospheres 93
6.4. CONCLUSION 93
7. CONCLUSIONS AND FUTURE DIRECTIONS 97
7.1. GEOMETRICALLY DIRECTED DELIVERY VECTORS 99
7.2. PHILOSOPHICAL OUTCOME (SIGNIFICANCE) 100
7.3. FUTURE DIRECTIONS 101
REFERENCES 103
ANNEXURE #1 117
LIST OF PUBLICATIONS 125

List of Figures

Figure 2.1.	Structural Evolution of Peptides and Proteins. Scheme to represent Ramachandran plot (R-plot) for L- and D-amino acids that define possible combinations of torsion angles (Φ, Ψ) in peptides, leading to different levels of structural organization in proteins starting from primary to secondary to tertiary and finally to quaternary structures.	11
Figure 2.2.	Tacticity types. Different type of tacticity observed in polypeptide chains a) isotacticity b) syndiotacticity c) heterotacticity. Isotactic polymers are composed of either L- amino acids or D- amino acids, whereas; an alternate arrangement of LDLD or DLDL amino acids in peptide chain forms syndiotactic peptides. Heterotactic peptides have random L- and D- amino acid combinations in their sequence.	12
Figure 2.3.	Examples of macrocyclic peptides. a) Cilengitide b) Simeprevir and c) Cyclosporine. Cilengitide is a ligand for $\alpha_v\beta_3$ and $\alpha_v\beta_5$ integrins which are biomarkers of tumor angiogenesis and metastasis of solid tumors. Simeprevir is used for the treatment of Hepatitis C, and Cyclosporine is used as an immunosuppressant in case of rheumatoid arthritis, organ transplantation, and psoriasis.	13
Figure 2.4.	Schematic representation of Phage Display Library (PDL). In this method, phages specific to tumors are recovered through affinity-based selection using combinatorial phage libraries.	16
Figure 2.5.	Binding and penetration mechanism of iRGD peptide. There is a proteolytic cleavage of iRGD peptide after binding to α_v integrins on tumor endothelium, leading to exposure of binding motif for Neuropilin-1 that mediates penetration of iRGD peptide into tumor cells.	19
Figure 2.6.	Cellular uptake mechanisms of CPPs. The involved mechanisms for cellular uptake of CPPs are non-endocytic and endocytic pathways. Non-endocytic pathways refer to the direct penetration of CPP through plasma membrane phospholipids, whereas; endocytic pathway involves pinching off membrane vesicles after endocytosis.	23
Figure 3.1.	**Rational modeling approach for peptide designs.** (A) The locked basins of Ramachandran map designated as 1, 1', 2, 2', 3, and 3' for different amino acids. (B) An example of 'RpD' trimer to show the process for generation of rotamer library having different combinations of ϕ (phi), Ψ (psi), and χ_1 (chi1) torsion angles. (C) All trimers were chosen selectively for theoretical calculations of Euclidean distances between CZ (Arg)_CG (Asp). (D) This shows the percentage of conformers and potent trimers that fit in the category of CZ (Arg)_CG (Asp) distance more than 12 Å.	31
Figure 4.1.	Solid Phase Peptide Synthesis. Scheme to represent amide bond formation in solid-phase peptide synthesis (Fmoc Chemistry) and details of N-terminal modification for the cargo attachment.	38

Figure 4.2.	Caspase Sensor System. (A) Schematic representation of the Linker sequence of a FRET-based sensor (NLS-SCAT3). (B, C) SCAT probe and representative images of NLS-SCAT3 transfected MDA-MB-231 cells with and without treatment depicting the change in CFP/YFP ratio from blue to green-yellow on the ratio scale. This change in fluorescence ratio corresponds to the activation of Caspase-3.	41
Figure 4.3.	Conceptual illustration of the peptide designs. (A) The sterically fixed regions of the Ramachandran plot for L- and D- amino acids (grey). (B) Geometrical parameters (Θ, d) of RXD/QXR motifs considered for systemic modeling. In the given figure, 'Θ_1' represents angles between CB of Arg and CB of Asp in RXD motif, and 'Θ_2' represents angles between CB of Gln and CB of Arg in QXR motif. Distance measurement '$d_{R\text{-}D}$' represents the Euclidean distance between CZ of Arg and CG of Asp, and '$d_{Q\text{-}R}$' represents the Euclidean distance between CD of Gln and CZ of Arg. CB, CG, CD, and CZ denotes the C_β, C_γ, C_δ, and C_ζ atoms of the amino acid, respectively. (C) Synthesized peptide library with peptide codes, amino acid sequences, locked basin combinations, and evaluated geometrical parameters from their coordinate files.	44
Figure 4.4.	**Electrostatic Fingerprinting of the designed peptide library.** The mapped potential values suggest design induced variations in the spatial electrostatics of the peptides. Delphi software is used for electrostatic potential calculations.	45
Figure 4.5.	Peptide Structure Characterization. The design induced structural variations in secondary structures of peptides by (A) CD Spectroscopy and (B) FTIR spectroscopy.	47
Figure 4.6.	Cellular uptake of the designed peptides. The comparative uptake of peptides is quantified in breast cancer (MDA-MB-231) cells, cervical cancer (HeLa) cells, LAMP-RFP transfected osteosarcoma (U2-OS) cells and mammary epithelial (MCF-10A) cells using flow cytometry. All cells were incubated with 10 µM of CF-tagged peptides (RG101-RG108) in serum-free DMEM for 4 h at 37 °C. Post-treatment cells were washed, harvested, and analyzed through flow cytometry. MFI represents Mean Fluorescence Intensity. Results are presented as mean ± SEM of three independent experiments. P values (**** P < 0.0001, *** P=0.0002, ** P=0.002, * P=0.03) were calculated using One-Way ANOVA.	48
Figure 4.7.	Cellular uptake in MDA-MB-231 cells. The cellular uptake of CF-tagged peptides (RG101-RG108) in breast cancer (MDA-MB-231) cells through confocal laser scanning microscopy. After peptide treatment, nuclei were stained with Hoechst 33342. In this figure, blue represents Hoechst staining, and green shows CF-tagged peptides. Scale bar corresponds to 50 µm.	49
Figure 4.8.	Cellular uptake in HeLa cells. The cellular uptake of CF-tagged peptides (RG101-RG108) in cervical cancer (HeLa) cells using confocal laser scanning microscopy. After peptide treatment, nuclei were stained with	49

Hoechst 33342. In this figure, blue represents Hoechst staining, and green shows CF-tagged peptide. Scale bar corresponds to 20 µm.

Figure 4.9. Cellular uptake in MCF-10A cells. The cellular uptake of CF-tagged peptides (RG101-RG108) in mammary epithelial (MCF-10A) cells through confocal laser scanning microscopy. After peptide treatment, nuclei were stained with Hoechst 33342. In this figure, blue represents Hoechst staining, and green shows CF-tagged peptides. Scale bar corresponds to 20 µm. 50

Figure 4.10. Cellular uptake in U2-OS cells. The cellular uptake of CF-tagged peptides (RG101-RG108) in LAMP-RFP transfected osteosarcoma (U2-OS) cells through confocal microscopy. After peptide treatment, nuclei were stained with Hoechst 33342. In this figure, blue represents Hoechst staining, green shows CF-tagged peptides, and red denotes lysosomes. Scale bar corresponds to 20 µm. 50

Figure 4.11. Cytotoxicity of the designed peptides using TMRM assay. MDA-MB-231 and MCF-10A cells were treated with MTX, peptides (UN) and peptide-MTX conjugates (MTX) at 25 µM, 50 µM, and 100 µM concentrations for 48 h at 37°C. The cells with TMRM loss and nuclear condensation were considered undergoing apoptosis and hence, taken for cell death analysis. (A & B) Representative fluorescence image panels of MDA-MB-231 and MCF-10A cells after treatment with RG102 peptide and its MTX conjugates. (C) Quantitative analysis of MDA-MB-231 and MCF-10A cells undergoing cell death by treatment with peptides (RG101-RG108) and their respective MTX conjugates. (D & E) Cytotoxicity of MTX drug alone on MDA-MB-231 and MCF-10A cells under identical experimental conditions (n=4). 52

Figure 4.12. Validation of apoptotic cell death. To confirm the cell death by apoptosis, MDA-MB-231 cells having the stable expression of CFP-YFP FRET-based caspase sensor, DEVD were used. MDA-MB-231 cells expressing this probe were subjected to treatment with MTX (red), peptides (black), and peptide-MTX (red) conjugates for 48 h. The cells with loss of FRET led to an increase in the CFP-YFP ratio and were considered for quantitative analysis. The graph represents the mean ± SD of the percentage (of cells) undergoing cell death through Caspase-3 activation (n=4). 54

Figure 4.13. Biocompatibility of peptides. The binding activity of peptides in the presence and absence of serum on (A) MDA-MB-231 cells (B) HeLa cells, (C) MCF-10A cells, and (D) U2-OS cells, measured by flow cytometry. The peptide stocks were pre-incubated with fetal bovine serum (FBS) for 1 h at 37°C before cell treatment. Cells were treated with 10 µM of serum untreated and treated CF-tagged peptides (RG101-RG108) for 4 h at 37 °C. The obtained fluorescence intensities were normalized by the intensities of the untreated cells. MFI represents Mean Fluorescence Intensity. 55

Figure 4.14. Hemotoxicity of peptides. Hemolytic assay of the designed peptides and their MTX conjugates against human red blood corpuscles (RBCs). Heme release was measured at 540 nm after treating human RBCs with buffer, and 100 µM of peptides (UN) and their MTX conjugates (MTX) for 2 h at 37°C. 56

The data was normalized by complete lysis with 0.5 % of Triton X-100. All results are presented as the mean ± SD of three independent experiments.

Figure 4.15. Comparative Histopathological Staining of peptides on clinical samples. We assessed the binding of the designed peptides (RG101-RG108) on patient-derived tumor and adjacent normal tissues through fluorescence imaging. (A) Representative bright-field microscopic images of selected invasive ductal carcinoma tissues (IDCT) and adjacent normal tissues (ANT) of the breast, stained with H&E and Ki-67 antibody. (B) The quantitative analysis of peptide binding on normal and tumor tissues is represented in terms of fluorescence intensity. The control group is with PBS and represents autofluorescence of tissues whereas, tissues treated with 5(6)-carboxyfluorescein (CF) alone represent negative control. All values were reported as mean ± SEM of fluorescence from different tissue sections treated under identical treatment conditions (n=4). For each treatment group, the normal and tumor treated tissues were compared by the Two-tailed Student's t-test. Scale bar corresponds to 50 µm. (C) Representative images of peptide binding on normal and tumor tissues. Blue shows nuclei stained with DAPI Fluormount, and green denotes the binding of CF-tagged peptide. 57

Figure 5.1. Design of peptide-based delivery vectors. (A) Informed walk across the sterically allowed regions of Ramachandran plot to fix the geometry of RGD and NGR motif. The highlighted text represents the conformational basins to introduce the topological fixation in RGD/QGR motifs of peptides. (B) Electrostatic potential distribution of the designed peptides signifying the differences in potential values obtained as an effect of the change in stereochemistry and amphipathicity. (C) CD Spectra of designed peptides indicating the design directed structural disparities in secondary structure. (D) FTIR spectra with C=O bond signature peak, suggesting extended conformation. 64

Figure 5.2. Cellular uptake of peptides. The comparative uptake of peptides in breast cancer (MDA-MB-231) cells, cervical cancer (HeLa) cells, LAMP-RFP transfected osteosarcoma (U2-OS) cells, and mammary epithelial (MCF-10A) cells using flow cytometry. All cells were incubated with 10 µM of CF-tagged peptides (RG201-RG204) in serum-free DMEM for 4 h at 37 °C and analyzed through flow cytometry. Corrected MFI represents Mean Fluorescence Intensity. Results are presented as mean ± SD of three independent experiments. 66

Figure 5.3. Cellular uptake of peptides using confocal laser scanning microscopy. Cellular uptake of CF-tagged peptides in (A) MDA-MB-231 cells, (B) HeLa cells, (C) MCF-10A cells, and (D) LAMP-RFP transfected U2-OS cells in serum-free DMEM for 4 h at 37 °C. Blue indicates Hoechst 33342 staining; green indicates peptide uptake, red shows lysosomes, and merged shows the cellular uptake. Scale bar: 50 µm (A) and 20 µm (B,C,D). 67

Figure 5.4. Cytotoxicity of designed peptides. Analysis of peptide toxicity in MDA-MB-231 cells and MCF-10A cells by peptide treatment employing TMRM 68

based assay. MDA-MB-231 and MCF-10A cells were treated with MTX (Xn), peptide vectors (Pn) and peptide-methotrexate (PXn) conjugates for 48 h at three different concentrations (n = 25 µM, 50 µM, and 100 µM) for 48 h at 37°C. The cells with TMRM loss and nucleus condensation indicate apoptosis.

Figure 5.5. Validation of apoptotic cell death. To confirm the cell death by apoptosis, MDA-MB-231 cells having the stable expression of CFP-YFP FRET-based caspase sensor, DEVD were treated with MTX, peptides (RG20X-UN) and peptide-MTX (RG20X-MTX) conjugates for 48 h. The loss of FRET in cells was measured in terms of their difference (increase) in the CFP-YFP ratio, and the cells with FRET loss were taken for analysis. The graph represents the percentage (mean ± SD) of cells undergoing cell death by Caspase-3 activation. 69

Figure 5.6. Biocompatibility of peptides. The binding activity of peptides in the presence and absence of serum on MDA-MB-231 cells, HeLa cells, U2-OS cells, and MCF-10A cells measured by flow cytometry. The peptide stocks were pre-incubated with fetal bovine serum (FBS) for 1 h at 37°C before cell treatment. Cells were treated with 10 µM of serum untreated and treated CF-tagged peptides (RG201-RG204) for 4 h at 37 °C. The obtained fluorescence intensities were normalized by the intensities of the untreated cells. MFI represents Mean Fluorescence Intensity. Results are presented as mean ± SD of three independent experiments. 70

Figure 5.7. Hemolytic activity of peptides. Hemolytic assay of the designed peptides and their MTX conjugates against human red blood cells (RBCs). Heme release was measured at 540 nm after treating human RBCs with buffer, and 100 µM of peptides (UN) and their MTX conjugates (MTX) for 2 h at 37°C. The data was normalized by complete lysis with 0.5 % of Triton X-100. All results are presented as the mean ± SD of three independent experiments. 71

Figure 5.8. Field emission scanning electron photomicrographs (FESEM) of peptides. (A) PhF6 peptide is taken as a positive control for nano-assembly formation (nanofibres) (B) RGDPAYQGRFL peptide is an already reported tumor homing peptide. (C-F) FESEM images of the designed peptides RG201-RG204 showing only amorphous aggregates. Scale bar corresponds to 100 nm. 72

Figure 5.9. Verification of peptide self-assembly. The self-assembly formation of peptides in solution was verified by Right Angle Scattering (A, B) and ThT Fluorescence Assay (C, D) at two time points 0 h (A, C) and 24 h (B, D). 72

Figure 5.10. Schematic illustration of the evolved concept for vector design. (A) Ramachandran Plot with the highlighted region to depict the fixed geometry of D-Proline in RGD and QGR motifs. (B) Geometrical parameters of D-Proline fixation showed in peptide RG201. (C, D, and E) The amino acid sequence of designed peptides RG202, RG203, and RG204, respectively, specifically indicating the tailed cationic (blue) and hydrophobic (grey) residues. (F) The syndiotactic segment of RG204 peptide, forming a 74

Gramicidin helix with a distinct cationic zone highlighted by the yellow arc. L- and D-amino acids are mentioned as upper case and lower case letters, respectively.

Figure 6.1. Electrostatic Mapping of the designed peptides. Electrostatic potential distribution of the designed peptides representing the obtained potential value differences as the consequence of altered stereochemistry and amphipathicity. 83

Figure 6.2. Circular Dichroism (CD) Spectroscopy. CD Spectra of designed peptides in water. 84

Figure 6.3. Cellular uptake of designed peptides. The comparative uptake of peptides in breast cancer (MDA-MB-231) cells, cervical cancer (HeLa) cells, and human embryonic kidney (HEK-293) cells using flow cytometry. All cells were incubated with 10 µM of CF-tagged peptides (TAT, RG301-RG304) in serum-free DMEM for four hours at 37 °C and analyzed through flow cytometry. Corrected MFI represents Mean Fluorescence Intensity. Results are presented as mean ± SD of three independent experiments. 85

Figure 6.4. Cellular uptake of designed peptides. The cellular internalization of designed peptides was observed in (A) MDA-MB-231 and (B) HeLa cells after treatment with 10 µM of peptides for four hours at 37°C. Scale bar corresponds to 20 µm. 86

Figure 6.5. Cellular uptake of designed peptides. (A) Breast (MDA-MB-231) and (B) cervical cancer (HeLa) cells were treated with 5 µM of CF-tagged designed peptides for one hour in different temperature condition and in the presence of sodium azide. The cellular uptake of designed peptides in both cell lines gets reduced to 40-50% at the low-temperature variable condition. However, the peptide uptake in the presence of sodium azide was just reduced to 70-80% of the control. 88

Figure 6.6. Biocompatibility of the designed peptides. Cellular uptake of designed peptides in the presence of serum was verified in (A) MDA-MB-231, (B) HeLa and (C) HEK-293 cells after treatment with 10 µM of designed peptides in serum and serum-free conditions. The uptake by all peptides in both conditions suggests that the serum presence in the media doesn't hinder their activity. 89

Figure 6.7. Cytotoxicity of designed peptides using MTT assay. (A) MDA-MB-231, (B) HeLa and (C) HEK-293 cells were treated with varying concentrations of peptides (n) and peptide-methotrexate (n-X) conjugates for 48 h at 37°C in serum-free conditions. (D) Cell viability of all cell types after similar treatment to them by only standard drug methotrexate (MTX). (n = 5 µM, 10 µM 20 µM, 50 µM and 100 µM). 91

Figure 6.8. Annexin V-PI Cytotoxicity assay. Flow cytometry analysis of Annexin-PI stained MDA-MB-231 cells after 48 h treatment with MTX drug and RG301-MTX conjugate at 50 µM concentration. (A) No treatment, (B) MTX treatment, and (C) RG301-MTX conjugate treated cells were harvested and 92

stained with Annexin V and PI before analysis. FL1-H represents FITC labeled Annexin-V staining, and FL3-H represents PI staining.

Figure 6.9. Hemotoxicity of peptides. Hemolytic assay of the designed peptides (UN) and their MTX conjugates (MTX) at 100 μM for 2 h at 37°C against human red blood corpuscles (RBCs). The data was normalized by complete lysis with 0.5 % of Triton X-100. All results are presented as the mean ± SD of three independent experiments. 92

Figure 6.10. Peptide uptake in 3D cultures. MDA-MB-231 tumorospheres were treated with CF-tagged RG301 peptide for 4 h at 37°C. After treatment, the tumorospheres were washed and imaged using confocal microscopy. (A) Peptide fluorescence acquired from different planes of the tumorosphere. (B) Peptide fluorescence merged with Bright field images of each plane to distinctly represent peptide uptake. (C) Three-dimensional view of peptide uptake in tumorosphere. (D) Maximum intensity projection images for the same tumorosphere to show the tumorosphere areas with peptide uptake. 94

Figure 7.1. Schematic representation of overall philosophy. H: Homing Domain, P: Penetrating Domain, and D: Drug molecule. 101

List of Tables

Table 2.1.	Approved peptide drugs and their respective functions.	9
Table 2.2.	RGD and NGR peptides in clinical trials.	17
Table 4.1.	List of Computational Tools used in the current study.	37
Table 4.2.	Characterization of Peptide Mass.	46
Table 5.1.	Amino acid Sequences and Mass Characterization of the designed peptides.	65
Table 6.1.	Amino acid sequence of designed peptides.	82

Abbreviations

3D	Three dimensional
Aib	2-Aminoisobutyric acid
Ala	Alanine
ANT	Adjacent normal tissue
ATCC	American Type Culture Collection
BPE	Bovine Pitutary Extract
CB	Beta carbon
CD	Circular dichroism
CF	5(6)-Carboxyfluorescein
CG	Gamma carbon
CLSM	Confocal Laser Scanning Microscope
CO_2	Carbon dioxide
CPP	Cell Penetrating Peptide
CZ	Zeta carbon
Da	Dalton
DKP	Diketopiperazine
DMEM	Dulbecco's Modified Eagle's Medium
DMF	Dimethylformamide
DOX	Doxorubicin
ECFP	Enhanced Cyan Fluorescent Protein
EDT	Ethanedithiol
ESI-MS	Electron Spray Ionization-Mass Spectrometry
FACS	Flow Activated Cell Sorter
FBS	Fetal Bovine Serum
Fmoc	Fluorenylmethoxycarbonyl
FRET	Fluorescence Resonance Energy Transfer
FTIR	Fourier Transform Infrared
Gly	Glycine

H&E	Hematoxylin and Eosin
HCCA	α-cyano-4-hydroxycinnamic acid
hEGF	Human Epidermal Growth Factor
HEK-293	Human Embryonic Kidney cell line
HeLa	Cervical cancer cell line
HMPA	4-Hydroxymethylphenoxyacetyl
IDCT	Invasive ductal carcinoma tissue
iRGD	Internalizing Arginine-Glycine-Aspartic acid
KGD	Lysine-Glycine-Aspartic acid
LAMP-RFP	Lysosomal associated membrane protein-red fluorescent protein
MALDI-TOF MS	Matrix-Assisted Laser Desorption Ionization- Time of Flight Mass Spectrometry
MCF-10A	Mammary epithelial cell line
MDA-MB-231	Breast cancer cell line
MEGM	Mammary Epithelial Cell Growth Medium
MFI	Mean Fluorescence Intensity
MMP	Mitochondrial membrane potential
MTT	[3-(4,5-dimethylthiazol-2-yl)-2,5-diphenyltetrazolium bromide]
MTX	Methotrexate
NGR	Asparagine-Glycine-Arginine
PBS	Phosphate Buffer Saline
Pro	Proline
QGR	Glutamine-Glycine-Arginine
RBC	Red Blood Corpuscle
RGD	Arginine-Glycine-Aspartic acid
RHD	Arginine-Histidine-Aspartic acid
RP-HPLC	Reverse Phase -High-Performance Liquid Chromatography
R-plot	Ramachandran plot
RYD	Arginine-Tyrosine-Aspartic acid
SPPS	Solid Phase Peptide Synthesis
TFA	Trifluoroacetic acid

THP	Tumor Homing Peptide
TMRM	Tetramethyl rhodamine methyl ester
TNF	Tumor Necrosis Factor
TPPs	Tumor Penetrating Peptides
U2-OS	Osteosarcoma cell line
Val	Valine
YFP	Yellow Fluorescent Protein

Abstract

Advancement in synthesis and characterization protocols and demand of new chemical entities (NCE) have contributed to the development of peptide-based therapeutics. The introduction of cell penetrating and tumor homing peptides has opened up new avenues for drug delivery applications using peptides. In the present thesis, we rationally designed sixteen peptides for targeted drug delivery, broadly classified into three different peptide series. The conceptual advancement of Series-1 to Series-3 peptides presents the evolution of a design tree, whose roots originate from the Ramachandran plot. The restriction of geometry through structural engineering is a common trait in all the peptide series. The progressive addition of syndiotactic penetrating domains in Series-2 and Series-3 molecules have remarkably shown the effect of the geometry encoded design. All designed molecules were synthesized, characterized, and tested on various cell lines, including breast cancer (MDA-MB-231), cervical cancer (HeLa), osteosarcoma (U2-OS), non-cancerous mammary epithelial cells (MCF-10A) and human embryonic kidney cells (HEK-293). 5(6)-carboxyfluorescein and methotrexate conjugated peptides were prepared to verify their potential to target cancer cells preferentially. Flow cytometry, fluorescence microscopy, spectroscopy, and cytotoxicity assays confirm their preferential cellular uptake, cytotoxicity, and cargo delivery potential in cancer cells. Each peptide molecule is imbibed with distinct electrostatics, evident from the electrostatic fingerprints and associated functional changes.

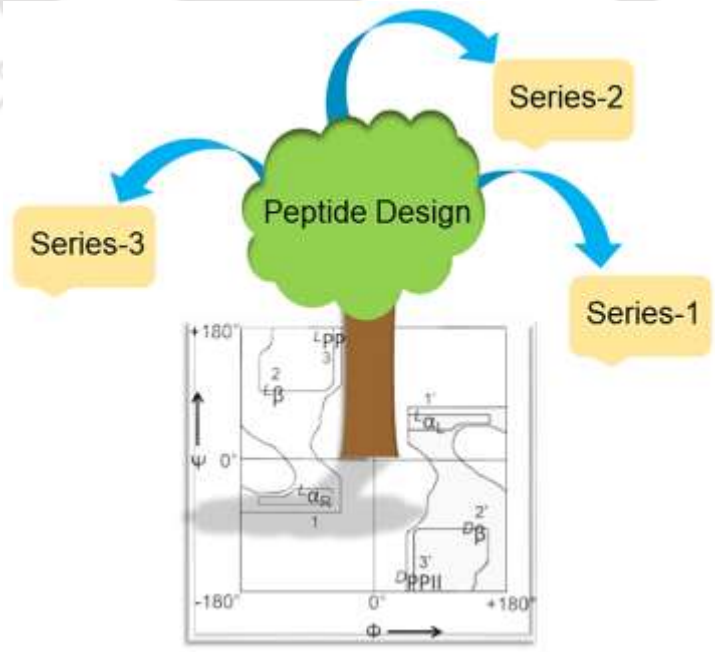

1

Introduction

Peptides are short polymers of amino acids. The therapeutic value of peptides got recognized in the first half of the 20th century. The ease of their chemical synthesis and scope for modifications and conjugations through chemical reactions have made them one among the preferred theranostic agents. Their diversity varies from the selection of amino acids, their sequence, and chain length, they are composed of. The permutations and combinations of amino acids can create a diverse array of peptides that represents a distinct peptidic universe. Their utility in medical science as hormones and drugs for diabetes, diarrhea, labor pain, cancer, etc. have already proven their therapeutic potential. In this chapter, we introduce the concept of therapeutic peptides for targeted drug delivery in brief, on the lines of the presented thesis work.

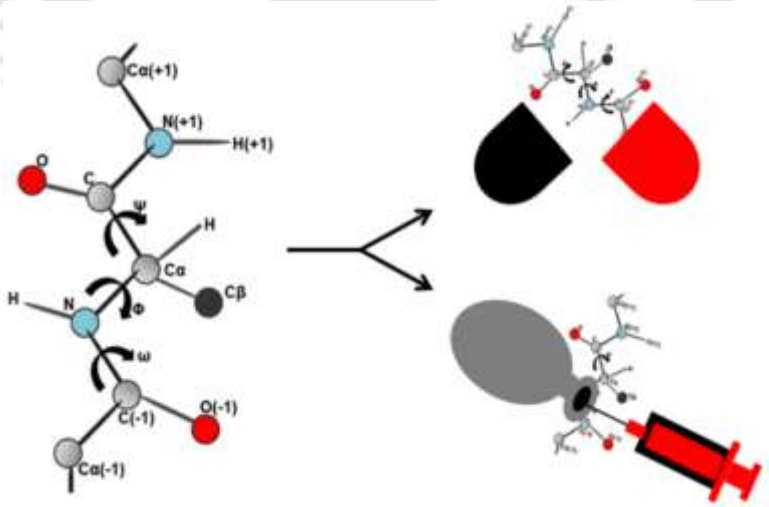

Life forms are driven by the organized, functional balance between biomolecules and metabolic pathways. According to the 'biochemical universals,' there is a unity of biomolecules and certain biochemical pathways in most life forms (*1*). Peptides and proteins are among one type of biomolecules capable of performing moonlighting functions. Peptides are the short polymer of amino acids that falls between small chemical compounds and large proteins in their size distribution contour. Conventionally, they are known to function as hormones, signaling molecules, transmitters, carriers, and supplements; but, the use of insulin, a peptide hormone for diabetes, opened up the possibilities of therapeutic peptides (*2*). Later, advances in synthetic chemistry led to the advent of several peptides as promising therapeutic options, including oxytocin, octreotide, calcitonin, and others.

Peptides are amongst preferred therapeutics over conventional synthetic drugs, due to their lesser side-effect, negligible toxicity, and predictable metabolism. Likewise, peptide-based drug delivery systems for cellular targeting are favored as they by-pass the issues of bio-distribution, biotransformation, and drug clearance due to multi-drug resistance. However, the use of naturally occurring peptides is limited due to their poor stability, short plasma half-life, high clearance, low oral bioavailability, and poor ligand selectivity. To deal with these problems, strategies like metal complexation, terminus or side chain modifications, cyclization, and scaffold-based peptidomimetics, were introduced to employ conformational and topological constraints (*3*). Such initiatives are helpful in the resurgence of peptide-based drug solutions for diseases like cancer.

Cancer has emerged as a global threat to the human race. From the historic era of Hippocrates (around 400 BC) to present medical literature, cancer etiology has evolved from Karkinos to Onkos, from the latter one 'oncology' discipline has acquired its modern name. Karkinos symbolizes a 'crab' in Greek literature, which reminded Hippocrates of tumors clutched with blood vessels around them (*4*). Presently, cancer has overshadowed many deadly diseases and is persistent in taking death tolls every year. In 2018, it accounted for 9.6 million deaths worldwide (*5*). Regardless of the major advancements in cancer research, the pitfalls associated with the recurrence-free cure of cancer is still a challenge.

The use of peptide-based therapeutics as targeted delivery vectors has emerged as an outstanding solution in combating the side-effects of chemo- and radiotherapies. Encouraging

pre-clinical and clinical trials of peptides against cancer offers the scope of their use as probable therapeutic solutions. In general, peptide-based targeting of cancer cells came into existence with the introduction of tumor homing and cell penetrating peptides.

The advancement of Cilengitide, iRGD, and NGR peptides for multiple cancers has manifested the usage of peptides for targeted drug delivery (*6*). Tumor homing peptides (THPs) were primarily discovered by phage display technology and combinatorial libraries (*7*). THPs are short stretches of amino acids with RGD and NGR trimers as common motifs (*7*). THPs like iRGD, Cilengitide, NGR-TNFα, etc. have been broadly investigated in clinical studies but couldn't get approval from Food and Drug Administration. The concerns related to proteolytic stability, tumor specificity, and response variations have mainly contributed as the obstructive factors for their clinical development (*8*).

In addition to homing peptides, cell penetrating peptides (CPPs) have presented their potential to deliver a wide range of molecules in cells. CPPs are generally 15-25 amino acids long amphipathic molecules capable of internalizing in cells, mainly by direct translocation across the plasma membrane and endocytosis. Historically, TAT and Penetratin peptides unveiled the prospects of payload translocation across plasma membranes (*9-11*). CPP molecules are mostly positively charged with optimum hydrophobicity to assist penetration in cells.

In the present thesis, we present the roadmap of peptide designs for cell-type specific vectors for targeted delivery. We discussed the evolution of three peptide series through *de novo* designing imbibed with the sequential conceptual advances. We used the knowledge of Ramachandran map, tacticity, torsion angle modifications, stereochemistry, topology restriction, and unnatural amino acids in the design of targeting peptides. The objective of the present study is to generate a complete molecular construct consisting of a homing domain, penetrating domain, and a cytotoxic molecule loaded on it for selective killing of cancer cells.

In the first series of peptide design, we designed a library of RGD and NGR/QGR mimics, employing an 'informed walk' across Ramachandran geometrical space, and experimentally verified them using standard protocols. (Chapter 4) The second series is the extension of the first one with the focus on the addition of the cell-penetrating function using the amphipathic syndiotactic tails (Chapter 5). In this series, the selection of stereo-specific amino acids at

defined positions imparts the unique electrostatic signature to each peptide molecule, which in turn, has influenced their behavior for the particular cell types. In the last series, we introduce the hybrid design of tumor homing peptides linked to the cell penetrating domain to generate tumor penetrating peptides (Chapter 6). The designed peptides were tested for selective binding to different cancer cell lines, representing different tissues. Later, their preferential binding to cancer tissues was also verified with the tissue samples of cancer patients.

The presented work is an attempt to re-engineer RGD-based homing peptides for selective cellular targeting and drug delivery by using geometrical directives. This study was primarily designed by embedding the translational perspective in it, which may help in addressing the massive problem of cancer worldwide. In addition to this, it offers insights for the conceptual innovations in the development of peptide-based therapeutic solutions using knowledge-based platforms.

2

Peptide-based Drug Delivery Systems

Peptides are versatile biomolecules that function as signaling messengers, hormones, carriers, and drugs. A variety of approaches are employed to engineer peptide-based systems for targeted drug delivery. They have been decorated with nanoparticles, conjugated with fluorophores, radiolabels, cytotoxic drugs, and modified with several polymers. Peptides themselves and their conjugates perform diverse functions based on their physicochemical and structural properties. In this chapter, recent developments in the field of peptide-based drug delivery systems as targeting peptides and cell penetrating peptides are discussed along with their clinical applications.

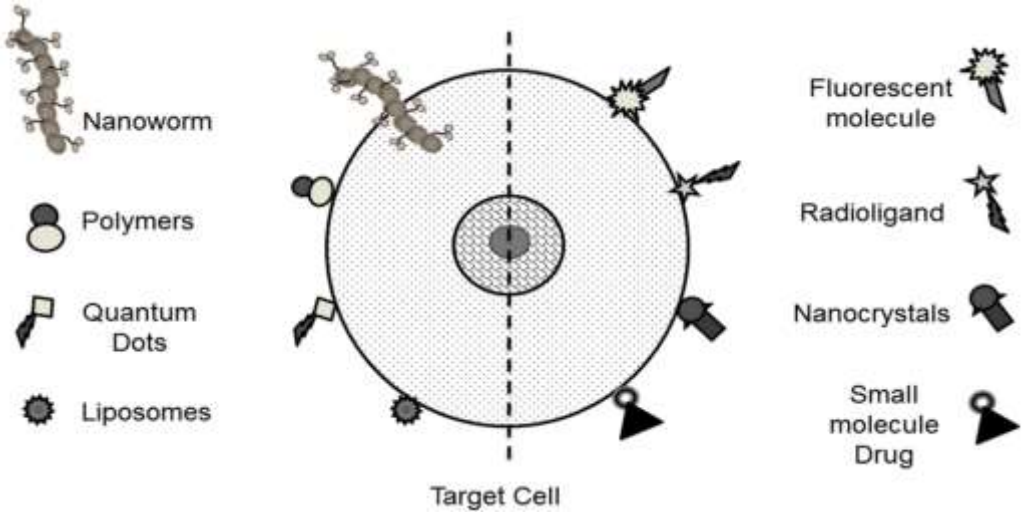

2.1. PEPTIDES IN TARGETED DRUG DELIVERY

Drug delivery, in particular, targeted drug delivery, represents a method of site-directed drug localization in the body. This concept gets recognized when Paul Ehrlich introduced the term 'Magic Bullet' in 1906. Drug delivery vehicles constitute a store of liposomes, polymeric micelles, nanoparticles, monoclonal antibodies, lipoproteins, quantum dots, radioligands, and fluorescent probes. These moieties are conjugated to peptide-based systems to circumvent the problem of stability, solubility, plasma half-life, bioavailability, and ligand specificity (*12*).

In drug databases, there are more than 100 peptide-based approved drugs available; Octreotide, Desmopressin, Cyclosporine, Oxytocin, Erythropoietin, Insulin glargine, etc. are some prominent examples (*13*) (Table 2.1). Presently, this 'peptide-based therapeutics' market is estimated to be more than US$40 billion/yr, amounting to 10% of the total drugs and pharmaceuticals market.

Table 2.1. Approved peptide drugs and their respective functions

Drug	Number of residues	Function
Octreotide	8	Inhibitor of growth hormone, glucagon, and insulin
Bradykinin	9	Increase peripheral circulation
Oxytocin	9	Maintains labor pain
Insulin	51	Maintains blood sugar level
Erythropoietin	165	Production of RBCs
LL-37	37	Anti-microbial peptide
DP-178	35	Anti-viral peptide
Ghrelin	28	Appetite-stimulating effect
Cyclosporine	11	Immunosuppressant

2.2. STRATEGIES FOR PEPTIDE-BASED DRUG DESIGN

Chemists and biologists employed many synthetic or biological moieties as targeted therapeutic molecules for diagnosis and treatment of any medical illness. Peptides are the preferred choice of therapeutics over conventional synthetic drugs due to their lesser side-effect, reduced toxicity,

and predictable metabolism. Likewise, peptide-based drug delivery systems for cellular targeting are in demand because they circumvent problems of bio-distribution, biotransformation, and drug clearance due to multi-drug resistance. However, the use of naturally occurring peptides is limited due to their poor stability, short plasma half-life, high clearance, low oral bioavailability, and poor ligand selectivity. To deal with these problems, strategies like metal complexation, terminus or side chain modifications, cyclization, and scaffold-based peptidomimetics, were introduced to employ conformational and topological constraints. Such initiatives are instrumental in the presently experienced renaissance in the discovery of peptide-based drug healthcare solutions.

First-generation peptide drugs like classical peptide drugs, peptidomimetic drugs, and macrocyclic peptide drugs are the result of primary modifications in peptide design such as amino acid substitution, amide bond modification, and peptide cyclization. Further, peptide scaffold and non-peptide template design strategies led to the second generation of peptidomimetic drugs, which consequently led to the development of target structure-based drug designs that can recognize structural patterns at their cognate ligands (*3*). These peptides are designed to adopt different conformations in space and to restrict their conformations to get topological control for receptor-mediated interactions. For instance, the development of an anti-cancer drug, Cilengitide, is based on such a reductionist approach of structure-based peptide design (*14*). Primary strategies adopted for peptide-based drug design, including torsion angle modifications, incorporation of unnatural residues, and cyclization, are also discussed in brief in this section.

2.2.1. Torsion angle and Peptide Backbone Alterations

The architecture of torsion angles (phi φ, psi Ψ, chi χ, omega ω) in peptides plays an important role in defining their 3D structural and conformational properties. Ramachandran plot of the peptide offers plausible combinations of these torsion angles to have different secondary structures like α-helix, β-turn, β-strand, ϒ-turns (Figure 2.1). This restriction of torsion angles in peptides determines their molecular flexibility. For example, trans-configuration is favored over cis-configuration, but torsion angle restriction in β-turn or ϒ-turn favors cis-configuration over trans-configuration for N-alkylated amino acid at C-terminus. In addition, different derivatives of amino acids like dehydro-amino acid, vinylogous-amino acid, β-amino acid, aza-amino acid,

peptoids, chimeric-amino acids, etc. limit the combinatorial possibilities of torsion angles and are reported to induce or stabilize α-helix, β-turn, β-strand, and ϒ-turn secondary structures. Apart from torsion angle alterations, peptide backbone modification like non-hydrolyzable amide bond isosteres led to the development of novel protease inhibitors like HIV protease inhibitors, including amprenavir, darunavir, indinavir, etc. (*15*). Principally, peptide backbone modifications include amide bond replacements like thioether, tetrazole, amino methylene, ester, and thioamide.

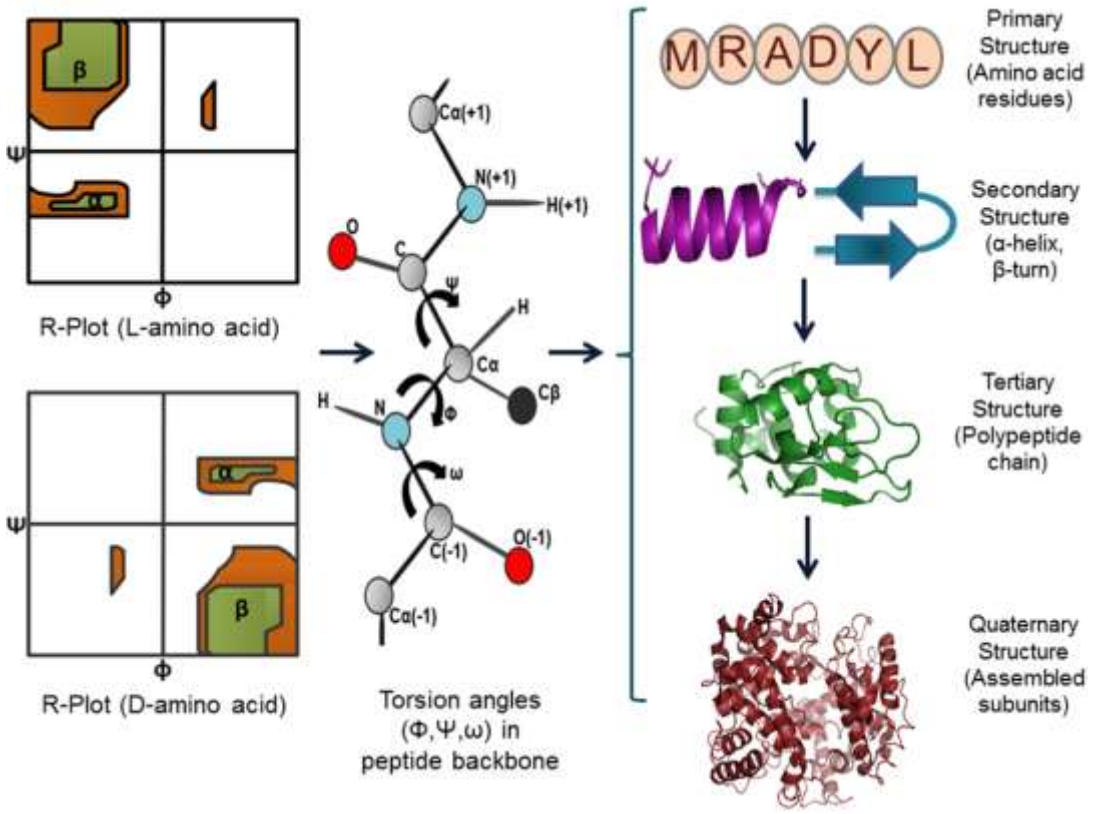

Figure 2.1. Structural Evolution of Peptides and Proteins. *Scheme to represent Ramachandran plot (R-plot) for L- and D-amino acids that define possible combinations of torsion angles (Φ, Ψ) in peptides, leading to different levels of structural organization in proteins starting from primary to secondary to tertiary and finally to quaternary structures.*

2.2.2. Peptidomimetics with Unnatural amino acids

Peptide engineering offers ample space to design application-oriented peptides for their particular utility. It addresses structure-based peptide design, peptide-peptide, peptide-protein and peptide-membrane interactions, bioactive peptides, and peptide-based materials. In a few

cases, peptides with superior properties are designed by incorporating D-amino acids and unnatural amino acids like aminobutyric acid. Several antimicrobial peptides like Gramicidin, Valinomycin, and others have D-amino acids in their sequence, which makes them resistant to proteases and metabolically more stable.

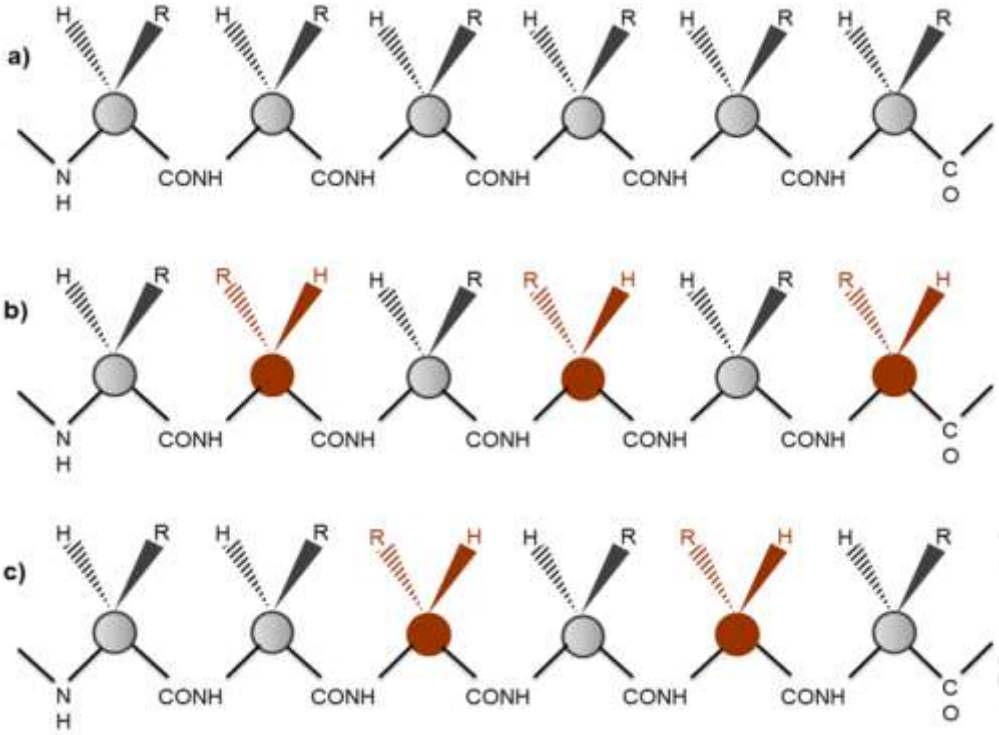

Figure 2.2. Tacticity types. *Different type of tacticity observed in polypeptide chains a) isotacticity b) syndiotacticity c) heterotacticity. Isotactic polymers are composed of either L- amino acids or D- amino acids, whereas; an alternate arrangement of LDLD or DLDL amino acids in peptide chain forms syndiotactic peptides. Heterotactic peptides have random L- and D- amino acid combinations in their sequence.*

Further, it is observed that the specific use of D-amino acids, unnatural amino acids, and dehydro amino acids in peptide design also favors a particular secondary structure (*16*). Studies are reported, where the use of L- and D- amino acids in different combinations and proportions yielded molecules with enhanced activities (*17*). The arrangement of L- and D- (R and S) monomers in a polymer chain is termed as tacticity. Based on tacticity, polymers can be isotactic, syndiotactic, or heterotactic. Isotactic polymers have either L- amino acids or D- amino acids in the peptide chain, whereas; an alternate arrangement of LDLD or DLDL amino acids forms syndiotactic peptides. Heterotactic proteins have completely random L- and D- amino acid combinations in their sequence (*18*) (Figure 2.2).

2.2.3. Macrocyclization of peptides

Cyclization of peptides by thioether linkages, ring-closing metathesis, and azide-alkyne are reported under the umbrella of druggable chemical space. Peptide cyclization topologies include backbone head-to-tail cyclization, side chain-side chain closet, backbone head-to-side chain, or side chain-to-backbone tail cyclization. In biological systems, they are reported to have better receptor selectivity and high metabolic stability. This approach of peptide cyclization has become prominent for mimicking the surface-exposed loops of target molecules. Some cyclopeptides that are employed for cellular targeting includes natural cyclopeptides like cyclosporine A (*19*), stapled α-helical peptides (dual MDM2/X antagonist (*20*)), protease inhibitors (hepatitis C virus protease inhibitor (*21*)), tumor homing peptides (*14*) and cell penetrating peptides (KRAS antagonist (*22*)) (Figure 2.3).

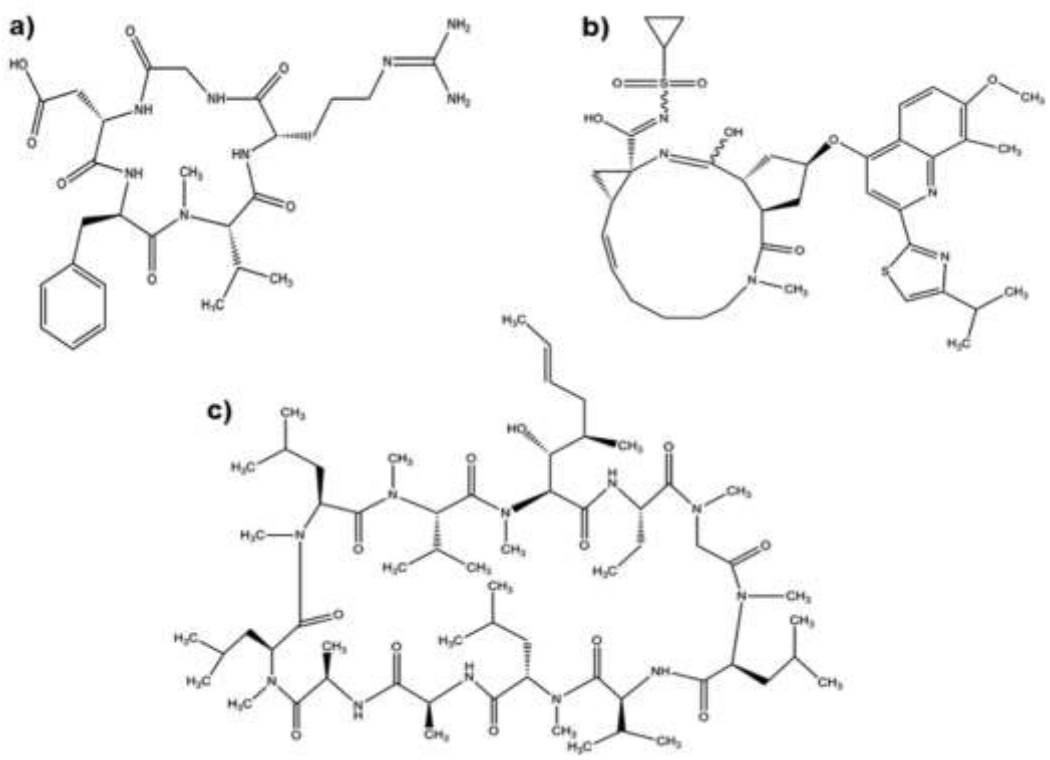

Figure 2.3. Examples of macrocyclic peptides. *a) Cilengitide b) Simeprevir and c) Cyclosporine. Cilengitide is a ligand for $\alpha_v\beta_3$ and $\alpha_v\beta_5$ integrins which are biomarkers of tumor angiogenesis and metastasis of solid tumors. Simeprevir is used for the treatment of Hepatitis C, and Cyclosporine is used as an immunosuppressant in case of rheumatoid arthritis, organ transplantation, and psoriasis.*

2.3. PEPTIDES AS CARRIERS FOR DRUG DELIVERY

Peptides with desirable traits of cell penetration, tumor homing, anti-microbial, target recognition, etc. are preferred in therapeutics as drug candidates for disease diagnosis and treatment. Peptide-based drug delivery vehicles have innumerable applications as targeting agents, imaging molecules, nanovectors, and cytotoxic molecules in the diagnosis and treatment of several diseases. The peptide-based active drug targeting is reported with Vasoactive Intestinal Peptides, RGD peptides, NGR peptides, NGF peptides, Luteinizing hormone-releasing hormone, aptamers, etc. (*23*). Moreover, homing peptides and cell penetrating peptides conjugated to cytotoxic drugs, oligonucleotides, liposomes, nanoparticles, radionuclides, and imaging agents have successfully been tested as delivery vehicles for selective targeting.

2.3.1. Targeting Peptides

Targeting or Homing peptides act as navigators for targeting specific cells or tissues in response to the overexpression of tumor-specific markers. Their function is not restricted to homing ability in response to targets, but they also perform cell or tissue penetration due to different secondary structures and deliver a variety of payloads into the cells. They are derived from natural ligands or combinatorial screens like Phage Display Libraries.

Among natural peptide ligands, somatostatin peptide (SST) arrests the proliferation of cancer cells by targeting the aberrant overexpression of somatostatin receptors (SSTR). In this context, Octreotide, an SSTR analog, is developed against SSTR 2 and SSTR 5 receptors, which are specifically overexpressed in breast cancer cells (*24*). Its radiolabelled conjugates with the trade name Octreoscan and NeoTect are FDA approved radiotracers for cancer treatment. Recent pre-clinical and patient studies on another natural peptide called Gastrin Release Peptide (GRP) also supports the development of targeting peptide as therapeutic drugs against breast and prostate cancers (*25-27*). The targeting of the tumor microenvironment is even possible with peptides like NT21MP peptide (*28*), Nef-M1 peptide (*29, 30*) and peptide R (*31*) which serve as an antagonist of a chemokine receptor CXCR4, that controls invasions of metastatic tumors by epithelial to mesenchymal transition (EMT). Advancements in the discovery of targeting peptides have produced peptides that can even target low pH (e.g., pHLIP (pH-Low Insertion Peptide) peptide) and high temperature (e.g., Leucine Zipper peptide, ELP peptide) in the tumor microenvironment (*32-34*). Another natural peptide α-MSH and its derivatives are

reported to act as antagonists of Melanocortin-1 receptors (MCR-1), which are overexpressed by primary melanomas (*35, 36*). These studies show that naturally occurring targeting peptides have the potential to develop as anti-cancer drugs.

Tumor Homing Peptides (THPs)

THPs are 3-15 residues long peptide sequences with common residues like Cys, Arg, Gly, Leu, and Ser. In recent decades, advanced techniques like phage display library (Figure 2.4) and combinatorial libraries give rise to many THPs that led to the creation of a manually curated Tumor Homing Database called TumorHoPe, which contains 744 experimentally validated THPs covering around 23 tumors like breast, melanomas, prostate, lung, etc. This database is an excellent source of compiled data of THPs, including statistics of an average amino acid composition of cyclic or non-cyclic THPs, distribution of peptides based on secondary structure composition, frequency of common motifs present in THPs, length-wise distribution of THPs, etc. (*7*). The receptor specificity of THP peptides makes them a suitable candidate for tumor targeting. Their range of receptors varies from intracellular to cell surface bound receptors. In the history of THPs, a first endothelial binding peptide called RGD peptide was reported against integrin receptors ($\alpha_v\beta_3$ and $\alpha_v\beta_5$) (*37, 38*). RGD peptides are conjugated with different nano cargoes (nanowires, quantum dots), cytokines, radiolabels, fluorescent tags, and cytotoxic drugs for targeting tumors. Some examples of RGD peptides include RGD-4C (CDCRGDCFC) peptide, iRGD peptide (CRGDK/RGPD/EC), Cilengitide [c(RGDf(NMe)V] and p160 (VPWMEPAYQRFL) derivatives (*14, 39, 40*). They are reported against $\alpha_v\beta_3$ and $\alpha_v\beta_5$ integrins which are biomarkers for angiogenesis and metastasis of solid tumors. Preclinical and clinical evaluation of these peptides confirmed their target-specific drug delivery with enhanced efficacy (Table 2.2).

Similar to RGD peptides, another tripeptide NGR is also associated with angiogenic vasculature (Table 2.2) as a ligand to Aminopeptidase N (CD13), a metalloproteinase highly expressed in angiogenic blood vessels (*41, 42*). Its conjugates with cytotoxic drugs (Cisplatin, Doxorubicin), proapoptotic peptide (KLA peptide), nucleic acids (polyethylenimine DNA polyplex), cytokines (TNFα, IFN) and others are in clinical trials (*43*). In tumor homing peptides, RGD and NGR motifs are known to impart selective targeting of tumor vasculatures by recognition of their cognate receptors. These motifs have similar charge disposition by arginine and aspartic

acid or asparagine. It was found that NGR motif has a strong propensity to undergo non-enzymatic

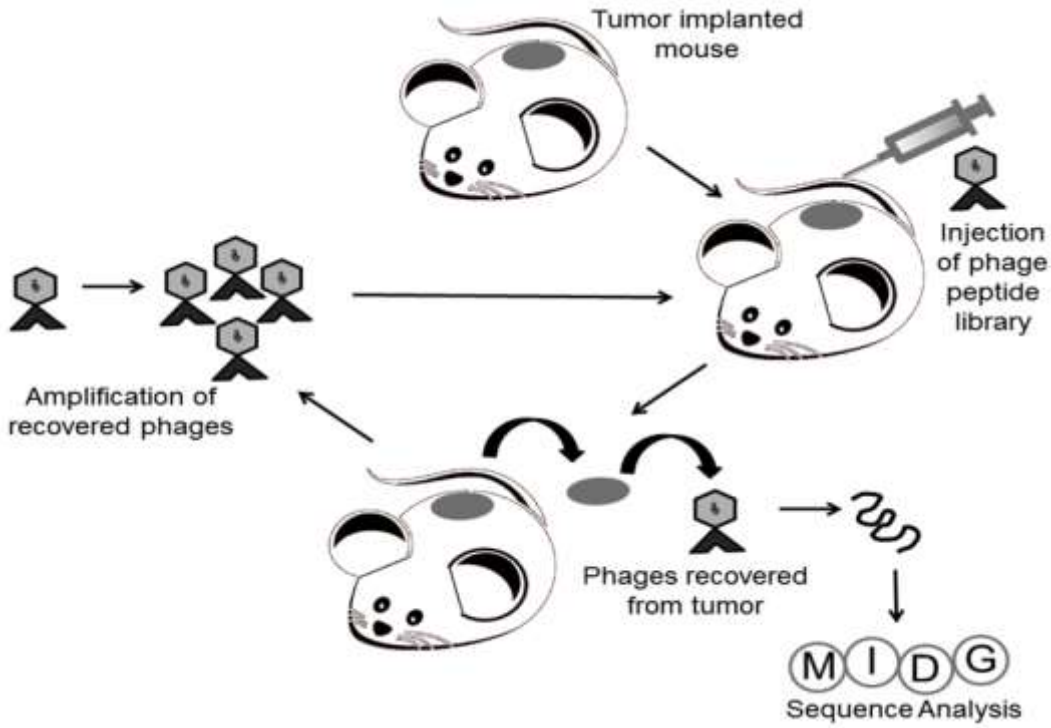

Figure 2.4. Schematic representation of Phage Display Library (PDL). *In this method, phages specific to tumors are recovered through affinity-based selection using combinatorial phage libraries.*

deamidation and becomes isoDGR, which led to receptor switching from CD13 to integrins (*44*). Enyedi et al., have used variants of cyclic NGR peptides in conjugation with daunomycin for dual targeting of CD13 and integrins in cancer cells (*45*).

Attempts have been tried to make RGD peptides as stimuli-responsive agents for targeting tumor vasculature. cRGDyK peptide modified with pH-responsive nanoparticles loaded with doxorubicin drug was used for targeting $\alpha_v\beta_3$ integrin receptors overexpressed in tumor vasculature. The receptor-mediated endocytosis and acidic-triggered drug release showed highly efficient uptake in cancerous cells (*46*).

Lymphatic Homing Peptides (LHPs)

Lymphatic homing peptides are another class of targeting peptides that are specific to markers of angiogenic tumor vessels. Angiogenic markers are different from normal markers of blood vessels and are known to have 'lymphatic zip codes,' selectively targeted for the destruction of

tumor lymphatics (*47*). LHPs possess the advantage of scanning whole body tumors through circulation as they specifically bind to tumor lymphatics. For instance, Lyp-1 peptide (CGNKRTRGC) acts like an LHP in tumors, as it showed selective binding to lymphatic endothelial markers as compared to blood vessel markers (*48*). Albeit, it is important to note that Lyp-1 peptide sequence doesn't have RGD or NGR motifs, which are frequently present in THPs. It has been reported that Lyp-1 peptide hosts anti-tumor activity apart from its tumor lymphatics homing activity by inhibiting tumor growth through its proapoptotic or cytotoxic effect (*49*). In another study on LHPs, Yao et al. identified peptide ligands CVSNPRWKC and CHVLWSTRC for vascular receptors, namely, EphA2 and EphA4 in islets of Langerhans in the murine pancreas through phage display method. They reported that endothelial cells of blood vessels in pancreatic islets preferentially express EphA4 receptors, and their expression gets upregulated in tumors (*50*).

Table 2.2. RGD and NGR peptides in clinical trials

S. No.	Cancer type	Status	Interventional Study	Phase	Year
1	Glioblastoma	Active	Delta-24-RGD Temozolomide	Phase I	2013
2	Prostate cancer	Recruiting	68Ga-NOTA-BBN-RGD	Phase I	2016
3	Glioblastoma	Active	18F-Galacto-RGD PET	Phase I	2013
	Breast cancer	Recruiting	68Ga-NOTA-BBN-RGD	Phase I	2016
4	Solid tumors	Recruiting	18 F FPPRGD2 PET/CT	Phase I & Phase II	2013
5	Solid tumors	Active	NGR-hTNFα	Phase I	2007
6	Malignant pleural mesothelioma	Active	NGR-hTNFα	Phase III	2009
7	Non-small cell lung cancer	Active	NGR-hTNFα; Cisplatin	Phase II	2010
8	Ovarian cancer	Active	NGR-hTNFα; Pegylated liposomal-doxorubicin; Doxorubicin	Phase II	2011

Source: http://clinicaltrials.gov

Later on, it is observed that LHP's development is associated with organ- and stage-specific changes in lymphatics. A peptide called LSD peptide (CLSDGKRKC) by Zhang et al. homed to C8161 melanoma tumors with the highest affinity. Similarly, REA peptide (CREAGRKAC) and AGR peptide (CAGRRSAYC) showed robust and specific binding to full-grown prostate tumors and prostatic intraepithelial neoplasia (PIN) lesions, respectively. They also noticed the stage-specific lymphatic signatures during tumorigenesis through another LHP called Lyp-2 peptide (CNRRTKAGC), which goes and binds to premalignant and malignant lesions in the cervix and also to lymphatics linked to dysplasias and squamous cell carcinomas of the skin (*47*). This shows that with tumorigenesis progression, there is an evolution of molecular specificities in lymphatic vessels. Getting benefited by these organ-specific peptide findings, studies are reported where LHPs are loaded with various payloads for their use in tumor regression therapies. One such example is of REA and LSD LHPs, which are conjugated with an apoptosis-inducing peptide $_D(KLAKLAK)_2$ that led to the reduction in counts of lymphatic vessels in PPC1 prostate tumors and C8161 melanoma respectively (*47*).

Tumor Penetrating Peptides (TPPs)

Despite the advances in peptide-based drug discovery, the success of organ or tissue-specific delivery of peptides confronts challenges with huge tumor vasculature due to poor penetration into tumors. This is due to poor perfusion of tumor vessels with blood and high interstitial pressure, which prevents the diffusion of drugs into tumors (*51*). To overcome this problem, a concept of peptides with tissue-penetrating properties comes into existence, which helped the peptide to deliver anti-cancer drugs deep into the tumor parenchyma. Tumor penetrating peptides undergo proteolytic cleavage after binding to a tumor-specific receptor, followed by binding to an intracellular receptor. This activates an endocytic transport or trans-tissue transport of attached cargoes on TPPs. Peptides like iRGD, iNGR, tLyP-1, TT1, F3, and others are amongst best known TPPs. They performed targeted delivery with penetration, concomitantly ensuring enhanced availability of drugs, antibodies, and nanoparticles.

In 2009, Sugahara et al. identified a strategy for THP-mediated delivery of compounds deep into the tumor parenchyma. They employed iRGD peptide (CRGDK/RGPD/EC) specifically against α_v integrins (where 'i' stands for internalizing) to investigate the ability of iRGD peptide

for delivering anti-cancer agents. For this, they used iRGD-coated iron oxide nano worms and iRGD-linked abraxane molecules and observed their selective targeting to tumors followed by their significant growth suppression. Mechanistically, it is found that this peptide contains a cryptic CendR motif that has a strong affinity for Neuropilin-1 (NRP-1), which is another biomarker for cancer. According to C-end rule (CendR), a C-terminal arginine or lysine in a consensus motif R/KXXR/K is essential for the internalization of the homing peptide (*40*). For iRGD peptide, homing and penetration is observed sequentially in three steps: RGD motif binds to α_v integrins on tumor endothelium, proteolytic cleavage occurs leading to exposure of binding motif for neuropilin-1 that mediates penetration into tissues and cells (Figure 2.5). Similarly, iNGR and tLyP-1 peptides also show internalization by binding to NRP-1 receptor due to the presence of CendR motif.

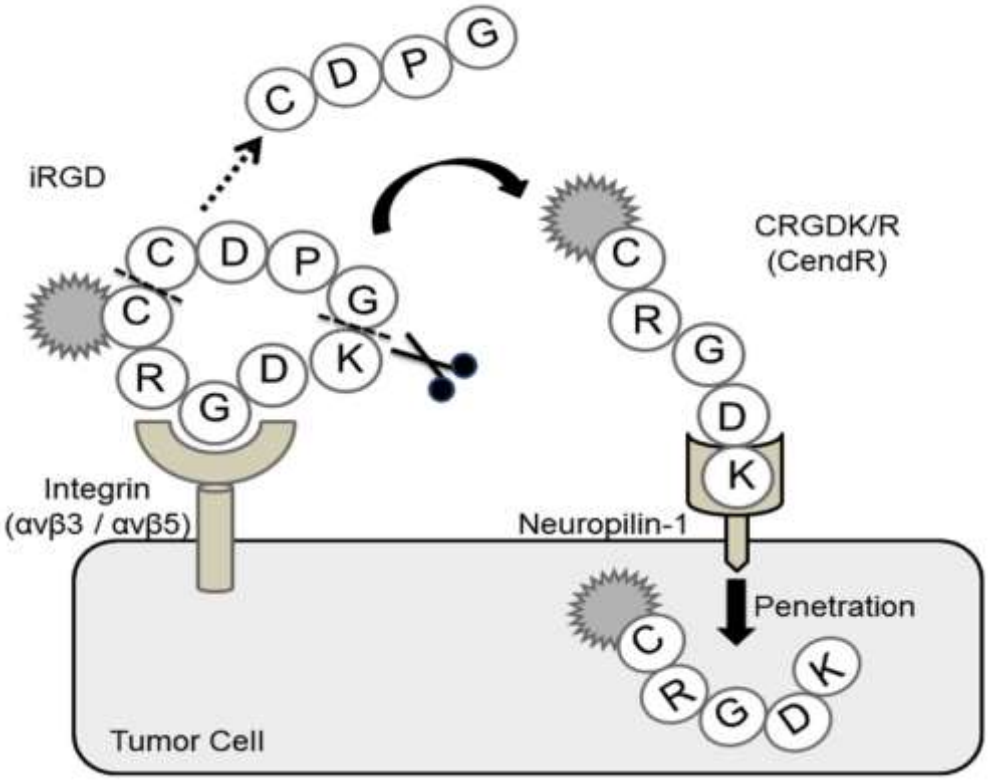

Figure 2.5. Binding and penetration mechanism of iRGD peptide. *There is a proteolytic cleavage of iRGD peptide after binding to α_v integrins on tumor endothelium, leading to exposure of binding motif for Neuropilin-1 that mediates penetration of iRGD peptide into tumor cells.*

Another tumor-penetrating peptide, F3, a 31-mer fragment of HMGN2 protein, is reported to internalize by cancerous cells through nucleolin-dependent pathway after binding to nucleolin

receptor at the cell surface (*52*). Normally, nucleolin resides in the nucleus, but in transformed cells, it shuttles between cell surface and nucleus (*53, 54*). It is investigated that F3 peptide can transport carriers like α-emitters in the proximity of DNA, leading to enhanced destruction of DNA and, ultimately, cell death (*55*). Furthermore, it's another conjugate 213Bi-DTPA-$[F3]_2$ found to accumulate in the nucleus of tumor cells and in *in vivo* studies; it showed double survival time of animal models with no toxicity. This facilitates the development of organ or tissue selective radiation-based tumor therapies (*56*).

Moreover, combined strategies for targeted gene delivery were also envisaged using a combination of TPPs like F3 peptide along with Lyp1. This combination of TPPs showed tumor-specific gene delivery in host cells (MDA-MB-435, MDA-MB-231, and MCF-10A) through the application of silk-based nano-complexes (*57*). In addition to this, metallic nanoparticles in conjugation with THP offer surplus opportunities for the design of stable peptide-based drug delivery systems that are reported with gold nanoparticles (AuNPs). AuNPs of 2 nm size functionalized with a therapeutic peptide PMI (p12) and a targeted peptide CRGDK enhanced intracellular uptake of AuNPs functionalized with peptide p12 in tumor cells (*58*).

Tumor-Specific Peptides (TSPs)

Among the aforementioned targeting peptides, some of them also target specific tumors like breast cancer, gastric adenocarcinoma, colon cancer, lung cancer, melanoma, and glioma. Peptides like TCP-1 and its conjugates with TNF-α and pro-apoptotic peptide displayed significant anti-tumor activity in colorectal cancer models (*59-61*). A renal targeting peptide $(KKEEE)_3K$ and its conjugates are found very effective in targeting kidneys through megalin receptors (*62*). Another peptide, CREKA, specific for breast cancer models conjugated with fluorescein, iron oxide nanoparticles, magnetic nano worms, paclitaxel, etc. for its application in imaging and anti-tumor therapy (*63-65*). For melanomas, peptide TH10 (TAASGVRSMH) specific to melanoma-associated antigen NG2 was also studied. TH10 conjugates with docetaxel-loaded nanoparticles target NG2 antigens highly expressed in melanoma tumors (*66*). Another TSP, SP5-52 peptide (SVSVGMKPSPRP) linked with doxorubicin-loaded liposome, is found to be specific for lung carcinoma in mice models (*67*). By PDL technology, peptide (CSNIDARAC) specific to H460 lung tumor cells also showed good specificity. This

peptide bound and internalized by H460 cells indicating that this peptide is a potent tumor homing peptide for lung cancer. Therefore, it is employed for imaging and targeted delivery of liposomal doxorubicin to lung tumors that subsequently led to the decrease in lung tumor growth many folds, compared to untargeted liposomes or free doxorubicin (*68*). Furthermore, glioma homing peptides MG11 (LWATFPPRPPWL) and GL1 (LLADTTHHRPWT) are also revealed by phage display screening (*69, 70*). The decoration of tLyP-1, RGD, iNGR, and F3 peptides with various nanoparticles, including RNAi, PEG-PLA, paclitaxel, etc. reinforced their potential for effective glioma therapies.

2.3.2. Cell Penetrating Peptides (CPPs)

Another major class of peptides refers to CPPs or protein transduction domains (PTDs), which are 15-25 amino acids long amphipathic molecules efficient in translocating through the membrane of cancer cells. Historically, studies with TAT, an HIV transactivating factor, and Penetratin, a third helix homeodomain of Antennapedia transcription factor of Drosophila, opened up the possibilities of translocation across cell membranes with the desired payloads (*9-11*). Molecules acting as CPP possess specific characteristic features that make them distinguishable from other peptides. Firstly, they are rich in positively charged residues, specially Arg because it contributes to cellular internalization more than Lys residues due to the extra H-bond donation of its guanidinium group. Secondly, they have optimal hydrophobicity, which leads to better uptake of CPP inside cells. Apart from sequence polarity, the secondary structure of CPPs also plays an important role in their cellular uptake. Structures adopted after interaction with cell membrane contributes more to cell penetration, but their inability of binding specifically to particular cells is a major demerit for their clinical applications (*71*). However, due to their phenonomenonal ability to penetrate inside cells, CPPs are widely used with targeting moieties for applications in the delivery of drugs and nanoparticles. These have been improved for the targeted delivery of drugs to tumors.

Activable cell penetrating peptides (ACPP) has been introduced, which gets active at the tumor extracellular pH of 6.8. Zhang et al., has formulated a prodrug composed of a known ACPP ($CR_8G_3PK_6$) capped with an acid-sensitive shielding group of 2,3-dimethyl maleic anhydride (DMA) and anti-cancer drug doxorubicin. At the tumor site, the extracellular pH 6.8 hydrolyze

DMA and activates CPP by charge reversal. This initiates the rapid uptake of CPP by tumor cells and thereby release the conjugated DOX and kills cells at the site (72). Similar to this, a study on the peptide-based pH-sensitive drug delivery system was reported using the hydrazone bridge as the pH-responsive probe. AP2H (IHGHHIISVG), a low-pH responsive decapeptide specific for lysosomal protein transmembrane 4 beta (LAPTM4B), was conjugated to doxorubicin drug (DOX) using hydrazine bond. The targeting through LAPTM4B offers selective death of cancer cells (73).

Uptake mechanisms for CPPs

Non-endocytic and endocytic are the two major uptake mechanisms proposed for CPP or CPP-cargo complexes so far. Non-endocytic uptake mechanism refers to the direct penetration of peptides through the cell membrane, and in this pathway, peptide gets localized directly in cytosol whereas, endocytic uptake mechanism refers to the internalization of peptides through endocytosis which is mediated by clathrin, caveolae or macropinocytosis (Figure 2.6). In the endocytic pathway, a peptide may or may not get released in the cytosol, but if not, then it gets localized in endocytic vesicular compartments. This cellular uptake process of CPPs can be active or passive in nature, which means they may or may not be energy driven. In general, it is known that carbohydrate moieties like proteoglycans, glycosaminoglycans, and negatively charged lipids play a major role in the interaction of CPPs with the cell surface and hence directly affect their penetration. Copolovivi et al. mentioned that cellular uptake of CPPs is also affected by factors like cell type and membrane composition; nature and secondary structure of CPP; their ability for interaction with cell surface and membrane lipid components and lastly, by nature, type and active concentration of cargoes (74).

Drug Delivery by CPP conjugates

So far, a good number of CPP-conjugated therapies have already established their efficacy for clinical use. For selective targeting of cancerous cells, CPPs are attached to targeting moieties like cell targeting peptides, activable cell penetrating peptides, and transducible agents. For instance, the injection of covalently conjugated cell-penetrating peptide TAT to p53 into rabbit eyes having human retinoblastoma xenografts enhanced tumor cell apoptosis without showing

toxicity to tissues in its vicinity (*75, 76*). Attachment of TAT with a CXC chemokine receptor 4 (CXCR4) ligand DV3 and two transducible anticancer peptides viz p53 activating peptide

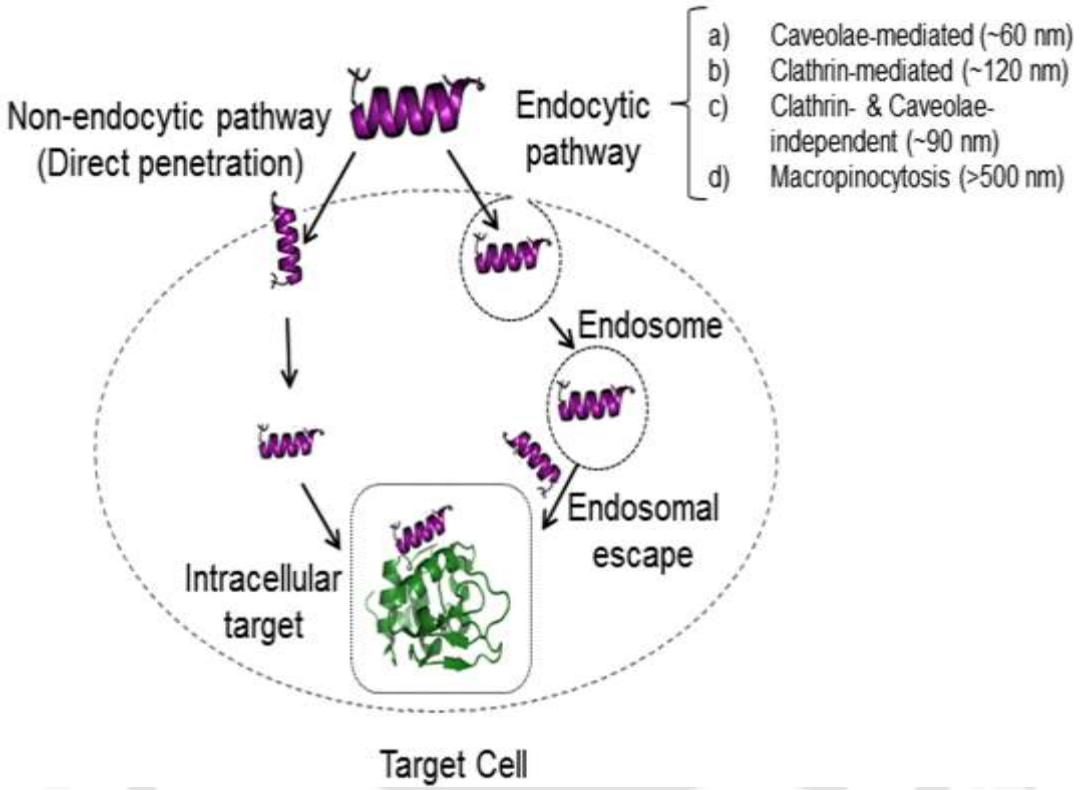

Figure 2.6. Cellular uptake mechanisms of CPPs. *The involved mechanisms for cellular uptake of CPPs are non-endocytic and endocytic pathways. Non-endocytic pathways refer to the direct penetration of CPP through plasma membrane phospholipids, whereas; endocytic pathway involves pinching off membrane vesicles after endocytosis.*

(p53C') and cdk2 antagonist peptide (RxL) has shown to double the killing efficiency of these anticancer peptides (*77*). The covalent coupling of CPPs like Transportan 10 (TP10) to modified nucleic acids like PNA is shown to promote their cytosolic delivery. In this context, both *in vivo* and *in vitro* studies have shown that siRNA (silencing RNA) against vascular endothelial growth factor (VEGF) complexed with CPP cholesteryl-R9 led to the increase in tumor regression efficacy of siRNA (*78*). The combinations of CPPs with THPs also enhanced their efficacy as anti-tumorogenic agents. Tumor-homing cell-penetrating peptide conjugate (PEGA-TAT) was used for targeting of Aminopeptidase P (APaseP) in the vascular endothelium of breast cancer (*79*). In a study, this approach was utilized with cell penetrating peptide pVEC, and tumor-homing peptide PEGA, where this conjugate (pVEC-PEGA) got selectively

accumulated in breast cancer cells and their conjugate with anti-cancer drug chlorambucil boosted the efficacy of drug over four times (*80, 81*). The conjugation of another homing peptide CREKA to p-VEC makes them suitable for targeted delivery of DNA alkylating agent, Chlorambucil, inside cells (*82*). For efficient gene delivery, nano-vectors are also constructed using CPPs. For instance, CPP octaarginine (R8) with target ligand folic acid (FA) and gene vector (PEI (600)-CyD, PC) showed excellent gene transfection in folate-receptor-positive tumor cells (*83*). For anti-cancer therapies, CPPs are also modified with different moieties like PNA, siRNA, drugs like doxorubicin (DOX), methotrexate (MTX) either by covalent coupling or by non-covalent complex formation. CPPs MPG8 and PEP3 were complexed with siRNA and PNA respectively through non-covalent interactions and showed to promote cellular uptake in cancerous cell lines. PEP3 and MPG8 form stable nanoparticles with PNA and siRNA respectively and enhances cellular uptake without any cytotoxicity (*84*). Activable CPPs (ACCPs) are also conjugated with anticancer drugs like doxorubicin (DOX) for site-directed action (*85*). Natural products like tea extracts have been employed with peptides for anti-cancer medicinal properties. A group has prepared a construct of the tumor-homing cell-penetrating peptide (PEGA-pVEC) linked to the colloidal mesoporous silica (CMS) encapsulated (-)-Epigallocatechin-3 gallate (EGCG), a major ingredient of green tea for breast cancer therapy. This conjugate (CMS@peptide@EGCG) showed around 89% tumor inhibition rate during in vivo treatment (*86*). These reported studies of CPP conjugates confirm their wide applicability in anti-cancer therapies.

2.4. FUTURE OF PEPTIDE-BASED DRUG DELIVERY SYSTEMS

The development of application-oriented peptides for diagnostics and therapeutics has been successfully highlighted in this chapter. At various places, one can see that multidimensional designs are incorporated into a single peptide to make it suitable for the desired function. For instance, Lin et al. incorporated characteristics of available anti-cancer peptides, tumor homing peptides, cell-penetrating peptides, and antimicrobial peptides in their new design of peptides (*87*). In fact, modification approaches of peptide conjugation and functionalization have proved very effective in several studies. Also, it is demonstrated that peptide-based drug delivery has been effective in both extracellular and intracellular targets. In addition, the adoption of mixed design strategies like heterochiral designs, cyclization, conjugation, and nanoparticle decoration

in peptide design makes them versatile by overcoming the barriers of protease instability, reduced half-life, non-specific binding, and others. Thus, it shows that there is a tremendous scope for peptide-mediated nanoparticle-based diagnosis and therapy, known as nano theranostics in recent literature.

3

Objectives and Research Design

The concept of cellular targeting by Paul Ehrlich and the discovery of the existence of cellular area codes by Erkki Rouslahti have prompted us to formulate our peptide design box with some probable unique solutions for cancer theranostics. The conceptual fusion of knowledge of Ramachandran plot and cellular area codes for selective tumor targeting has contributed to the framing of objectives and research design mentioned in this chapter.

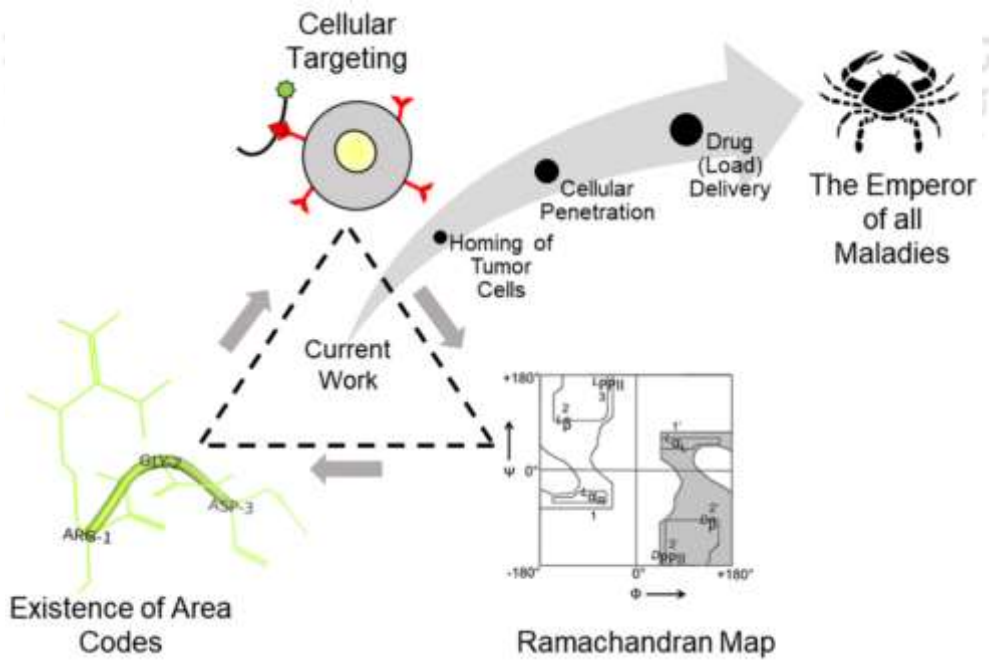

Patent: Ruchika Goyal, Gaurav Jerath, and Vibin Ramakrishnan. Peptide-based Molecular Constructs for Tumor Homing and Cell Penetration. Patent number TEMP/E 1/36087/2019-KOL; 2019 (Filed)

3.1. OBJECTIVES

The present study was designed to address the following objectives:

I. Design of conformationally locked tumor homing peptides (THPs) to generate unique peptides for targeted drug delivery in cancer cells.

II. Design three series of peptides with the following objectives:
   a. Geometry Encoded Functional Programming of Drug Delivery Vehicles, by designing a series of eight molecules with locked Ramachandran basins (Series-1).
   b. Extension of peptides with pre-defined geometrical locks and short tumor cell penetrating segments (Series-2).
   c. Generation of complete tumor-targeting molecular conjugates, with homing, cell penetration, and apoptosis-inducing chemical moieties encoded (Series-3).

III. Synthesis of the designed peptides by Solid Phase Peptide Synthesis, purification by High-Performance Liquid Chromatography, and primary characterization by Mass Spectrometry.

IV. Evaluate the specificity for differential uptake and drug delivery potential against various cell lines and also in three-dimensional tumor tissue models (tumorospheres).

V. Validation of designed THPs in clinical samples and/or tumorogenic mouse models, as possible therapeutic solutions.

3.2. RESEARCH DESIGN DIRECTIVES TO GENERATE DRUG DELIVERY VECTORS

The precise targeting of tumors appears as a challenging task in the treatment of solid tumors using chemotherapy. Tumor homing peptides (THPs), in combination with chemotherapeutic drugs and diagnostic agents, have entered many clinical and pre-clinical trials. Arg-Gly-Asp (RGD) and Asn-Gly-Arg (NGR) motifs frequently present in THPs are the ligands of $\alpha_v\beta_3$ integrin and aminopeptidase N (CD13) receptors, respectively. These motifs provide selective targeting of tumor vasculatures by recognition of these receptors in cancer cells. These motifs become more important for dual targeting of CD13 and integrins in cancer cells due to the receptor switching from CD13 to integrins by isoDGR formation of NGR motif (*44, 45*).

The mentioned facts about these two trimeric peptidic motifs have inspired our investigation to look into the geometry of the middle residue, 'Gly' in these motifs, without which these motifs were proved ineffective (*88*). The presence of 'Gly' in these motifs, enables the tripeptide to assume geometries that are otherwise not accessible to L-amino acids in the Ramachandran Map. To investigate the role of Glycine geometry, we deliberately locked the Glycine residue conformation to specific basins in the D-region of Ramachandran Map, with the desired non-natural amino acid substitutes, to look into their corresponding effect in homing tumors with better specificity, and across cancer cell types with better selectivity.

Theoretically, we hypothesize that during interactions of RGD or NGR peptides with their targets, there is a possibility of 'Gly' being in any plausible conformation in Ramachandran map. Achiral nature of Cα carbon atom and no side-chains helps Glycine to occupy 57% region of Ramachandran plot (R-plot) whereas, the other amino acids are restricted to a meagre 21% (*16*). This means that Glycine can access both L-chiral and D-chiral amino acid basins of the Ramachandran map. The conformational propensities of L- and D- amino acids in the Ramachandran map are mirror images of each other due to asymmetry and backbone dipole directionality (*89, 90*). With this understanding, we tactfully locked the 'middle residue' in one particular conformation by D-valine, D-proline, 2-aminoisobutyric acid (Aib), etc. in peptide designs. We call them 'conformational lockers' as they are restricted to particular basins of the Ramachandran map with specified dihedral angle range (Figure 3.1 A). These basins are mentioned as the right-handed alpha-helical region, beta-sheet region, and polyproline II (PP II) region for the L- and D- amino acids, respectively (Figure 3.1 A). Substitution of 'Gly' with basin specific residue provides a distinct advantage to look into the effect of conformational restriction on the activity of RXD peptides. In the designed THPs, we purposely substituted 'Gly' with D-Pro, D-Ala, Aib, and D-Val to fix basin 3', 1', 1 and 2', for theoretical calculations (Figure 3.1 A). We ensured the occupancy in all six basins of Ramachandran map by selecting distinct combinations of tri-peptides (RGD, rGd, RpD, rPd, RqD, rQd, RvD, rVd, rBd, RaD, and rAd). Substitution of 'Gly' with basin specific residues provides a distinct advantage to investigate the effect of conformational restriction on the activity of RXD peptides. For example, as a test case, if the middle residue (Gly) is mutated with L-proline, it will force the flanking residues to adopt the polyproline conformation. If the middle residue is mutated with D-proline, then it will get locked in a unique conformation, and we hypothesize that this conformation may

induce specificity while interacting with specific cancer cell types, showing more affinity to one (or two) compared to the rest.

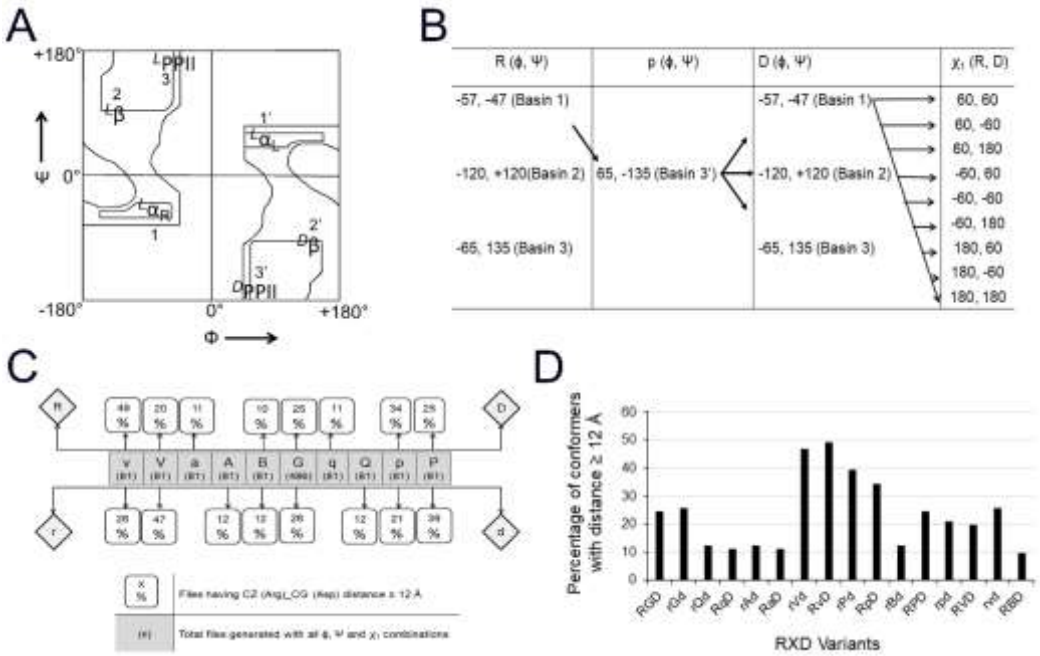

Figure 3.1. Rational modeling approach for peptide designs. *(A) The locked basins of Ramachandran map designated as 1, 1', 2, 2', 3, and 3' for different amino acids. (B) An example of 'RpD' trimer to show the process for generation of rotamer library having different combinations of ϕ (phi), Ψ (psi), and χ_1 (chi1) torsion angles. (C) All trimers were chosen selectively for theoretical calculations of Euclidean distances between CZ (Arg)_CG (Asp). (D) This shows the percentage of conformers and potent trimers that fit in the category of CZ (Arg)_CG (Asp) distance more than 12 Å.*

To explore the effect of maximum possible conformations, different combinations of ϕ (phi), Ψ (psi) and χ_1 (chi1) dihedral angles are considered for each tripeptide (an example is shown in Figure 3.1 B), subsequently leading to the generation of multiple (80-500 in number) structure files for a single tripeptide (Figure 3.1). Inspired by pentapeptide Cilengitide's drug development reports in clinical trials, we proceeded for a Euclidean distance calculation between the specific chromophoric points (CZ atom of Arg and CG atom of Asp) in the designed conformers. The structure of Cilengitide has a distance separation of 13.98 Å between CZ of Arg and CG of Asp. We also performed similar calculations for all basin combinations of RGD tri-peptides. The distance calculation data obtained from exhaustive modeling were pruned based on CZ (Arg) to CG (Asp) distance (Annexure Table 1). We observed that the distance in the

range of 13 Å, could be realized by substitution of Glycine (G) with Pro or Val (Figure 3.1 C&D).

This conceptual basin fixation of prominent motifs of THPs led to the design of seven new tumor homing peptides (RG102 to RG108) with heterochiral sequences (Series-1). Molecule RG101 is an already reported tumor homing peptide (*91, 92*), which we considered as a positive control. Further, the peptide designs were extended to Series-2 (chapter-5) and Series-3 (chapter-6) to improve the penetration ability of peptides in tumor vasculatures after homing. The theoretical assumptions we propose are validated through a series of experimental approaches, as discussed in the succeeding chapters.

Translational Value of Thesis
The objectives of the thesis are inclined to develop a complete tumor targeting peptide-based system capable of penetrating and delivering a drug in the tumor vasculature. The presented work is designed keeping in view the translational perspective of the defined problems.

4

Geometry Encoded Functional Programming of Drug Delivery Vehicles

Poly-peptide molecules have shown promising applications in drug delivery and tumor targeting. A series of tumor homing peptides were designed by exhaustively sampling low energy geometrical basins of amino acids at specific sites of a peptide molecule to induce a conformational lock. This peptide library was pruned to a limited set of eight mol1ecules, employing electrostatic interactions, and molecular modeling. These design optimized peptides were synthesized and tested on various cell lines, including breast cancer (MDA-MB-231), cervical cancer (HeLa), osteosarcoma (U2-OS) and non-cancerous mammary epithelial cells (MCF-10A) using confocal microscopy and flow cytometry. Flow cytometry data revealed that peptides show differential uptake in cancerous MDA-MB-231, HeLa, U2-OS, and non-cancerous MCF-10A cells. Confocal imaging verified their ability to penetrate even in 3D tumorospheres of MDA-MB-231 cells. Further, experiments of mitochondrial membrane potential depolarization and Caspase-3 activation confirmed that their cytotoxic effects are by apoptosis. Fluorescence imaging with clinical samples of human origin has further confirmed that the in vitro studies are qualitatively identical and quantitatively comparable in their ability to recognize tumor cells selectively. Overall, we present a roadmap for the functional programming of peptide-based homing and penetrating molecules that can perform selective tumor targeting.

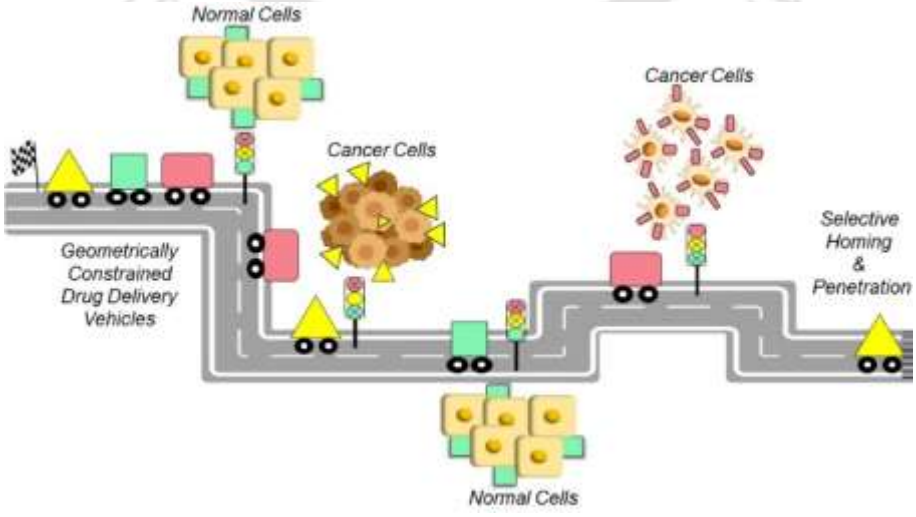

4.1 INTRODUCTION

The side effects of chemotherapy have paved the way for the development of targeted therapies for cancer treatment (*93, 94*). Tumor homing peptides (THPs) have emerged as promising tools for cancer theranostics in recent years (*7, 95, 96*). These tumor homing peptides are resourceful biomolecules that have been employed to engineer peptide-based systems for targeted drug delivery in various cancer types (*97-100*). Peptide-based therapeutics, including cell penetrating peptides, tumor homing peptides, and anti-cancer peptides, are favored for drug delivery due to their lesser side effects, predictable metabolism, and biocompatibility (*87, 101-103*). Receptor-mediated interaction of THPs favors high specificity and low cross-reactivity in recognition of cancer cells due to the presence of frequently occurring peptidic motifs like RGD, NGR, etc. These RGD (Arg-Gly-Asp) and NGR (Asn-Gly-Arg) tripeptides have been used for targeting tumors and tumor-associated vasculatures by targeting integrin $\alpha_v\beta_3/\alpha_v\beta_5$ and Aminopeptidase N (CD13) receptors, respectively, which are overexpressed in cancerous cells.

The origin of RGD story dates back to 1968 when Erkki Ruoslahti got the notion for the existence of "area code" at the cellular and molecular level, and investigations for the next fifteen years resulted in the remarkable discovery of RGD tripeptide (*104, 105*). Since then, this peptide has got significant recognition in terms of being important for cellular attachment and recognition in anomalies such as arthritis, osteoporosis, and cancer metastasis (*106-108*). RGD derivatives have been used for targeting tumor-associated vasculature as they enhance penetration of delivery systems in tumors (*109, 110*). This augments the therapeutic efficacy of RGD based drugs by regulating intratumoral distribution (*111, 112*). A series of various permutations in the sequence followed then. Interestingly, Ruoslahti et al., showed that the KA/aE sequence similar to RGD sequence in terms of charge disposition does not support cell attachment, reflecting the specific role of RGD sequence in cell adhesion (*104*).

However, it is reported that few amino acids are compatible with RGD function, as evidenced by the presence of KGD, RYD, and RHD motifs in integrin binding sites of different proteins (*113-115*). Approaches of synthetic chemistry involving both peptide-based and non-peptide based RGD mimetics have created libraries of small molecules similar to RGD. The basic principles of conformational biasing through turn-inducers, cyclization, rigid cores, etc. have been adopted to explore RGD mimetics (*116*). As a general rule, the distance of 12 C-C bonds

between C-terminal carboxylic acid and N-terminal guanidine group is considered optimal for the generation of $\alpha_v\beta_3$ antagonists (*117*). However, studies have been reported where minimizing this distance also enhanced selectivity for $\alpha_v\beta_3$ integrins (*116, 118-120*). In addition to this, the β-turn or γ-turn conformations centered on Glycine favors bioactive conformation (*116, 121, 122*). Gentilucci et al., have used the β-turn mimetic approach by introducing D-Proline in RGD tripeptide (*117*). Similarly, Royo et al., have used the rigid scaffold approach for synthesizing constrained RGD ligands by involving diketopiperazine (DKP) and hydantoin structures (*123*). Various small molecules like Cilengitide have been therapeutically explored as integrin antagonists through structure-based drug design (*14*). In an approach to construct a small library of cyclic pentapeptide by introducing bicyclic lactams, a new compound ST1646 showed high affinity towards $\alpha_v\beta_3$ and $\alpha_v\beta_5$ integrins (*124*). Similarly, non-peptide RGD mimetics were achieved through structures like diketopiperazine, 3-aminophenyl piperazine, hydantoin, tetrahydroazoninone, phenylbiguanide, biphenylalanine urea, etc. (*123-125*). The principles of introducing conformational constraints through turns are known to create bioactive peptides (*126, 127*).

Given these remarkable advancements, only a few THPs (Cilengitide, NGR-hTNFα, and iRGD peptide) have progressed to the advanced stages of clinical trials for cancer indications so far, though none of them have reached to the market yet. The gaps associated in their developments lies in the partial understanding of receptor conformations, difference in mouse and human responses, inadequate target validation models, and unpredictable human disease conditions (*8*). In light of these facts, our investigation pivots around the understanding that the development of RGD/NGR based mimetics lies in the correct spatial orientation or topology of flanking residues around a central core (*125*). With this perspective, we designed a library of RGD and NGR/QGR mimics, employing an 'informed walk' across Ramachandran geometrical space, and experimentally verified them using standard protocols. The designed peptides are conjugated with fluorophore and methotrexate drug at N-terminus using solid phase peptide synthesis. Methotrexate was chosen for coupling because of the following reasons:

1) Methotrexate drug has free carboxylic group which help in conjugation to the peptides towards the end of synthesis through simple amide bonding.

2) It is a broad-spectrum drug molecule which acts by blocking dihydro folate reductase receptors present in many cancer cell types.

3) We have used MTX-resistant cell line (MDA-MB-231) in our study. Taking MTX, helped us in evaluating the delivery potential of peptides over MTX free drug in MTX-resistant cells.

4.2. MATERIALS AND METHODS

The methods used for modeling and validation of designed peptides by various experimental approaches are mentioned in this section. In this chapter, a total of eight peptides (RG101-RG108) were designed and verified by the methods mentioned here.

4.2.1. Molecular Modeling. For peptide designing and modeling studies, various tools were used. In brief, they are described in Table 4.1.

Table 4.1. List of Computational Tools used in the current study

S. No.	Tool	Purpose
1	Ribosome / pdb make	Generates pdb files of input peptide sequences with defined phi (ϕ), psi (Ψ), and/or chi (χ) angles.
2	PROSS	Gives dihedral angles as an output of any input pdb file
3	Py-Mol, version 1.7.2	Visualizes and models protein or peptides.
4	Swiss PDB Viewer (spdbv), version 4.1	Visualizes and models protein or peptides.
5	Delphi	Calculates Electrostatic Potential by Poisson Boltzmann Equation

4.2.2. Electrostatic Profiling of Peptides. The peptide structures were constructed using the Ribosome software of George D Rose's lab. Using Delphi software (*128*), electrostatic potentials were mapped for every amino acid side chain in a peptide structure by solving Finite Difference Poisson Boltzmann equation. The obtained electrostatic profile of peptides represents a particular fingerprint for the designed peptide series.

4.2.3. Peptide Synthesis and Characterization. The designed peptides were synthesized by solid-phase peptide synthesis (SPPS) using Fmoc chemistry on HMPA resin (Figure 4.1). For SPPS, required amino acids, resin, activators, and solvents were purchased from Merck and

Sigma-Aldrich with 99% purity. Couplings were done on a solid support HMPA resin with three-fold excess of amino acids and activators after Fmoc deprotection by 20% piperidine.

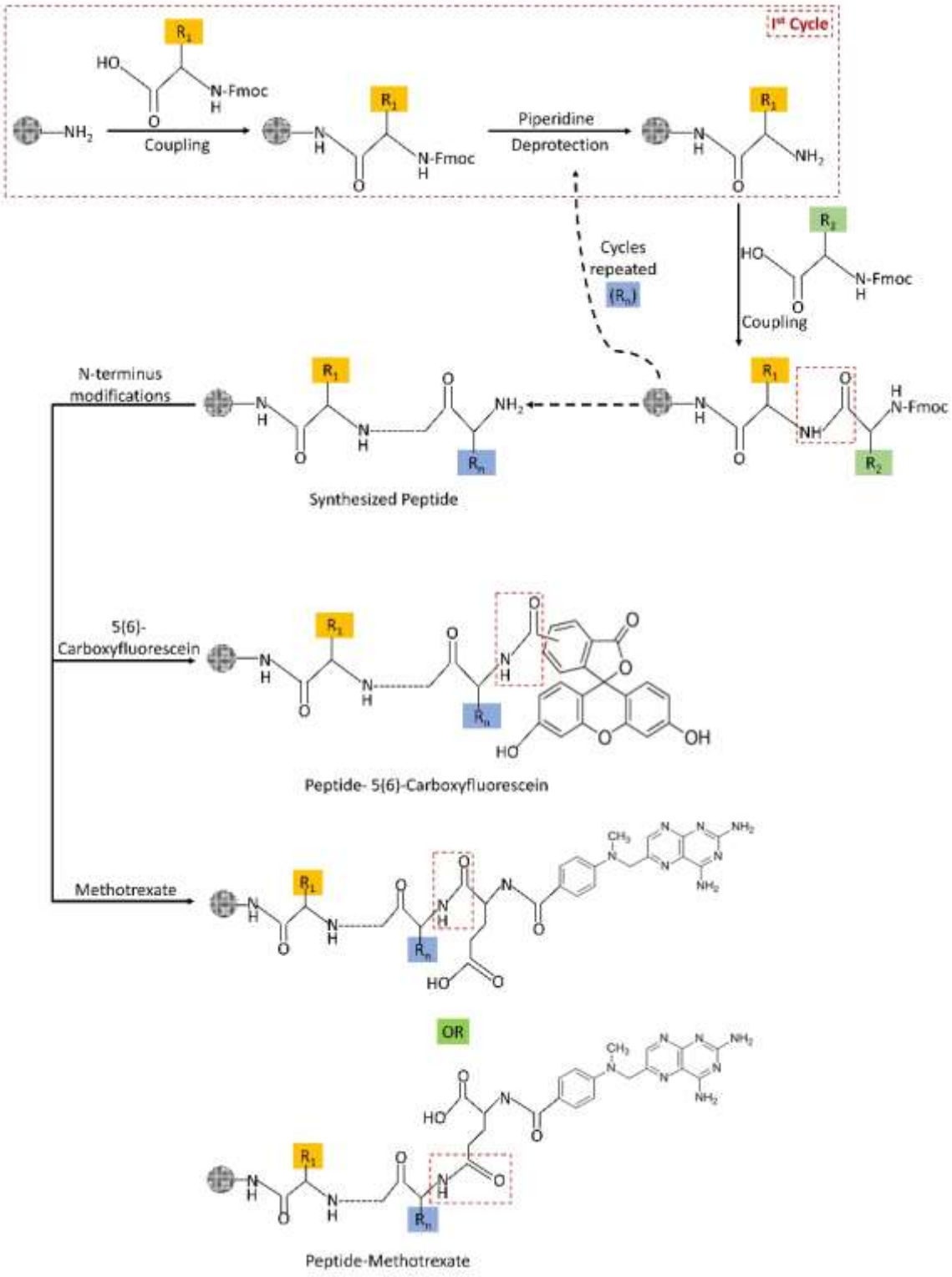

Figure 4.1. Solid Phase Peptide Synthesis. *Scheme to represent amide bond formation in solid-phase peptide synthesis peptide synthesis (Fmoc Chemistry) and details of N-terminal modification for the cargo attachment.*

After completion of synthesis, peptides were conjugated with 5(6)-Carboxyfluorescein (CF) and Methotrexate (MTX) at N-terminus and deprotected using the deprotection cocktail composed of m-cresol/ thioanisol/ ethanedithiol/ trifluoroacetic acid as 2:2:1:20 (v/v/v/v). CF attachment is followed by two piperidine washes for ten and forty minutes, respectively, with intermittent DMF washes, until neutral pH was achieved (*129*). The crude peptides were precipitated with cold diethyl ether and subsequently characterized by RP-HPLC (Shimadzu, LC 20AD) and MALDI-TOF MS (Bruker, Autoflex Speed). The gradient run in HPLC was performed by running a gradient of 10% Acetonitrile in milli-Q water to 100% Acetonitrile with a flow rate of 0.5 mL/min using a C-18 column in reverse phase. HPLC peaks were collected and subjected to Mass Spectrometry analysis. α-cyano-4-hydroxycinnamic acid (HCCA) was used as a matrix for sample embedding. After mass characterization, the peptides were purified by semi-preparative RP-HPLC and lyophilized.

4.2.4. Circular Dichroism (CD) Spectroscopy. The purified peptides were dissolved in water to obtain 10 µM concentration for secondary structure characterization by CD Spectroscopy. Far-UV CD spectra were recorded in a quartz cuvette having a 1 mm path length by using Jasco J-1500 spectropolarimeter with a scan rate of 100 nm/min. For each spectrum, five scans were averaged, and the observed ellipticity is converted to mean residual ellipticity as described previously (*130*).

4.2.5. Fourier Transform Infrared (FTIR) Spectroscopy. The same peptide stocks of 10 µM were used for recording the FTIR spectra in attenuated total reflection (ATR) mode using Shimadzu IR Affinity-1S Fourier transform infrared spectrophotometer equipped with a diamond ATR crystal. Each spectrum is an average of 64 scans at a resolution of 4 cm^{-1}.

4.2.6. Cell Culture. MDA-MB-231 breast cancer cells (purchased from NCI, USA), HeLa cervical cancer cells (procured from ATCC) and U2-OS osteosarcoma cells (procured from ATCC) were cultured in Dulbecco's Modified Eagle Media (DMEM) supplemented with 10% fetal bovine serum (FBS), 1% antibiotic cocktail (10,000 units/mL penicillin and 10 mg/mL streptomycin and 25 µg/mL Amphotericin B) and $NaHCO_3$ salt. Non-cancerous mammary epithelial cells MCF-10A (procured from Sigma) were cultured in Mammary Epithelial Cell Growth Medium (MEGM, Lonza, USA) supplemented with BPE, hEGF, insulin, hydrocortisone, and GA-1000. The cells were grown as sub-confluent monolayers in T-25 cell

culture flasks at 37°C under the water-saturated environment with 5% CO_2. Mammalian expression vector, Lamp1-RFP, was procured from Addgene, USA (Plasmid #1817) to transfect U2-OS cells and FRET caspase 3 sensor expression vector ECFP-VENUS SCAT 3 was a gift from Dr. Masayuki Miura, RIKEN Brain Science Institute, Japan.

4.2.7. Flow cytometry for comparative peptide uptake. For quantitative analysis of differential binding, MDA-MB-231, HeLa, U2-OS, and MCF-10A cells were seeded in 24-well plates at a density of 30,000 cells per well. After overnight incubation, the cells were washed with PBS and treated with 10 μM of CF-labelled peptides in serum-free DMEM for 4 h at 37 °C. Cells with no treatment were taken as a negative control in the experiment. After that, cells were washed thrice with PBS and harvested by trypsinization, followed by repeated washing to ensure the removal of unbound peptides. Finally, cell pellets were suspended in 400 μL of PBS and kept on ice until analysis. The fluorescence intensity was detected by flow cytometer (FACS Aria III, BD Biosciences).

4.2.8. Fluorescence imaging to confirm cellular uptake. MDA-MB-231, HeLa, U2-OS, and MCF-10A cells were seeded in 96 well glass bottom plates. After overnight incubation, the cells were washed with PBS and treated with CF-labelled peptides (RG101-RG108) in serum-free DMEM. After incubation for 4 h, the cells were washed thrice with PBS and stained with Hoechst 33342 (1 μg/mL) for 5 min to stain the nucleus of live cells. Finally, the excess stain was rewashed, and phenol-red and serum-free DMEM was added to each well for fluorescent imaging by Confocal Laser Scanning Microscope (NikonA1R).

4.2.9. TMRM Cytotoxicity Assay. For Tetramethyl rhodamine methyl ester (TMRM) cytotoxicity assay, MDA-MB-231 and MCF-10A cells were seeded in 96-well glass-bottom plates. After 24 h, the cells were washed with PBS and stained with Hoechst 33342 (1 μg/mL) for 5 min, followed by 100 nM TMRM treatment for 10 min at 37°C. Cells were rewashed to remove the unbound dye and replenished with peptide treatment in 20 nM TMRM phenol-red and serum-free DMEM at various concentrations for imaging mitochondrial membrane potential (MMP) loss. The fluorescent images were taken in blue and red channels by Pathway Bio-imager 435 (BD Biosciences, San Jose, CA, USA) after 48 h using a dry x20 objective with NA 0.7. After the acquisition, the images were analyzed for chromatin condensation and TMRM loss.

4.2.10. Cell death by apoptosis. Peptide's cytotoxicity through the apoptotic pathway is confirmed by Caspase-3 activation. MDA-MB-231 cells with stable expression of FRET-based caspase sensor (DEVD) (Figure 4.2) were seeded in 96-well glass-bottom plates. After 24 h, the cells were washed with PBS, followed by peptide treatment in phenol-red and serum-free DMEM at various concentrations. Ratiometric imaging of CFP/YFP FRET was performed after 48 h through high-throughput Pathway Bio-imager 435 (BD Biosciences, San Jose, CA, USA) in different channels. The images were acquired as 2x2 montages, which later stitched as a single image for each well and subjected to generate quantitative data using the ratiometric scale color code, which ranges from 0 to 2.

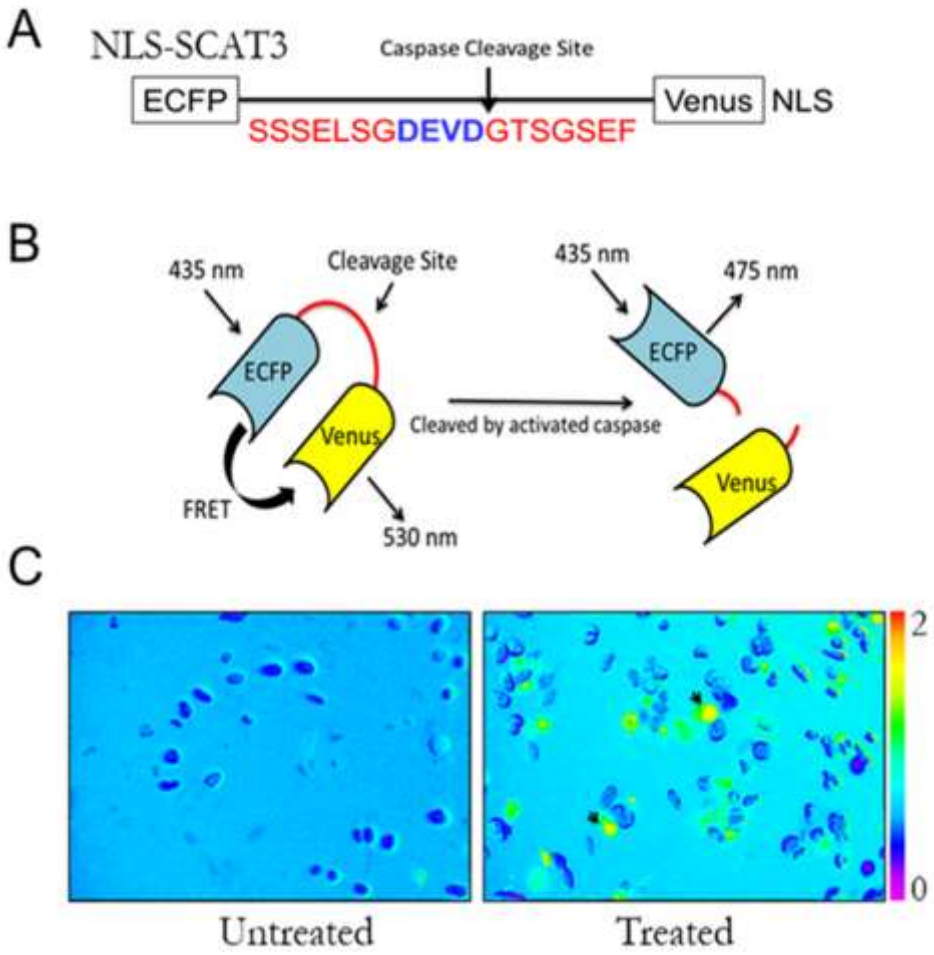

Figure 4.2. Caspase Sensor System. *(A) Schematic representation of the Linker sequence of a FRET-based sensor (NLS-SCAT3). (B, C) SCAT probe and representative images of NLS-SCAT3 transfected MDA-MB-231 cells with and without treatment depicting the change in CFP/YFP ratio from blue to green-yellow on the ratio scale. This change in fluorescence ratio corresponds to the activation of Caspase-3.*

4.2.11. Hemolytic activity. The hemotoxicity of peptides and their MTX conjugates was assayed by using fresh human blood samples collected in a vacutainer blood collection tube. The collected blood sample was centrifuged at 800 g for 5 min and washed thrice with PBS to obtain the erythrocytes pellet. The pellet was resuspended to obtain 10% hematocrit which subsequently, was incubated with an equal volume of peptides of 200 µM concentration for 2 h at 37°C in shaking incubator. After incubation, the samples were centrifuged at 800 g for 5 min, and the supernatant was collected. The absorbance of the supernatant was recorded at 540 nm to quantify heme release after RBC lysis. The data were normalized with the value obtained from complete lysis, i.e., with 0.5 % of Triton X-100.

4.2.12. Biocompatibility of peptides. CF-tagged peptides were incubated with FBS in equal volume for 1 h at 37°C. MDA-MB-231, HeLa, U2-OS, and MCF-10A cells were seeded in 24-well plates at a density of 30,000 cells per well for overnight. Then, the cells were washed and treated with serum pre-treated and untreated peptides for 4 h at 37°C. Post-treatment, the cells were rewashed and harvested to quantify the uptake in both conditions using flow cytometry, as described previously in section 4.2.7.

4.2.13. Comparative Histopathological Staining of peptides. Patient-derived tissues, including cancerous and non-cancerous types, were collected from Department of Pathology, Dr. B. Borooah Cancer Institute, a unit of Tata Memorial Center, Mumbai, India. The formalin-fixed and paraffin-embedded tissues were sliced into 5 µm sections and subjected to sequential steps of deparaffinization, rehydration, antigen retrieval, blocking, and peptide staining. The obtained sections were also stained for hematoxylin-eosin (H&E) to evaluate tumor morphology and confirmation of tumor malignancy by pathologists. The tissue slices were incubated with CF-labelled peptides (RG101-RG108) for 6 h at 37°C. After washing with PBS, the slides were mounted with DAPI Fluormount G, cover glass, and subjected for fluorescence imaging. The green channel from the acquired images was extracted and used for the quantification of the peptide signal. This work has been carried out through the approval of the patients as well as Institute Human Ethics Committee.

4.2.14. Statistical analysis. All experiments were performed with a minimum sample size of three per experiment. Results are presented as mean ± SD or SEM of two or three independent experiments, depending on the experiment type. For comparison between two groups, Two-

tailed Student's t-test with P-value: $P < 0.05$ and for comparison between more than three groups One-Way ANOVA with the following P values: **** $P < 0.0001$, *** P=0.0002, **P=0.002, * P=0.03 were used as the cut-off for statistical significance.

4.3. RESULTS AND DISCUSSION

4.3.1. Geometry encoded functional programming

The library of eight peptides in Series-1 represents eight different conformational locks of RGD and QGR motifs. Molecule RG101 is an already reported tumor homing peptide (*91, 92*), which we used as the positive control. The other seven heterochiral sequences are coded as RG102 to RG107 (Figure 4.3). This study describes the possibility of an 'informed walk' across Ramachandran geometrical space in search of conformational lockers. It can, in principle, be the first attempt to make tumor homing 'programmable' by permuting and fixing the topology of RGD and QGR motifs. It provides an opportunity to monitor the effect of the designed conformation, and the resultant electrostatic fingerprint of 'Gly substituted residues' on the activity of THPs, thus giving access to the topological control.

The variants of the designed THP library are zwitterionic with RGD/NGR motifs. Besides this, hydrophobic nature of other residues likes alanine, phenylalanine, and proline in the sequence may facilitate their penetration through cell membrane after homing. The electrostatic fingerprints generated as a result of Ramachandran basin engineering has been validated by performing potential mapping through Finite Difference Poisson Boltzmann (FDPB) equation using Delphi software (*128*) (Figure 4.4).

The obtained variations in the electrostatic distribution of the designed peptides are important in modulating the topology combined with composition induced functional changes in the activity of peptides. Further, the effect of the desired substitutions was investigated by calculating the geometrical parameters like distance and angle between the terminal residues of the RXD/QXD motifs (Figure 4.3 C).

4.3.2. Peptide Synthesis and Characterization

The designed peptides were synthesized using standard protocols of solid-phase peptide synthesis (Fmoc chemistry) and characterized by reverse-phase High-Performance Liquid Chromatography (RP-HPLC) and MALDI-TOF mass spectrometry (MALDI-TOF MS).

Peptides were conjugated with 5(6)-carboxyfluorescein (CF) and methotrexate (MTX) for uptake and cytotoxicity estimation. HPLC, combined with mass spectrometric analysis, confirmed the purity of the designed peptides and their conjugates (Table 4.2).

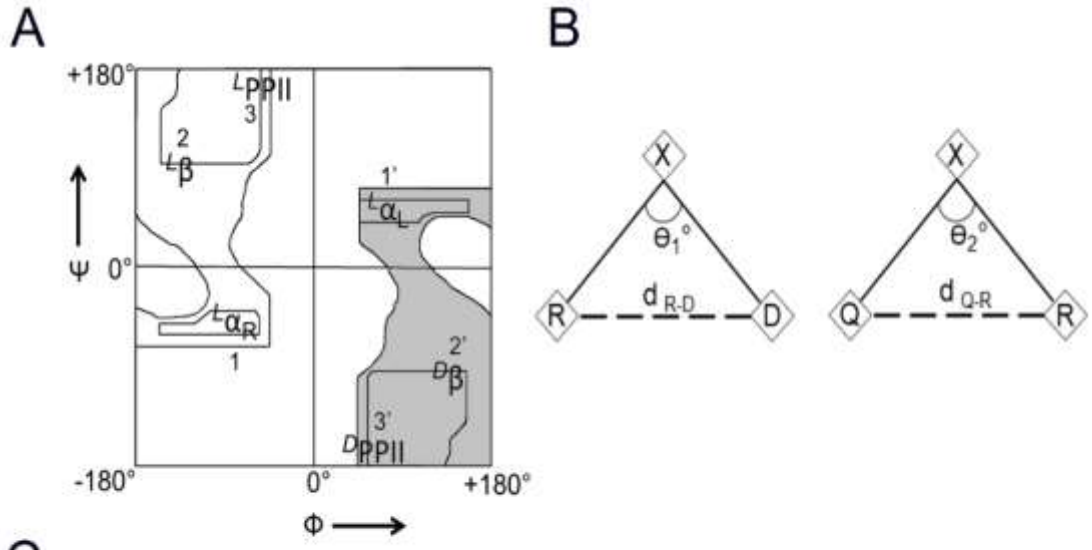

C

Peptide codes	Amino acid sequence	Basins Locked	d_{R-D}	d_{Q-R}	RXD (Θ_1°)	QXR (Θ_2°)
RG101	RGDPAYQGRFL	-	12.0	15.0	139.3	145.4
RG102	RvDPAYQvRFL	(2', 2')	12.4	15.1	145.0	150.3
RG103	rGdpaygGrfl	-	8.6	7.9	100.3	88.4
RG104	RpDPAYQpRFL	(3', 3')	11.5	14.4	132.0	137.5
RG105	rBdpaygBrfl	(1, 1)	12.3	12.8	94.2	93.1
RG106	RaDPAYQaRFL	(1', 1')	12.4	15.1	145.0	150.3
RG107	RpDPAYQvRFL	(3', 2')	11.5	15.1	132.0	150.2
RG108	RvDPAYQpRFL	(2', 3')	12.4	14.4	145.0	137.6

Figure 4.3. Conceptual illustration of the peptide designs. *(A) The sterically fixed regions of the Ramachandran plot for L- and D- amino acids (grey). (B) Geometrical parameters (Θ, d) of RXD/QXR motifs considered for systemic modeling. In the given figure, 'Θ$_1$' represents angles between CB of Arg and CB of Asp in RXD motif, and 'Θ$_2$' represents angles between CB of Gln and CB of Arg in QXR motif. Distance measurement 'd$_{R-D}$' represents the Euclidean distance between CZ of Arg and CG of Asp, and 'd$_{Q-R}$' represents the Euclidean distance between CD of Gln and CZ of Arg. CB, CG, CD, and CZ denotes the C$_\beta$, C$_\gamma$, C$_\delta$, and C$_\zeta$ atoms of the amino acid, respectively. (C) Synthesized peptide library with peptide codes, amino acid sequences, locked basin combinations, and evaluated geometrical parameters from their coordinate files.*

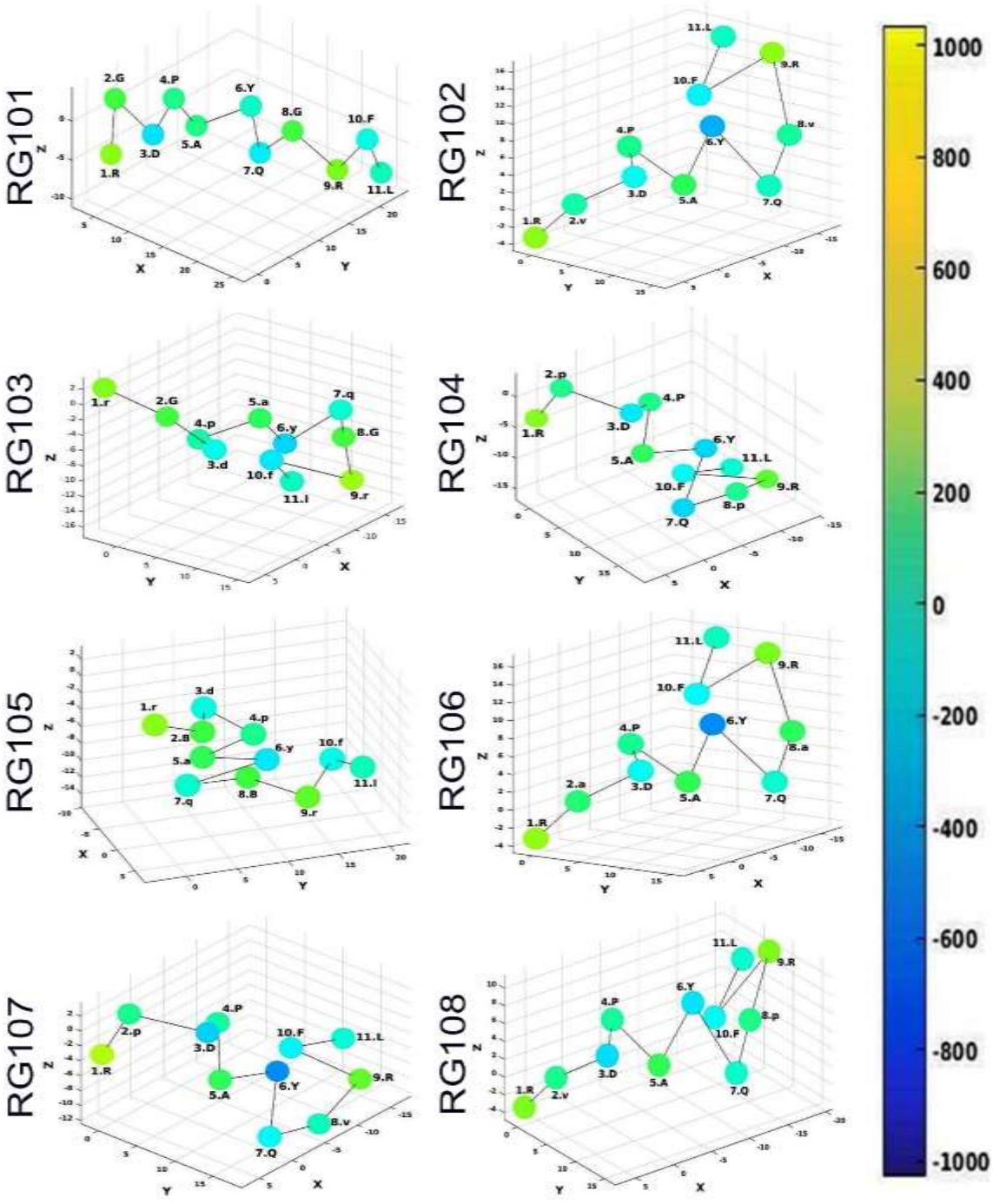

Figure 4.4. Electrostatic Fingerprinting of the designed peptide library. *The mapped potential values suggest design induced variations in the spatial electrostatics of the peptides. Delphi software is used for electrostatic potential calculations.*

Table 4.2. Characterization of Peptide Mass

S. No.	Peptide Code	Expected Molecular Mass			Observed Molecular Mass		
		UN	5(6) CF	MTX	UN	5 (6) CF	MTX
1	RG101	1278.6	1636.9	1714.6	1280.06	1638.42	1716.34
2	RG102	1362.7	1721	1799	1364.9	1723.11	1801.8
3	RG103	1278.6	1636.9	1714.6	1280.87	1638.17	1716.56
4	RG104	1358.6	1717	1794.6	1361.08	1719.31	1796.81
5	RG105	1335.8	1694.1	1771.8	1336.95	1694.49	1772.61
6	RG106	1306.6	1664.9	1742.6	1308.90	1666.46	1744.34
7	RG107	1361	1719	1797	1362.62	1720.25	1798.4
8	RG108	1361	1719	1797	1362.95	1721.37	1799.87

Note: *The designed peptide sequences and their conjugates were characterized by MALDI-MS post-synthesis. The expected and observed molecular masses of the synthesized peptides with and without conjugates are mentioned herein Daltons (Da). UN represents peptide with free N-terminus (unlabeled), 5(6)-CF represents peptide conjugates with 5(6) carboxyfluorescein, and MTX shows peptide conjugates with methotrexate.*

4.3.3. Secondary Structure Characterization

Topological variations manifested through secondary structural changes are verified by Circular dichroism (CD) spectroscopy, and Fourier transform infrared (FTIR) spectroscopy. The substitution of guest residues in the parent sequence resulted in corresponding changes in CD spectral characteristics. CD spectral analysis confirms that the secondary structure characteristics of each sequence are distinctly different as envisaged in the design. Since the sequences are heterochiral in nature, they do not show any secondary structure peak signatures, typical of poly L sequences. However, the peak signatures (Figure 4.5 A) broadly resemble extended conformation, which was also expected. The results from FTIR studies further supports CD data, with a major peak obtained at 1654 cm^{-1} (*131*) (Figure 4.5 B).

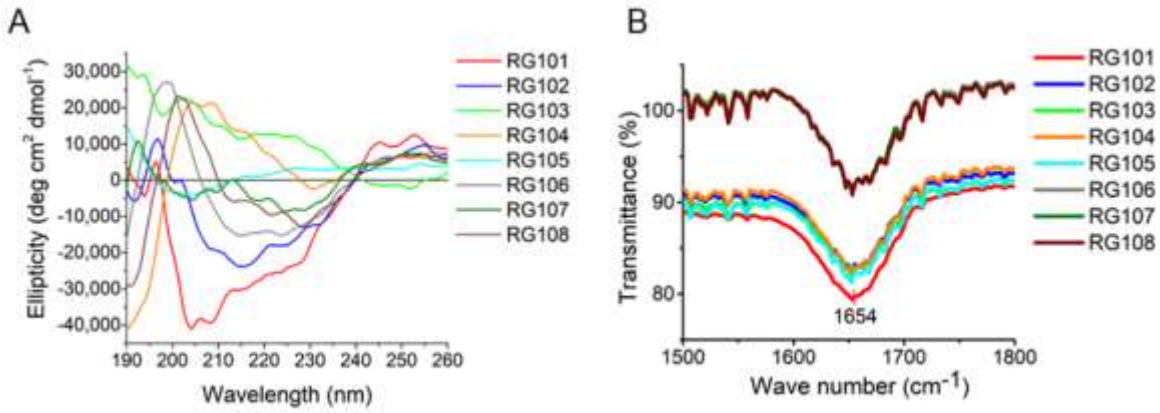

Figure 4.5. Peptide Structure Characterization. *The design induced structural variations in secondary structures of peptides by (A) CD Spectroscopy and (B) FTIR spectroscopy.*

4.3.4. Cellular uptake of peptides by flow cytometry

Tumor homing peptides (THPs), are molecules designed to show significantly high affinity to tumor cells and tumor-associated vasculatures. To confirm the differential cellular uptake of the designed peptides; breast cancer (MDA-MB-231), cervical cancer (HeLa), osteosarcoma (U2-OS cells transfected with lysosome-associated membrane protein fused with a red fluorescent protein (LAMP-RFP)) and non-cancerous mammary epithelial cells (MCF-10A) were treated with 10 μM of purified CF-labelled peptides in serum-free media (Dulbecco's Modified Eagle Media (DMEM)) for four hours and analyzed using flow cytometry. The obtained results suggest that the designed molecules have differential uptake towards different cell types under identical experimental conditions. All peptides showed more affinity to MDA-MB-231 and U2-OS cells in varying degrees, compared to HeLa and MCF-10A cells (Figure 4.6). The difference in peptide binding is not just between cancerous and non-cancerous cells, but also between cancer cell types as well (MDA-MB-231, U2-OS, HeLa). This was expected because sequence selection in RXD and QXR motifs of THPs, was primarily aimed at presenting different topological and electrostatic signatures while interacting with the cell membrane. This also suggests cell-specific variations on surface electrostatics resulting from the difference in topology and constitution of the plasma membrane of different cell types.

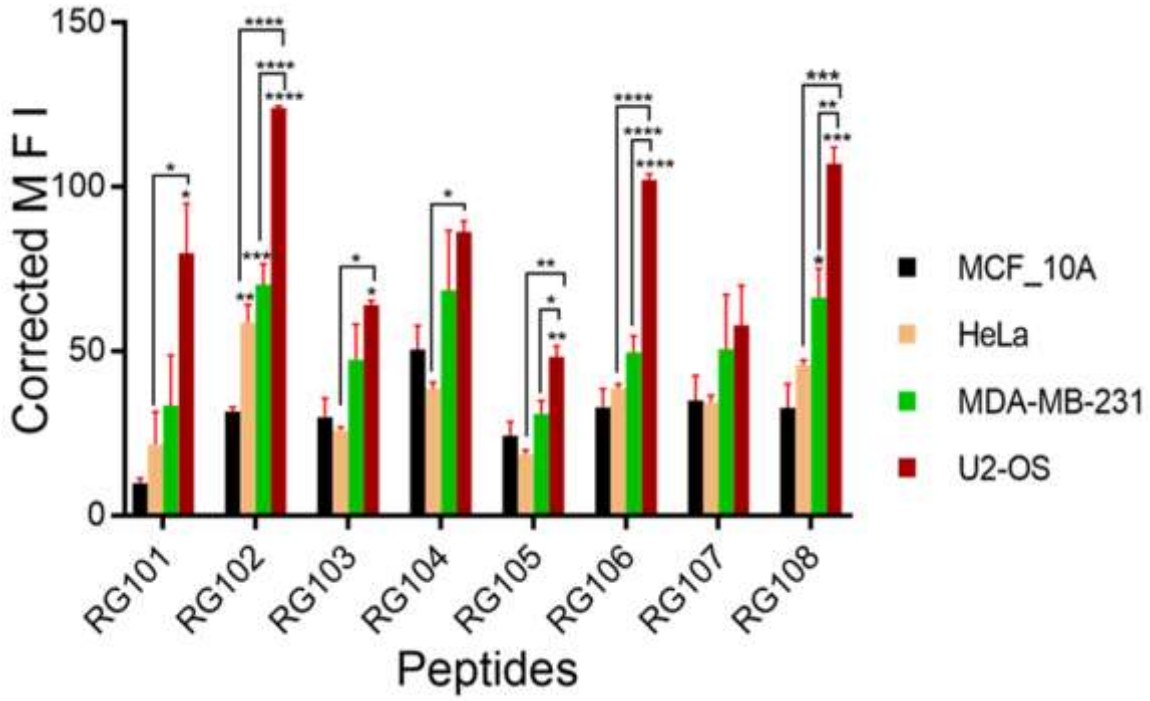

Figure 4.6. Cellular uptake of the designed peptides. *The comparative uptake of peptides is quantified in breast cancer (MDA-MB-231) cells, cervical cancer (HeLa) cells, LAMP-RFP transfected osteosarcoma (U2-OS) cells and mammary epithelial (MCF-10A) cells using flow cytometry. All cells were incubated with 10 µM of CF-tagged peptides (RG101-RG108) in serum-free DMEM for 4 h at 37 °C. Post-treatment cells were washed, harvested, and analyzed through flow cytometry. MFI represents Mean Fluorescence Intensity. Results are presented as mean ± SEM of three independent experiments. P values (**** P < 0.0001, *** P=0.0002, ** P=0.002, * P=0.03) were calculated using One-Way ANOVA.*

4.3.5. Cellular uptake of peptides by confocal imaging

The intracellular uptake of the designed peptides was further verified using confocal laser scanning microscopy (Figure 4.7 - 4.10). Interestingly, it was observed that the designed peptides get fairly internalized into the cells except for poly-D peptides (RG103 and RG105), which showed weak internalization in all cell types, confirming the topology mediated interactions of peptides with the cell surface. We used osteosarcoma cells (LAMP-RFP transfected U2-OS cells) to confirm the subcellular localization of peptides.

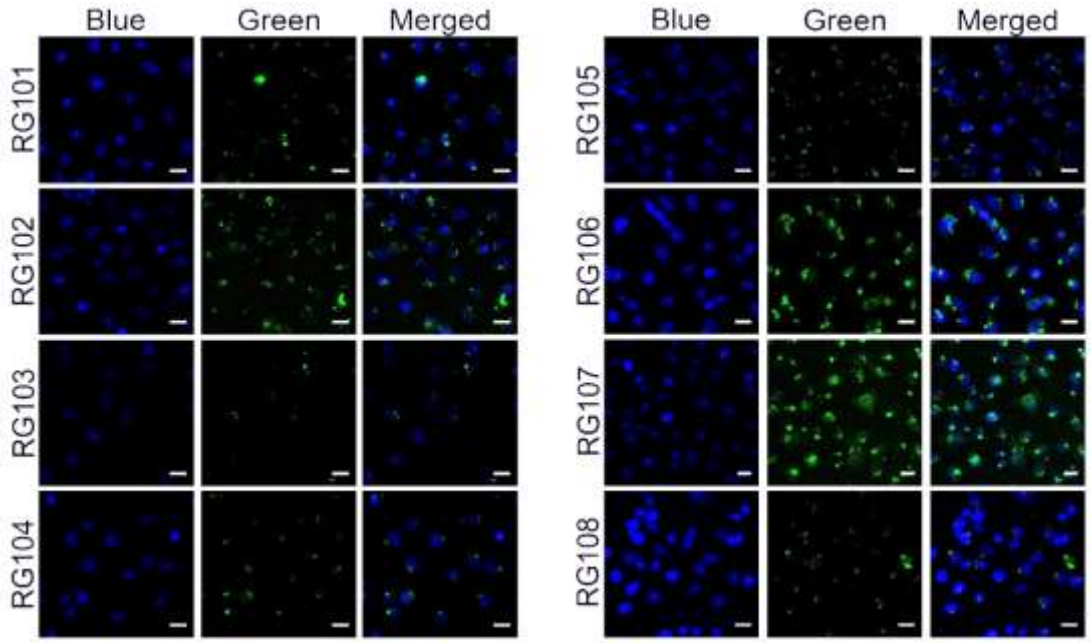

Figure 4.7. Cellular uptake in MDA-MB-231 cells. *The cellular uptake of CF-tagged peptides (RG101-RG108) in breast cancer (MDA-MB-231) cells through confocal laser scanning microscopy. After peptide treatment, nuclei were stained with Hoechst 33342. In this figure, blue represents Hoechst staining, and green shows CF-tagged peptides. Scale bar corresponds to 50 µm.*

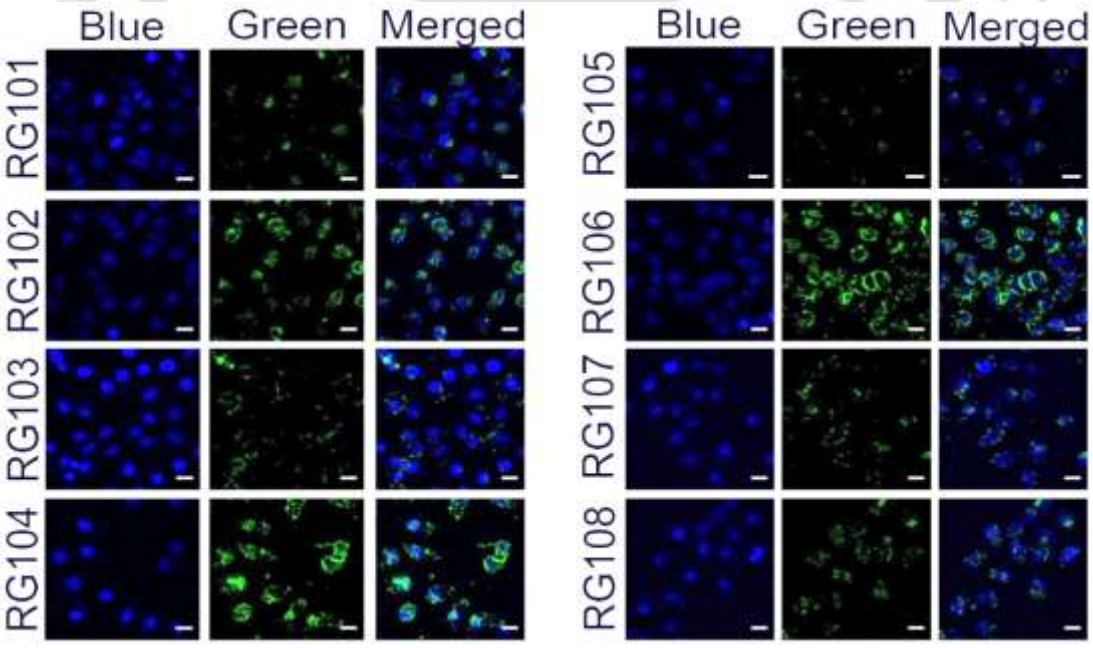

Figure 4.8. Cellular uptake in HeLa cells. *The cellular uptake of CF-tagged peptides (RG101-RG108) in cervical cancer (HeLa) cells using confocal laser scanning microscopy. After peptide treatment, nuclei were stained with Hoechst 33342. In this figure, blue represents Hoechst staining, and green shows CF-tagged peptide. Scale bar corresponds to 20 µm.*

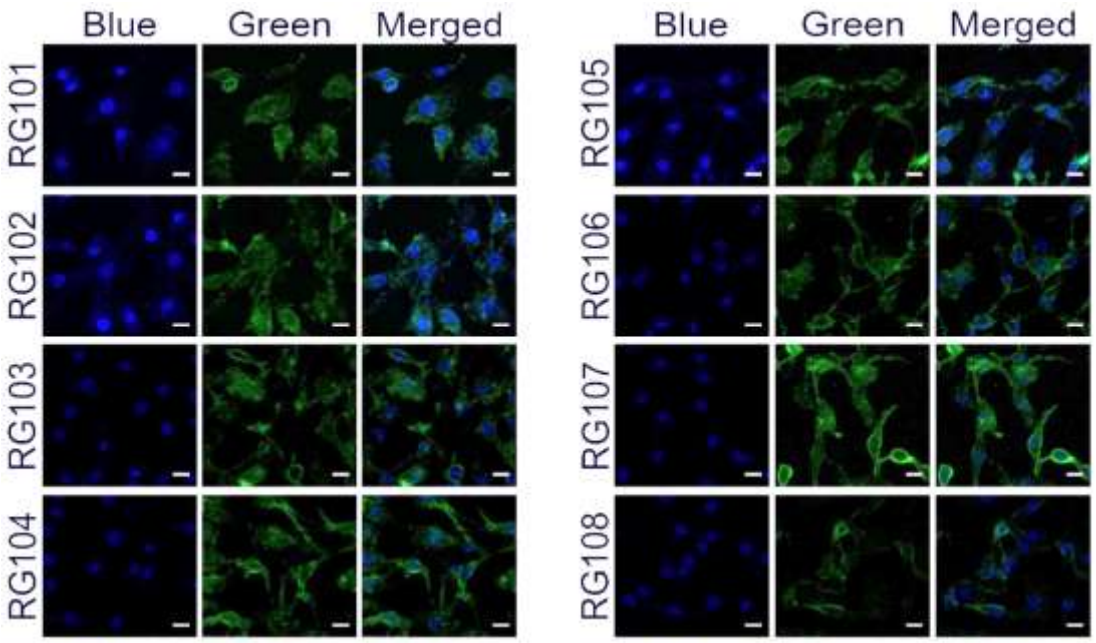

Figure 4.9. Cellular uptake in MCF-10A cells. *The cellular uptake of CF-tagged peptides (RG101-RG108) in mammary epithelial (MCF-10A) cells through confocal laser scanning microscopy. After peptide treatment, nuclei were stained with Hoechst 33342. In this figure, blue represents Hoechst staining, and green shows CF-tagged peptides. Scale bar corresponds to 20 µm.*

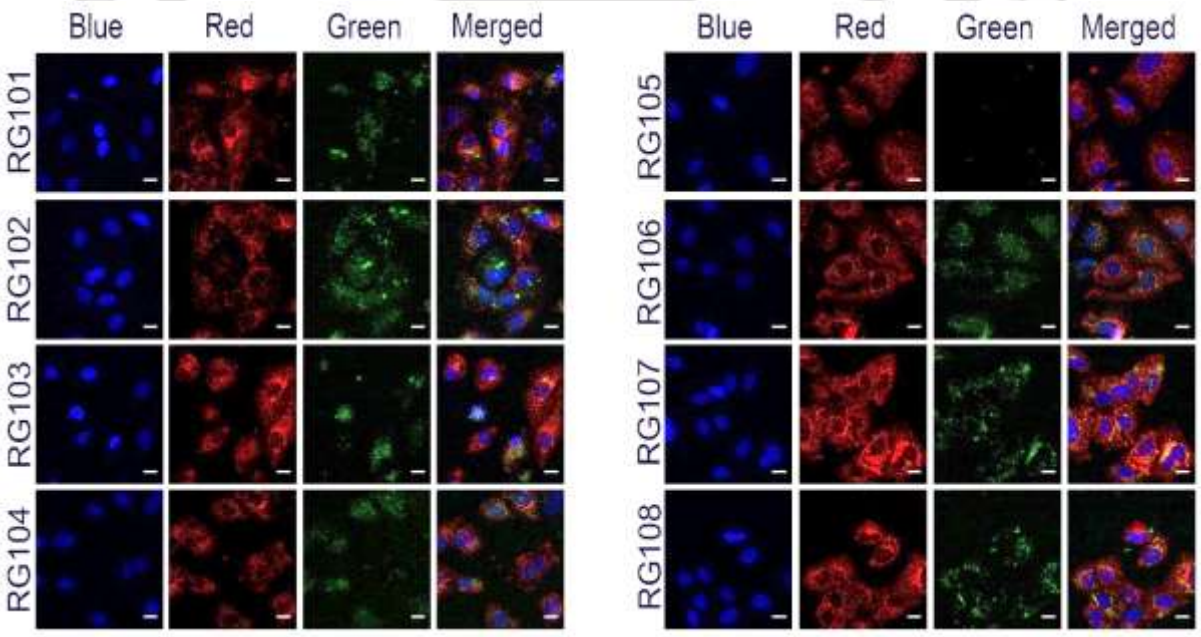

Figure 4.10. Cellular uptake in U2-OS cells. *The cellular uptake of CF-tagged peptides (RG101-RG108) in LAMP-RFP transfected osteosarcoma (U2-OS) cells through confocal microscopy. After peptide treatment, nuclei were stained with Hoechst 33342. In this figure, blue represents Hoechst staining, green shows CF-tagged peptides, and red denotes lysosomes. Scale bar corresponds to 20 µm.*

The fair uptake of RG102, RG104, RG106, RG107, and RG108 peptides can be seen in lysosomes of LAMP-RFP transfected U2-OS cells through the merged images, indicating the internalization of peptides in sub-cellular compartments (Figure 4.10). Although, this subcellular localization of peptides is verified as an additional property of peptides rather than the main focus of the present study.

4.3.6. Cytotoxicity of designed peptides

After cellular binding and penetration, the next desirable feature of an effective THP is the selective killing of cancerous cells either by themselves or by acting as drug delivery vehicles. With this premise, our following investigation is associated with the delivery of a standard drug Methotrexate (MTX) after conjugating it with the designed THPs. The cytotoxicity potential of the designed peptides and their MTX conjugates were evaluated against MTX resistant breast cancer MDA-MB-231 cells (*132*) and mammary epithelial MCF-10A cells at different concentrations using Tetramethylrhodamine methyl ester (TMRM) based assay. TMRM is a potentiometric fluorescent dye which localizes in mitochondria of the living cells in a voltage-dependent manner (*133*). Under abnormal physiological conditions, mitochondrial dysfunction causes depolarization of Ψm which opens the mitochondrial permeability transition pore (PTP) and eventually leads to the leakage of intermembrane proteins like cytochrome c, etc. (*134*). In the present study, the loss of TMRM for depolarization of mitochondrial membrane potential (MMP) and enhanced blue fluorescence for chromatin condensation, both indications of apoptosis, could be observed for the treated cells (Figure 4.11; Annexure Figure 1, 2). From the corresponding data quantification, it is very evident that peptide-MTX conjugates possess significant toxicity as compared to only MTX or peptide under the same conditions (Figure 4.11 C-E). Moreover, it signifies the minimal toxicity in mammary epithelial cells (MCF-10A) up to 50 µM, whereas, at 100 µM concentration, toxicity to MCF-10A indicates the threshold value of drugs required to induce toxicity non-selectively. The amplified toxicity at the other two concentrations (25 µM and 50 µM) against MTX-resistant MDA-MB-231 cancerous cells can be attributed to the increase in bioavailability of MTX through selective targeting and cell penetration of peptide-MTX conjugates.

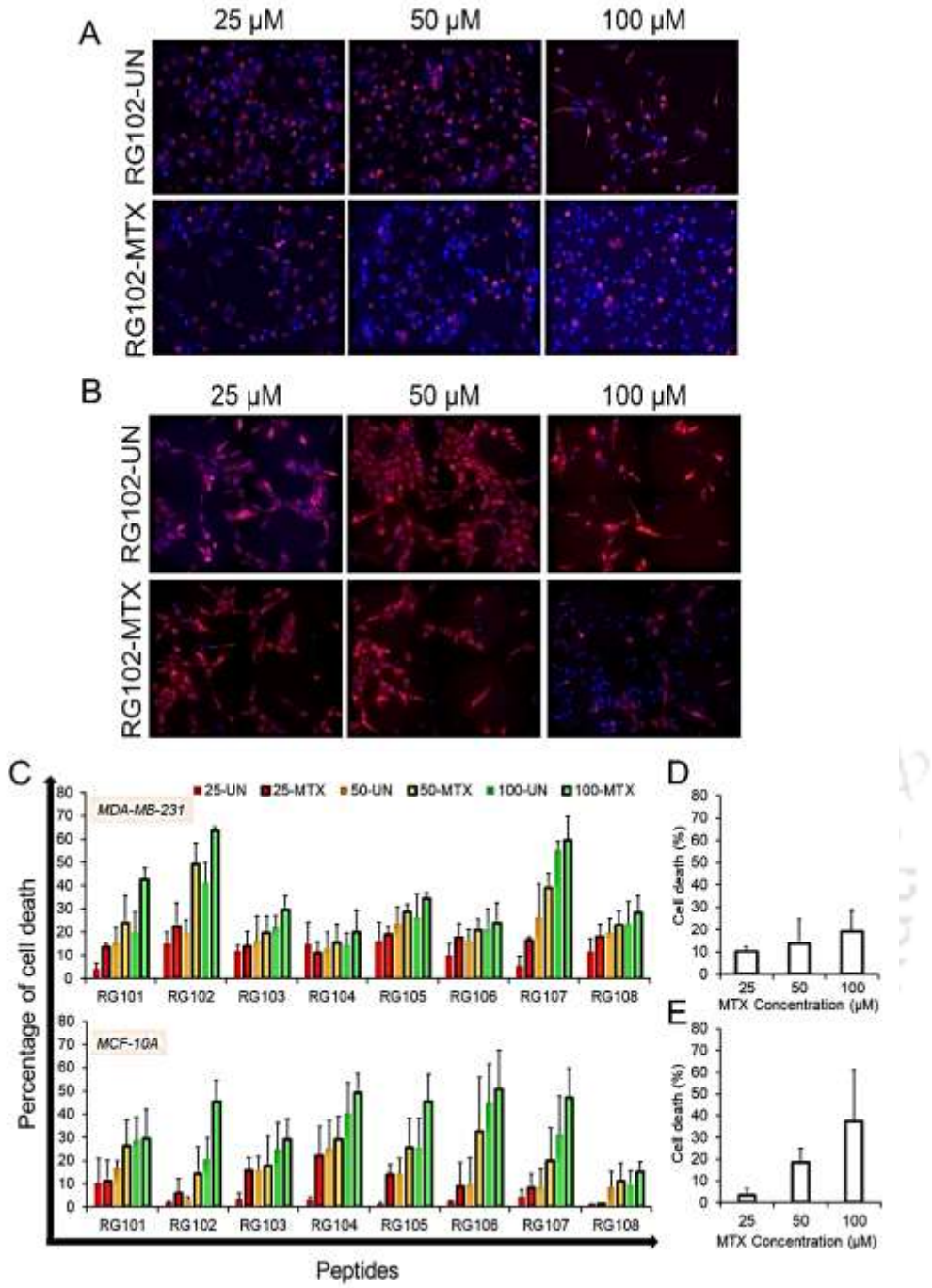

Figure 4.11. Cytotoxicity of the designed peptides using TMRM assay. *MDA-MB-231 and MCF-10A cells were treated with MTX, peptides (UN) and peptide-MTX conjugates (MTX) at 25 µM, 50 µM, and 100 µM concentrations for 48 h at 37°C. The cells with TMRM loss and nuclear condensation were considered undergoing apoptosis and hence, taken for cell death analysis. (A & B) Representative fluorescence image panels of MDA-MB-231 and MCF-10A cells after treatment with RG102 peptide and its MTX conjugates. (C) Quantitative analysis of MDA-MB-231 and MCF-10A cells undergoing cell death by treatment with peptides (RG101-RG108) and their respective MTX conjugates. (D & E) Cytotoxicity of MTX drug alone on MDA-MB-231 and MCF-10A cells under identical experimental conditions (n=4).*

4.3.7. Activation of Caspase-3 by ratiometric fluorescence-based assay

The living cells undergo cell death primarily through necrosis or apoptosis. The apoptotic or programmed cell death is a tightly regulated multistep phenomenon of cell death, unlike necrosis, which is more like traumatic cell death. The cytotoxic drugs which initiate cellular death through apoptosis are preferred as they cause cell death in a series of biochemical processes, including membrane blebbing, cell shrinkage, chromatin condensation, etc. (*135, 136*). In fact, RGD based therapeutics are known to cause apoptotic cellular death (*137*). The results of this experiments, especially the loss of TMRM and chromatin condensation, gave us indications of programmed cell death. However, to confirm apoptosis, we assessed the cytotoxicity of peptides in cells by cell-based fluorescence resonance energy transfer (FRET) ratiometric imaging (*138*). This assay was performed by using MDA-MB-231 cells with stable expression of the CFP-YFP FRET-based probe. In this probe, a cyan fluorescent protein (CFP) and yellow fluorescent protein (YFP or Venus) are joined together by linker peptide sequence, which has a Caspase-3 cleavage site (DEVDG) (Figure 4.12). The increase in CFP/YFP ratio indicates the loss of FRET and hence, the activation of Caspase-3 (Figure 4.12). Caspase-3 being an executioner caspase, take cells towards irreversible cell death by apoptosis. The results revealed that there is a noticeable change in the CFP/YFP ratio in MDA-MB-231 treated cells as compared to the untreated cells (Annexure Figure 3). Comparatively, peptide-MTX conjugates demonstrate an increment of 30-60 % apoptosis induction as compared to free peptides or MTX, which is significantly high compared to a treatment option with the peptide or MTX alone (Figure 4.12). This further enhances the potential of our designed THPs to mediate the delivery of MTX, thereby increasing its bioavailability for inducing apoptosis.

4.3.8. Biocompatibility of peptides

The utility of peptide-based therapeutics has not been used to its optimum potential due to the loss of their function in biological fluids (*139*). The compatibility of the designed peptides in serum was also evaluated as a measure of their homing ability (*130*). We cross-checked the cellular uptake in MDA-MB-231, HeLa, U2-OS, and MCF-10A cells, by objectively comparing with serum pre-incubated and serum-free peptide solutions using flow cytometry (Figure 4.13

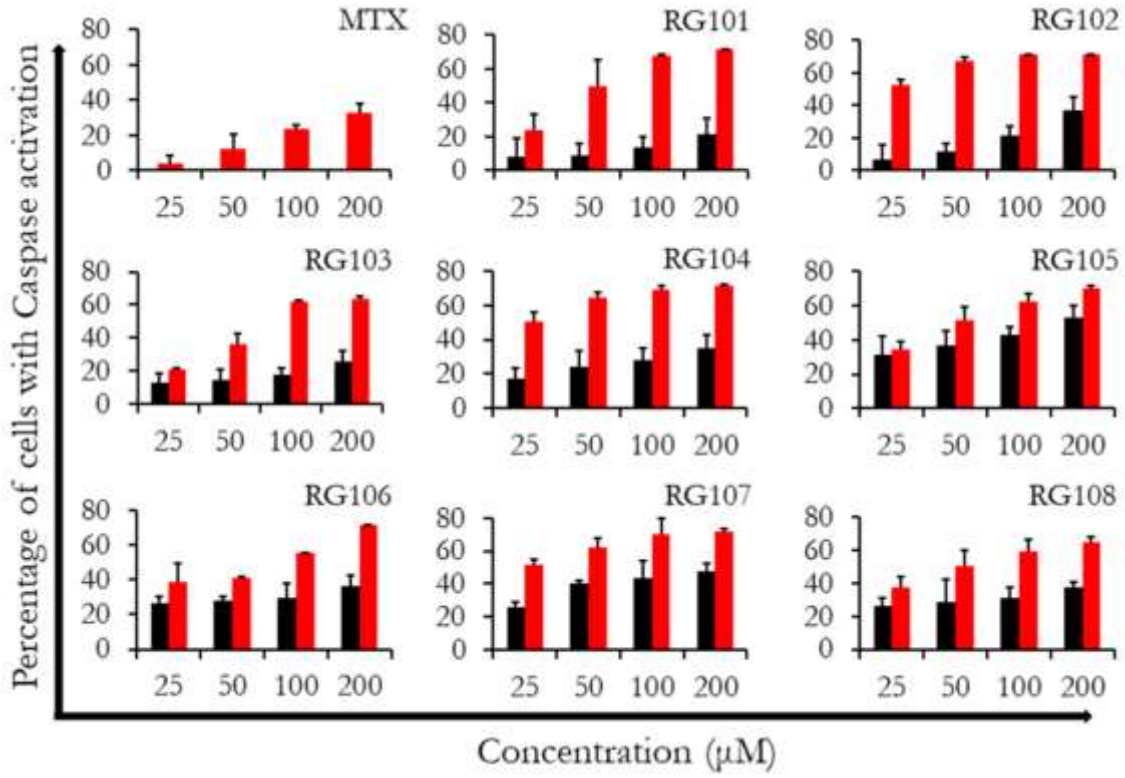

Figure 4.12. Validation of apoptotic cell death. *To confirm the cell death by apoptosis, MDA-MB-231 cells having the stable expression of CFP-YFP FRET-based caspase sensor, DEVD were used. MDA-MB-231 cells expressing this probe were subjected to treatment with MTX (red), peptides (black), and peptide-MTX (red) conjugates for 48 h. The cells with loss of FRET led to an increase in the CFP-YFP ratio and were considered for quantitative analysis. The graph represents the mean ± SD of the percentage (of cells) undergoing cell death through Caspase-3 activation (n=4).*

A-D). The cellular uptake in both conditions was found to be in a similar range, indicating the retention of more than 90 % peptide functional activity.

4.3.9. Hemotoxicity of peptides

The extent of hemotoxicity has been performed against human RBCs at 100 μM concentration of peptides and peptide-MTX conjugates. In our study, the heme release measured at 540 nm after treating human RBCs is less than 3% in all cases, indicating the non-hemolytic nature of peptides and peptide-MTX conjugates (Figure 4.14).

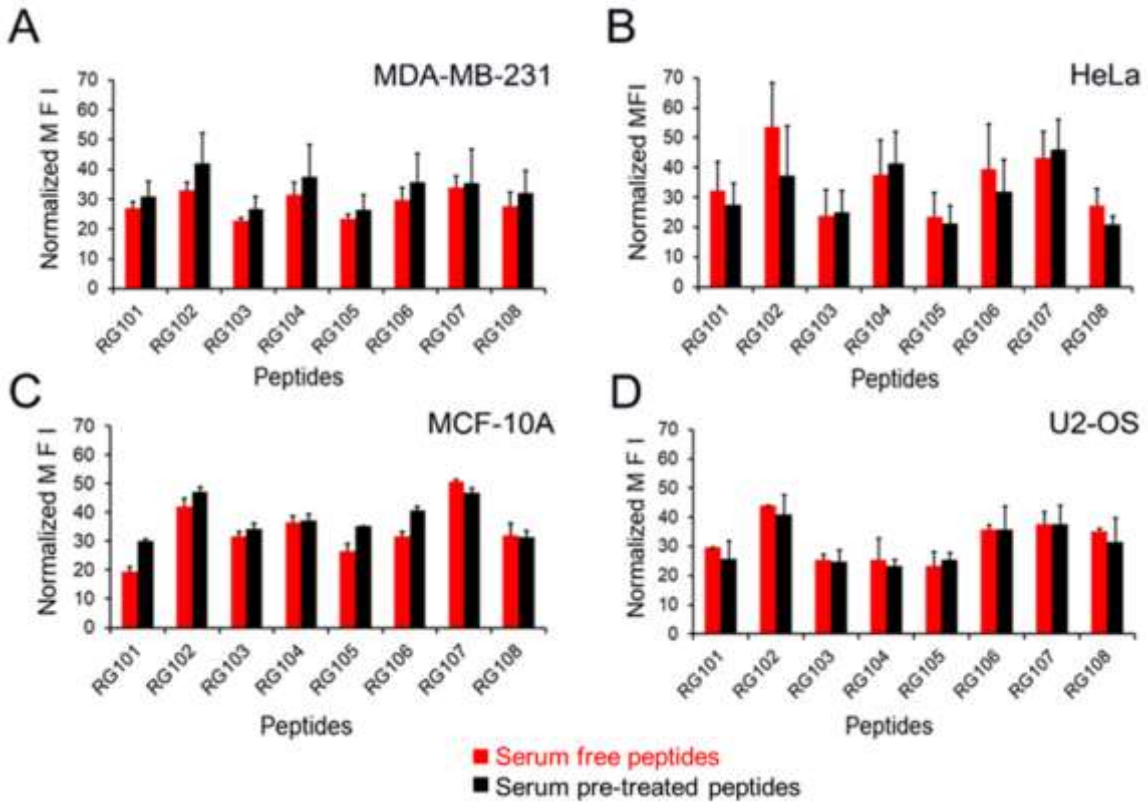

Figure 4.13. Biocompatibility of peptides. *The binding activity of peptides in the presence and absence of serum on (A) MDA-MB-231 cells (B) HeLa cells, (C) MCF-10A cells, and (D) U2-OS cells, measured by flow cytometry. The peptide stocks were pre-incubated with fetal bovine serum (FBS) for 1 h at 37°C before cell treatment. Cells were treated with 10 µM of serum untreated and treated CF-tagged peptides (RG101-RG108) for 4 h at 37 °C. The obtained fluorescence intensities were normalized by the intensities of the untreated cells. MFI represents Mean Fluorescence Intensity.*

4.3.10. Comparative histopathological peptide staining

The homing and selective recognition of tumors *in vivo* occurs in a complex microenvironment. In our study of clinical investigation, we aim to use tumor biopsy samples from patients to understand the behavior of designed peptides on real tumor samples of human origin. Benefiting from the desirable potency of the designed peptides, we checked their binding potential to the patient-derived tumor and adjacent normal tissues through fluorescence imaging. The pathological status of the tissues was confirmed by H&E and Ki-67 staining (Figure 4.15 A). H&E staining defines the type of tissue and their malignancy status, whereas Ki-67 is a prognostic marker for cellular proliferation (*140*). This evaluation of tumor morphology and confirmation of tumor malignancy has been performed by the pathologist. Under identical conditions of treatment and image acquisition, different peptides showed differential binding

behavior to normal and tumor tissues (Figure 4.15 B, C; Annexure Figure 4). All peptide model systems showed considerable difference in binding compared to the respective negative control, which is only 5(6)-carboxyfluorescein stained tissues. Estimation of homing and penetration with cell lines and clinical samples are qualitatively identical and quantitatively comparable, with this new breed of *de novo* designed peptides with diversified stereochemistry.

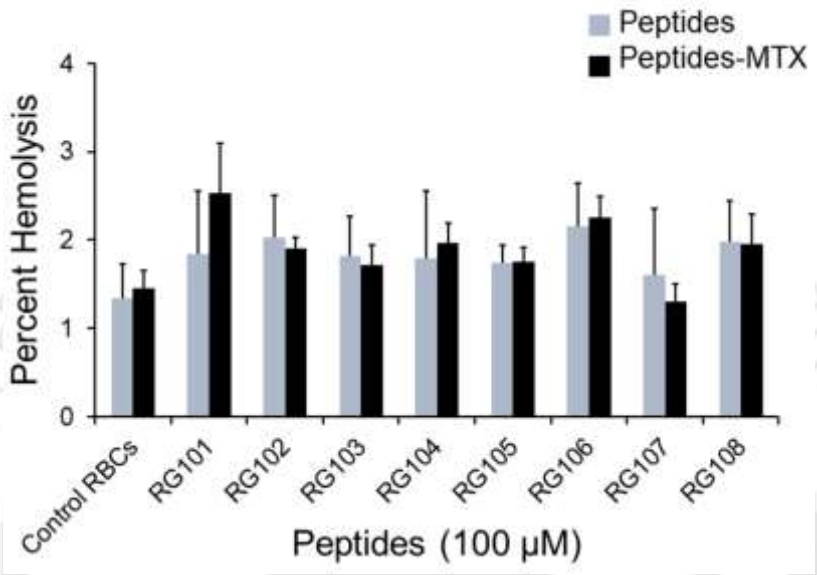

Figure 4.14. Hemotoxicity of peptides. *Hemolytic assay of the designed peptides and their MTX conjugates against human red blood corpuscles (RBCs). Heme release was measured at 540 nm after treating human RBCs with buffer, and 100 µM of peptides (UN) and their MTX conjugates (MTX) for 2 h at 37°C. The data was normalized by complete lysis with 0.5 % of Triton X-100. All results are presented as the mean ± SD of three independent experiments.*

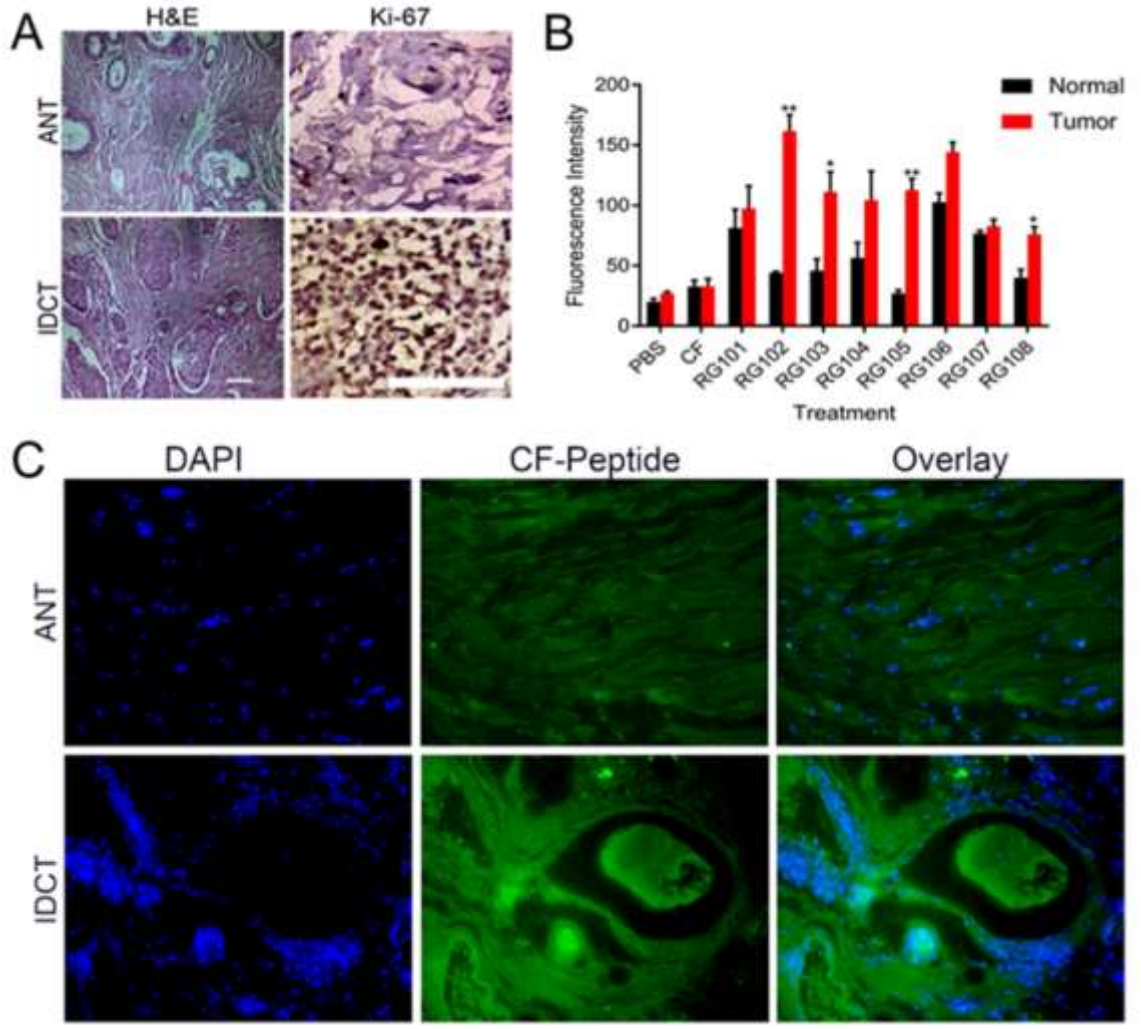

Figure 4.15. Comparative Histopathological Staining of peptides on clinical samples. *We assessed the binding of the designed peptides (RG101-RG108) on patient-derived tumor and adjacent normal tissues through fluorescence imaging. (A) Representative bright-field microscopic images of selected invasive ductal carcinoma tissues (IDCT) and adjacent normal tissues (ANT) of the breast, stained with H&E and Ki-67 antibody. (B) The quantitative analysis of peptide binding on normal and tumor tissues is represented in terms of fluorescence intensity. The control group is with PBS and represents autofluorescence of tissues whereas, tissues treated with 5(6)-carboxyfluorescein (CF) alone represent negative control. All values were reported as mean ± SEM of fluorescence from different tissue sections treated under identical treatment conditions (n=4). For each treatment group, the normal and tumor treated tissues were compared by Two-tailed Student's t-test. Scale bar corresponds to 50 µm. (C) Representative images of peptide binding on normal and tumor tissues. Blue shows nuclei stained with DAPI Fluormount, and green denotes the binding of CF-tagged peptide.*

4.4. CONCLUSION

In the present study, we rationally designed a library of eight tumor homing peptides by topologically restricting the RGD and QGR motifs in geometrical basins of Ramachandran map. This study unfolds the possibility of an 'informed walk' across Ramachandran geometrical space in search of conformational lockers. It can, in principle, be the first attempt to make tumor homing 'programmable' by permuting and fixing the topology of RGD and QGR motifs. It offers a space for conceptual innovations in drug design at the conformational level. Modeling and electrostatic profiling studies confirmed the efficacy of our designs. CD and FTIR spectroscopy suggested that these peptides are distinctly different in their conformations, as envisaged by design. We demonstrated that these peptides displayed differential cellular uptake in cancerous cell types, revealing their potential for selective targeting. The designed poly-D peptides show comparatively less uptake in cancerous cells. This corroborates our hypothesis that the topological specifications coded in the peptide design and the resulting electrostatic fingerprint play a critical role while interacting with the cell surface. All members in the designed THP library retained their functional activity in serum, indicating their biocompatibility and showed negligible toxicity to mammalian red blood corpuscles (RBCs). Improved cytotoxicity to MTX resistant breast cancer (MDA-MB-231) cells by peptide-MTX conjugates, compared to the free MTX or THPs, guarantees the enhanced drug accumulation in cells, leading to the effective delivery of the designed molecules.

Further, ratiometric fluorescence-based assay confirms that the strong anticancer activity is induced by apoptosis, a desirable trait for a typical drug delivery vehicle. As a separate study, we intend to validate this design framework in tumorigenic mouse models. However, studies with clinical isolates confirmed that the topological signatures encoded in the design of each member in the THP library, have manifested as differential binding to normal and tumor tissues. The two- to three-fold difference in selective binding to tumor tissues would, therefore, qualify them for further evaluation as a therapeutic option against breast cancer.

5

Peptide-Based Delivery Vectors with Pre-defined Geometrical Locks

Design of peptide-based targeted delivery vectors with attributes of specificity and selective cellular targeting by fixing their topology and resulting electrostatic fingerprint is the objective of this study. We formulated our peptide design platform by utilizing the possibilities of side-chain induced geometric restrictions in a typical peptide molecule. Conceptually, we locked the conformation of the RGD/NGR motif of tumor homing peptides (THPs) by mutating Glycine residue in these motifs with D-Proline and tailed the peptides with a syndiotactic amphipathic segment for cellular penetration. The designed peptides were synthesized, characterized, and tested in vitro on various cell lines, including breast cancer (MDA-MB-231), cervical cancer (HeLa), osteosarcoma (U2-OS) and non-cancer mammary epithelial cells (MCF-10A), by flow cytometry and confocal microscopy. The results showed differential cellular uptake in different cell types, as a result of distinct electrostatic fingerprint encoded in their design. The uptake of serum pre-treated peptides by cells reveals the retention of peptide activity even after the incubation with serum. In addition, the peptide-methotrexate (MTX) conjugates showed enhanced apoptotic cell death in MTX-resistant MDA-MB-231 cells, indicating the increase in MTX bioavailability.

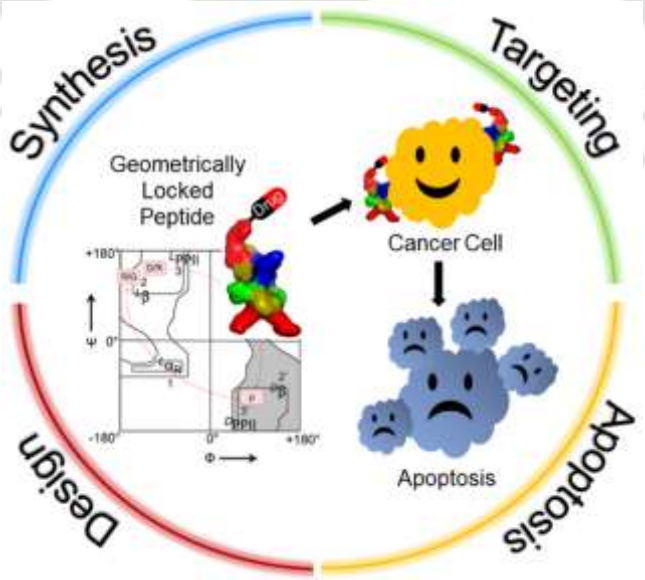

5.1. INTRODUCTION

Chemotherapy is one of the most effective therapeutic options for the treatment of cancer. Efficacy of such systemically administered drugs is often limited by their non-selectivity, poor water solubility, and low therapeutic index. The purpose of using a drug delivery vector is to transport drugs to the site of action with high specificity. This report focuses on the design and development of a delivery vector with tumor homing and cell penetrating peptide segments conjugated with a drug molecule.

Peptides, the short polymer of amino acids, falls between small chemical compounds and large proteins in their size distribution profile. Peptides were known to function as hormones, signaling molecules, carriers, and supplements. The use of insulin, a peptide hormone for diabetes, unfastened the science of peptides as therapeutics (*2*). Later, when chemical synthesis and sequence identification became plausible, many peptides have emerged as promising therapeutic options, including oxytocin, vasopressin, octreotide, and calcitonin. The persistent curiosity in peptide research led to the identification of bioactive peptides even from biological secretions of cephalopods and arthropods (*141*). However, short-half life and less oral bioavailability influenced their development as potential therapeutics (*142*). Yet, they are preferred for being natural components of biological systems. Strategies such as cyclization, D-amino acids, nano-conjugations, and functionalization have been adopted to overcome such limitations. Such ingenuities have significantly improved the pharmacokinetic properties of peptide drugs. Peptides like exenatide and teriparatide are even used as injectable, respectively, for type 2 diabetes and osteoporosis (*143, 144*). Recent statistics report more than 60 FDA approved peptide drugs (US, Europe, and Japan), 150 in clinical development, and another 260 tested in human clinical trials (*141*).

Peptides or their conjugates perform diverse functions based on their physicochemical and structural properties. They have been used for imaging, diagnosis, and treatment of diseases as targeting agents, nanovectors, drug delivery vehicles, and cytotoxic molecules (*23*). The development of peptides for targeted delivery of drugs is very evident from the studies of Cilengitide, iRGD, and NGR peptides for multiple cancers. During 1991-2014, FDA has approved 116 anti-cancer drugs; among them, 82 belong to the targeted class (*145*).

The preferential affinity of certain rationally designed peptide sequences to cancer cells and even between specific cancer cell types have introduced the concept of tumor homing peptides. Cell penetrating peptides have the ability to translocate cargoes ranging from small molecules to large proteins into the cells (*101, 102, 146, 147*). Tumor homing peptides, on the other hand, can be employed to enhance the accumulation of drugs on tumor sites (*112*). RGD (Arginine-Glycine-Aspartic acid) and QGR (Glutamine-Glycine-Arginine) motifs are known for their ability to selectively home tumor vasculature. THPs like iRGD, Cilengitide, NGR-TNFα, etc. have been widely tested in various clinical studies (*6*). However, none of them succeeded in getting FDA approval. The major limiting factors for their development in the clinics include proteolytic stability, cell specificity, and response variations in *in vitro*, *in vivo* and clinical studies (*8*). Herein, we present a plausible strategy to address the first two limitations by focussing on the design and development of a delivery vector with tumor homing and cell-penetrating motifs conjugated with a drug molecule. The third limitation can only be confirmed after in vivo studies and clinical trials.

5.2. MATERIALS AND METHODS

The methods used in this chapter are same as described previously in Chapter 4, section 4.2, except the mentioned additional experiments.

5.2.1. Right Angle Scattering of designed peptides. The self-assembly formation of peptides in solution was monitored by performing the 90° scattering assay. Time course measurement spectra were recorded for all peptides at 0 h and 24 h, respectively, at 450 nm using a spectrofluorometer (Jasco FP 8500; slit width = 2.5 nm).

5.2.2. Thioflavin T (ThT) Fluorescence assay. The assembly formation of peptides was evaluated by ThT binding assay. Freshly prepared ThT dye solution was added to the peptide samples of 0 h and 24 h, respectively. Fluorescence spectra (Ex/Em: 450/485 nm; slit width Ex/Em: 2.5/5 nm) were recorded in the spectrofluorometer (Jasco FP 8500) at 25°C using quartz cuvette (Helma, Sigma Aldrich) with 1 cm path length.

5.2.3. Field emission scanning electron microscopy (FESEM). Peptide samples (30 µl) dropped cast on the clean glass surface and allowed to air dry. The glass-coated samples were loaded on the FESEM sample holder with the carbon tape and uniformly coated with

Platinum to enhance the conductivity. The images were acquired by JSM-7610F electron microscope (JEOL).

5.3. RESULTS

5.3.1. Design of D-Proline Induced Geometrical Locks

Our efforts for the rational peptide design through the principles of Ramachandran map incorporates stereochemically varied residues to produce enriched THPs. Earlier studies have shown that if glycine (G) in RGD or NGR motif is mutated, then their efficacy is largely compromised (*88*). This observation directly points to the possibility of Glycine assuming a (ϕ, ψ) dihedral angle combination, that falls in the D-region of Ramachandran Map (Figure 5.1A) (*16, 89*). D-Proline is one residue with which we can fix this geometry firmly in the designated region in (ϕ, ψ) map. So, we intentionally mutated Glycine with D-Proline in RGD/QGR motifs to produce a topologically specific, yet constrained peptide; based on a reported homing peptide RGDPAYQGRFL (*91*) (Figure 5.1A). We have earlier shown that design directives such as stereochemistry, amphipathicity, and electrostatics can be suitably incorporated in modulating the cell penetration of a peptide sequence with a good degree of selectivity (*130*). In this study, we have combined the homing and penetration motifs in one sequence, in an attempt to design an optimum carrier for targeted delivery of small molecules. In the design, the tumor homing segment was followed by a short tail of syndiotactic (peptide chain with alternating L, D stereochemistry), amphipathic sequence (Table 5.1). Amphipathicity in the tail sequence was achieved by designing lysine and leucine side-chains protruding in opposite directions resulting in two distinct zones of different polarities (Figure 5.1B).

5.3.2. Electrostatic Fingerprinting of designed delivery vectors

Electrostatic interactions have a pivotal role in the specificity and efficacy of homing and cell penetration. The electrostatic potential distribution of each peptide was calculated through the Finite-Difference Poisson-Boltzmann (FDPB) equation using DelPhi software (*128*). Keeping the amino acid composition identical up to eleventh residue in all four sequences, the extended tail with Lys-Leu-Lys (KLK) in RG202, Lys-(D-Lys)-Leu (KkL) in RG203 and Lys-(D-Lys)-Leu-(D-Leu)-Lys (KkLlK) in RG204 has significantly altered the electrostatic fingerprint of the parent sequence (Figure 5.1B). Thus, each designed molecule has its own electrostatic

signature, which directly modulates its functional properties, as discussed in the following sections.

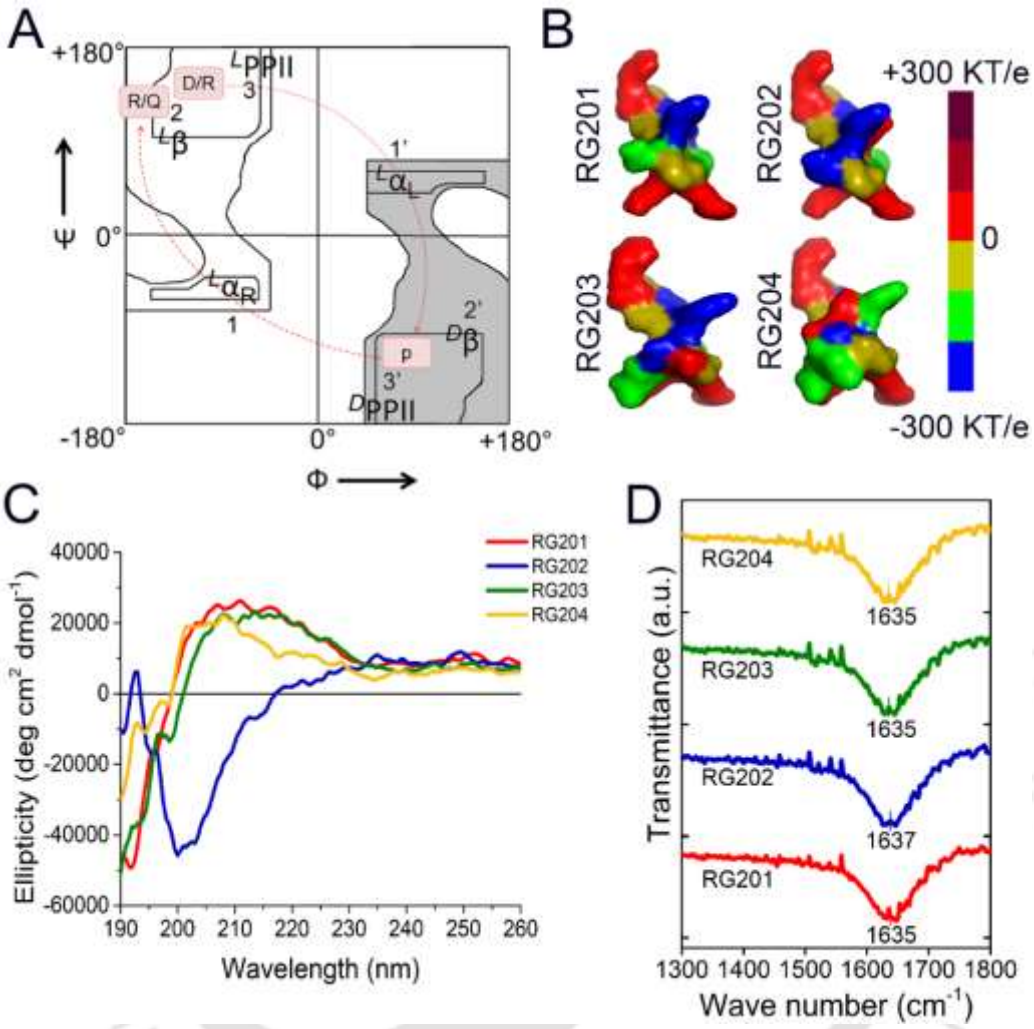

Figure 5.1. Design of peptide-based delivery vectors. *(A) Informed walk across the sterically allowed regions of Ramachandran plot to fix the geometry of RGD and NGR motif. The highlighted text represents the conformational basins to introduce the topological fixation in RGD/QGR motifs of peptides. (B) Electrostatic potential distribution of the designed peptides signifying the differences in potential values obtained as an effect of the change in stereochemistry and amphipathicity. (C) CD Spectra of designed peptides indicating the design directed structural disparities in secondary structure. (D) FTIR spectra with C=O bond signature peak, suggesting extended conformation.*

5.3.3. Peptide Synthesis and Characterization

The designed peptides were synthesized using solid-phase peptide synthesis and characterized by reverse-phase High-Performance Liquid Chromatography (RP-HPLC) and Mass

spectrometry (MALDI-TOF-MS) (Table 5.1). N-terminus modifications with 5(6)-carboxyfluorescein (CF) or methotrexate (MTX) were aimed to investigate their efficacy and specificity upon membrane interaction. Further, the design incorporated structural changes were verified by Circular dichroism (CD) spectroscopy, and Fourier transform infrared (FTIR) spectroscopy. CD spectral analysis suggests that the designed peptides adopted different conformations at room temperature, suggesting no typical secondary signatures (Figure 5.1 C). FTIR experiments also indicate a major peak of 1635 cm^{-1}, which corresponds to C=O bond stretching (Figure 5.1 D) (*131*). CD and FTIR spectroscopy results broadly suggest that the designed peptide sequences are mainly in the extended conformation.

Table 5.1. Amino acid Sequences and Mass Characterization of the designed peptides

Peptide Code	Amino acid Sequence	Expected Molecular Mass			Observed Molecular Mass		
		UN	CF	MTX	UN	CF	MTX
RG201	RpDPAYQpRFK	1373.7	1731.7	1809.7	1376.0	1733.2	1811.5
RG202	RpDPAYQpRFKLK	1614.8	1972.8	2050.8	1617.0	1974.2	2052.7
RG203	RpDPAYQpRFKkL	1614.8	1972.8	2050.8	1616.9	1975.3	2052.3
RG204	RpDPAYQpRFKkLIK	1856	2214	2292	1857.8	2216.0	2295.0

Note: *The amino acid sequences of the designed THP peptides. L- and D-amino acids are written as upper case and lower case characters, respectively. The expected molecular mass for the designed peptides with their 5(6)-Carboxyfluorescein (CF) and Methotrexate (MTX) conjugates is shown in Dalton (Da). The observed molecular mass corresponds to the mass observed from MALDI-TOF analysis of the purified peptides.*

5.3.4. Cellular Uptake of the designed peptide-based delivery vectors

The comparative uptake of peptides was quantitatively assessed through flow cytometry in breast cancer (MDA-MB-231), cervical cancer (HeLa), LAMP-RFP transfected osteosarcoma (U2-OS) and mammary epithelial (MCF-10A) cells. The obtained results suggest that we could accomplish the two broad objectives envisaged in the design; (i) differential uptake between cancerous and non-cancerous cells and (ii) differential uptake between different cancer cell types. We observed the maximum cell surface binding of designed peptides in the U2-OS cell line followed by MDA-MB-231 and HeLa or MCF-10A cell lines. Interestingly, in HeLa and MCF-10A cells, the peptide binding and/or uptake is almost similar and is 2-3 times less than that of peptide binding in U2-OS cells (Figure 5.2). This observation of lower cellular uptake in

cervical cancer cells and mammary epithelial cells markedly represents the differential uptake and selective targeting of designed peptides.

Further, the penetration ability of these peptides and delivery of small molecules was verified in the same cell types by confocal microscopy. Strikingly, fluorescence imaging observations also support that the uptake of designed peptides varies with the cell types. We observed that the peptide RG203 and RG204 show penetration in MDA-MB-231 cells, while in the case of U2-OS cells, they are observed to be mostly membrane-bound (Figure 5.3). Similarly, only RG202 molecule enter HeLa cells, unlike in MDA-MB-231 cells, where the penetration was observed by all molecules.

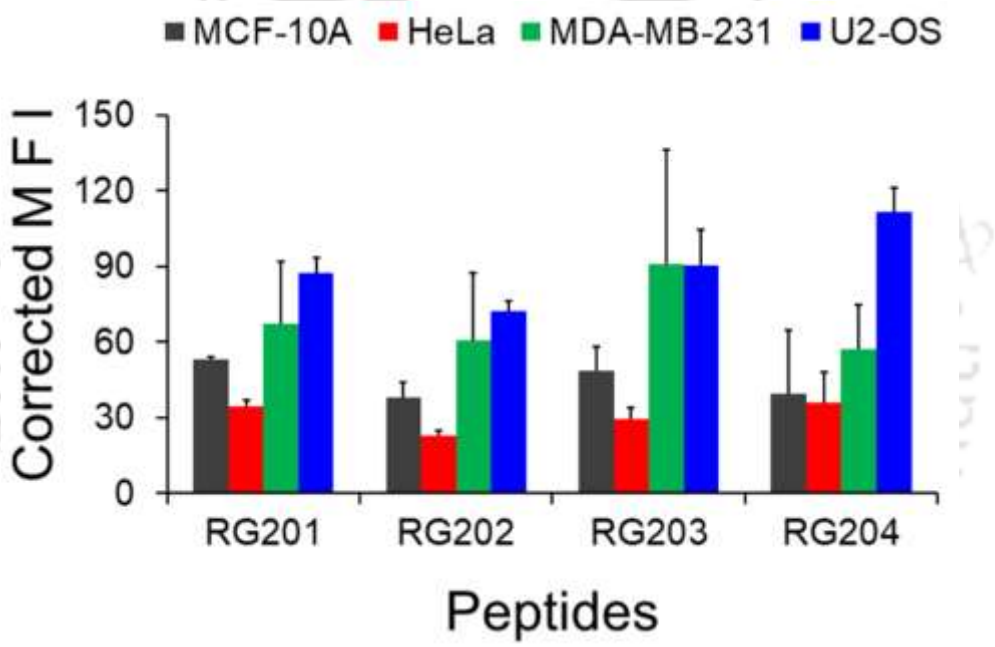

Figure 5.2. Cellular uptake of peptides. *The comparative uptake of peptides in breast cancer (MDA-MB-231) cells, cervical cancer (HeLa) cells, LAMP-RFP transfected osteosarcoma (U2-OS) cells, and mammary epithelial (MCF-10A) cells using flow cytometry. All cells were incubated with 10 µM of CF-tagged peptides (RG201-RG204) in serum-free DMEM for 4 h at 37 °C and analyzed through flow cytometry. Corrected MFI represents Mean Fluorescence Intensity. Results are presented as mean ± SD of three independent experiments.*

These observations clearly reflect the manifestation of differential electrostatic signature and stereochemical modifications encoded in the design of peptides to interact differently with membranes of different cell types. This observation underlines an earlier report by Roland Brock

and coworkers, clearly pointing out that the cell surface binding and internalization are two distinct mechanisms with separate structure-activity relationships involved (*148*).

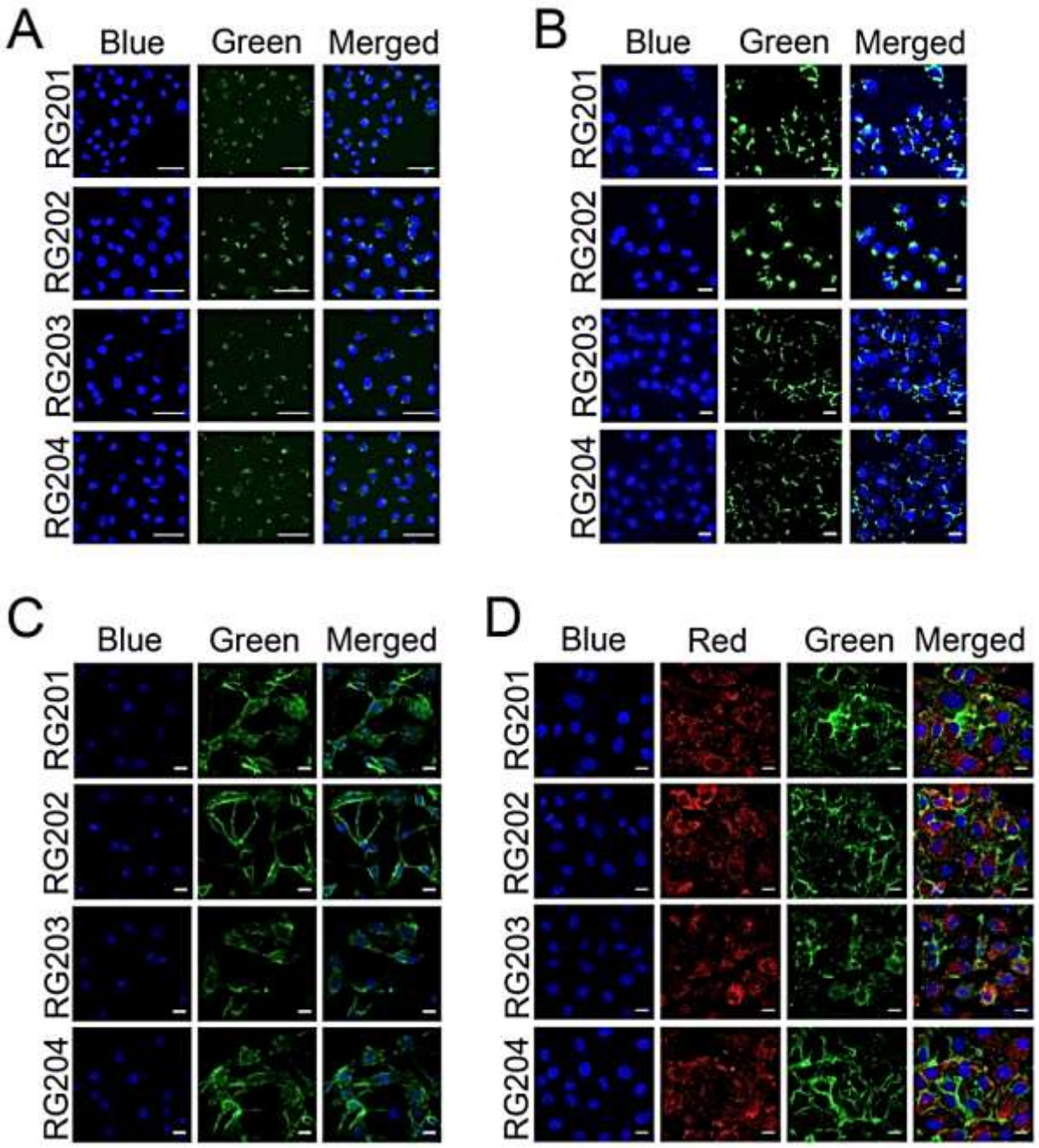

Figure 5.3. Cellular uptake of peptides using confocal laser scanning microscopy. *Cellular uptake of CF-tagged peptides in (A) MDA-MB-231 cells, (B) HeLa cells, (C) MCF-10A cells, and (D) LAMP-RFP transfected U2-OS cells in serum-free DMEM for 4 h at 37 °C. Blue indicates Hoechst 33342 staining; green indicates peptide uptake, red shows lysosomes, and merged shows the cellular uptake. Scale bar: 50 µm (A) and 20 µm (B,C,D).*

5.3.5. Cytotoxicity assessment

The designed peptides were also conjugated with an anti-cancer drug, Methotrexate (MTX), at N-terminus to investigate their cellular toxicity as a drug delivery vector. The cytotoxic activity of these peptides, along with free MTX and MTX conjugated peptides was evaluated in MTX-resistant MDA-MB-231 (*132*), and MCF-10A cells using Tetramethylrhodamine methyl ester (TMRM) based assay. The release of TMRM dye from mitochondria indicates apoptotic cell death due to the depolarization of mitochondrial membrane potential. In our study, the cells with TMRM loss and karyopyknosis were considered undergoing programmed cell death and hence, considered for analysis. As compared to MTX alone, peptide-MTX conjugates possess augmented toxicity to MDA-MB-231 cells, compared to MCF-10A cells, thereby supporting the earlier observation of higher uptake rates in cancer cells (Figure 5.4, Annexure Figure 5, 6).

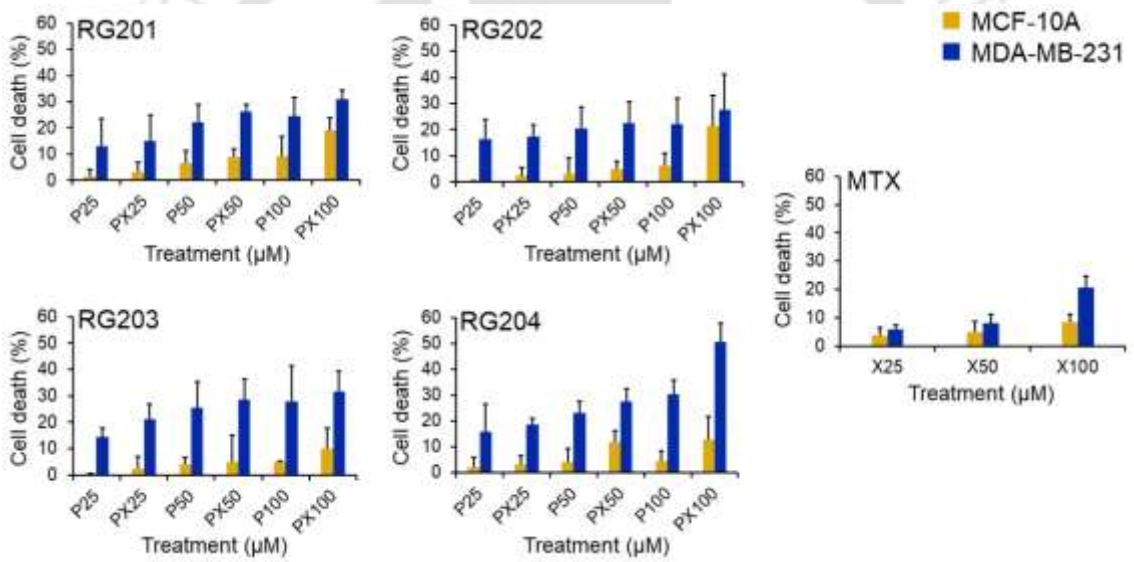

Figure 5.4. Cytotoxicity of designed peptides. *Analysis of peptide toxicity in MDA-MB-231 cells and MCF-10A cells by peptide treatment employing TMRM based assay. MDA-MB-231 and MCF-10A cells were treated with MTX (Xn), peptide vectors (Pn) and peptide-methotrexate (PXn) conjugates for 48 h at three different concentrations (n = 25 μM, 50 μM, and 100 μM) for 48 h at 37°C. The cells with TMRM loss and nucleus condensation indicate apoptosis.*

5.3.6. Caspase-3 activation

To confirm the cell death through apoptosis, MDA-MB-231 cells having the stable expression of CFP-YFP FRET-based caspase sensor (DEVD) were used for apoptosis detection. This probe is composed of a cyan fluorescent protein (ECFP) and yellow fluorescent protein (EYFP

or Venus), which are fused by the linker having a Caspase-3 cleavage site (DEVDG). The increase in the CFP/YFP ratio as a result of the loss of fluorescence resonance energy transfer (FRET) indicates Caspase-3 activation (*138*). These transfected cells were treated with MTX, peptides, and peptide-MTX conjugates at different concentrations. After treatment, the loss of FRET in cells is observed by using the ratiometric fluorescence imaging (*138*). The obtained results represent high Caspase-3 activation in cells treated with peptide-MTX conjugates, compared to cells treated with only MTX or peptides alone (Figure 5.5, Annexure Figure 7).

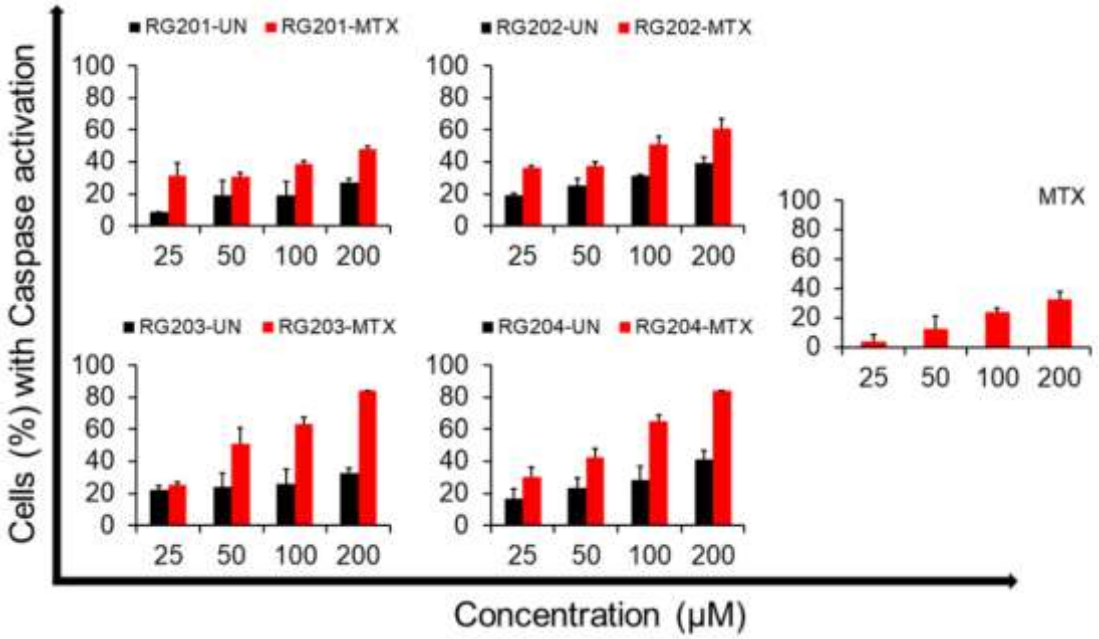

Figure 5.5. Validation of apoptotic cell death. *To confirm the cell death by apoptosis, MDA-MB-231 cells having the stable expression of CFP-YFP FRET-based caspase sensor, DEVD were treated with MTX, peptides (RG20X-UN) and peptide-MTX (RG20X-MTX) conjugates for 48 h. The loss of FRET in cells was measured in terms of their difference (increase) in the CFP-YFP ratio, and the cells with FRET loss were taken for analysis. The graph represents the ratio (mean ± SD) of cells undergoing cell death by Caspase-3 activation.*

5.3.7. Biocompatibility of peptides

Peptide biocompatibility in biological fluids like serum is the foremost concern for their bioavailability in the physiological system, and therefore, their functional activity was verified in the presence of serum. The cellular uptake of the CF-tagged designed peptides at 10 μM concentration was tested using serum pre-treated peptides and untreated peptides by flow cytometry in MDA-MB-231, HeLa, U2-OS, and MCF-10A cells. There is almost 90%

retention in peptide function after treatment with serum irrespective of the cell types. The similar cellular uptake of peptides in both conditions confirms that the peptides are biocompatible in biological serum and have the potential for their development as drug delivery vectors (Figure 5.6).

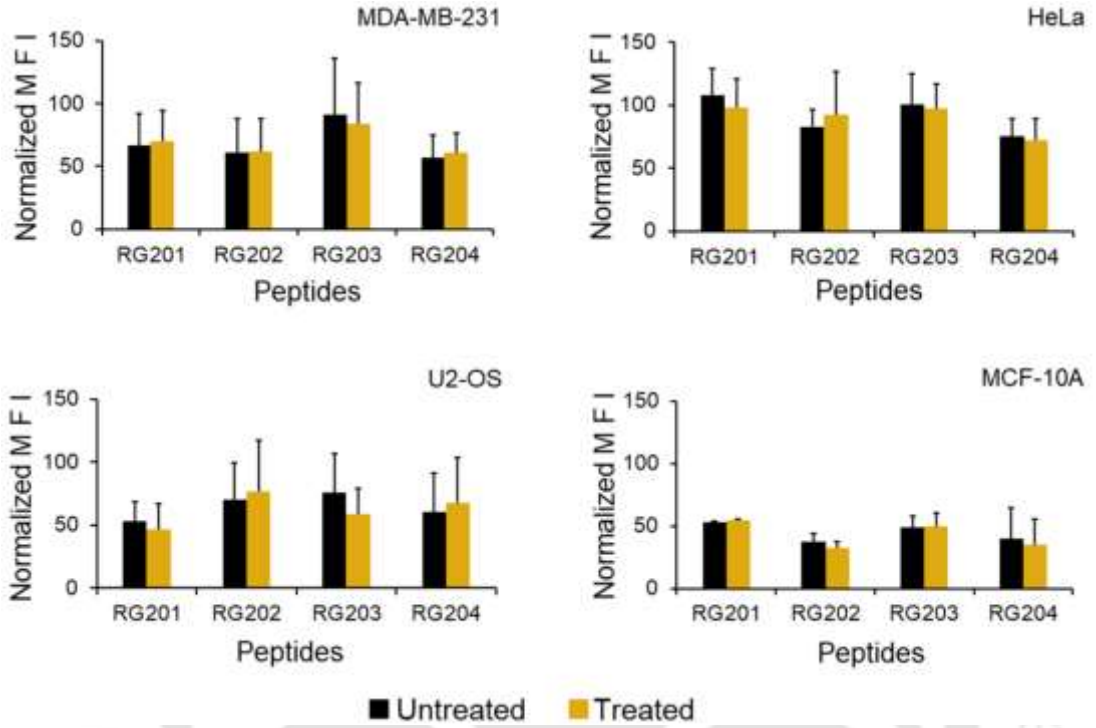

Figure 5.6. Biocompatibility of peptides. *The binding activity of peptides in the presence and absence of serum on MDA-MB-231 cells, HeLa cells, U2-OS cells, and MCF-10A cells measured by flow cytometry. The peptide stocks were pre-incubated with fetal bovine serum (FBS) for 1 h at 37°C before cell treatment. Cells were treated with 10 µM of serum untreated and treated CF-tagged peptides (RG201-RG204) for 4 h at 37 °C. The obtained fluorescence intensities were normalized by the intensities of the untreated cells. MFI represents Mean Fluorescence Intensity. Results are presented as mean ± SD of three independent experiments.*

5.3.8. Hemotoxicity of peptides

The therapeutic potential of the designed peptides was assessed in mammalian red blood corpuscles (RBCs). This experiment was performed with an aim to verify the toxic effects of designed peptides and their methotrexate (MTX) conjugates on RBCs because most chemotherapeutic drugs are administered intravenously for enhanced bioavailability, and blood is the first tissue that comes in direct contact with the injected drug. The toxic effects can lead to various side effects like blood thinning, anemia, etc. Therefore, it is of utmost

importance to verify the toxic effects of any drug delivery vehicle to the RBCs. In our study, we observed that the peptide, along with the peptide-MTX conjugates are non-hemolytic in nature, as they showed less than three percent toxicity to mammalian RBCs up to a concentration of 100 µM (Figure 5.7).

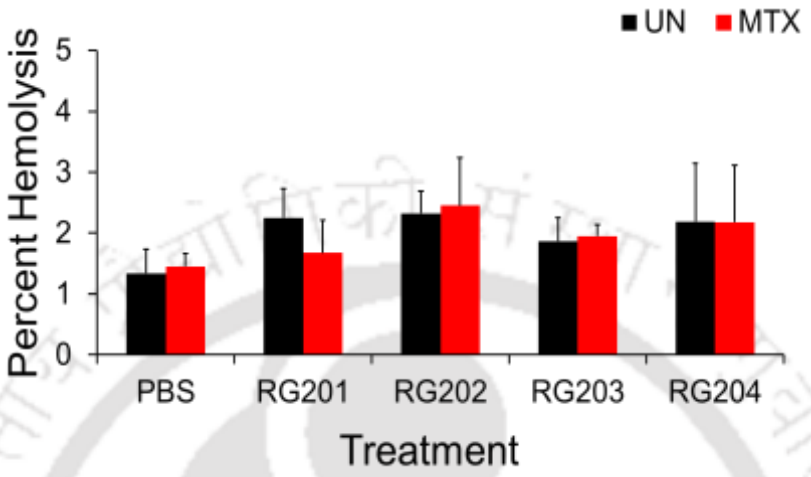

Figure 5.7. Hemolytic activity of peptides. *Hemolytic assay of the designed peptides and their MTX conjugates against human red blood cells (RBCs). Heme release was measured at 540 nm after treating human RBCs with buffer, and 100 µM of peptides (UN) and their MTX conjugates (MTX) for 2 h at 37°C. The data was normalized by complete lysis with 0.5 % of Triton X-100. All results are presented as the mean ± SD of three independent experiments.*

5.3.9. Verification of peptide aggregation propensity

The self-assembly of peptides is driven by the synergistic effect of the involved interactions like metal-ion coordinations, non-covalent interactions, stacking-pair interactions, etc. The composition of amino acids in a peptide chain is the major decisive factor for the nature of peptide self-assembly formation. Peptide nano-assemblies are crucial in imparting or augmenting the specified function of peptides like the anti-tumor effect (*149-151*). Looking into this fact, we have verified the self-assembly formation of peptides by using standard methods like scanning electron microscopy (FE-SEM), right-angle scattering, and ThT fluorescence assay. Interestingly, results from all the experiments confirm that the designed peptides are non-aggregating in nature and do not form any defined nano-structures, even in the solution form (Figure 5.8 and Figure 5.9). This suggests that the observed differential behavior of peptides towards different cell types is only due to the fundamental properties of the designed peptides.

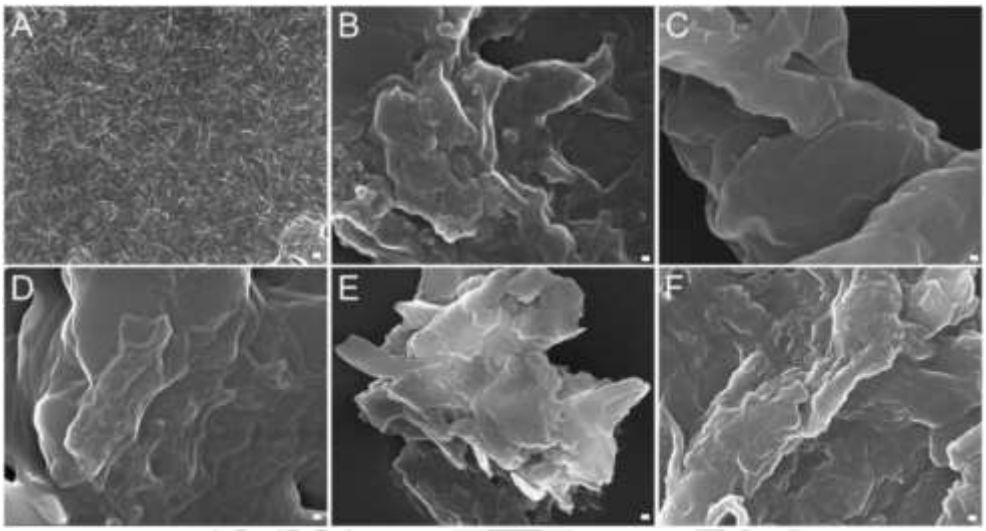

Figure 5.8. Field emission scanning electron photomicrographs (FESEM) of peptides. *(A) PhF6 peptide is taken as a positive control for nano-assembly formation (nanofibres)(152). (B) RGDPAYQGRFL peptide is an already reported tumor homing peptide (91). (C-F) FESEM images of the designed peptides RG201-RG204 showing only amorphous aggregates. Scale bar corresponds to 100 nm.*

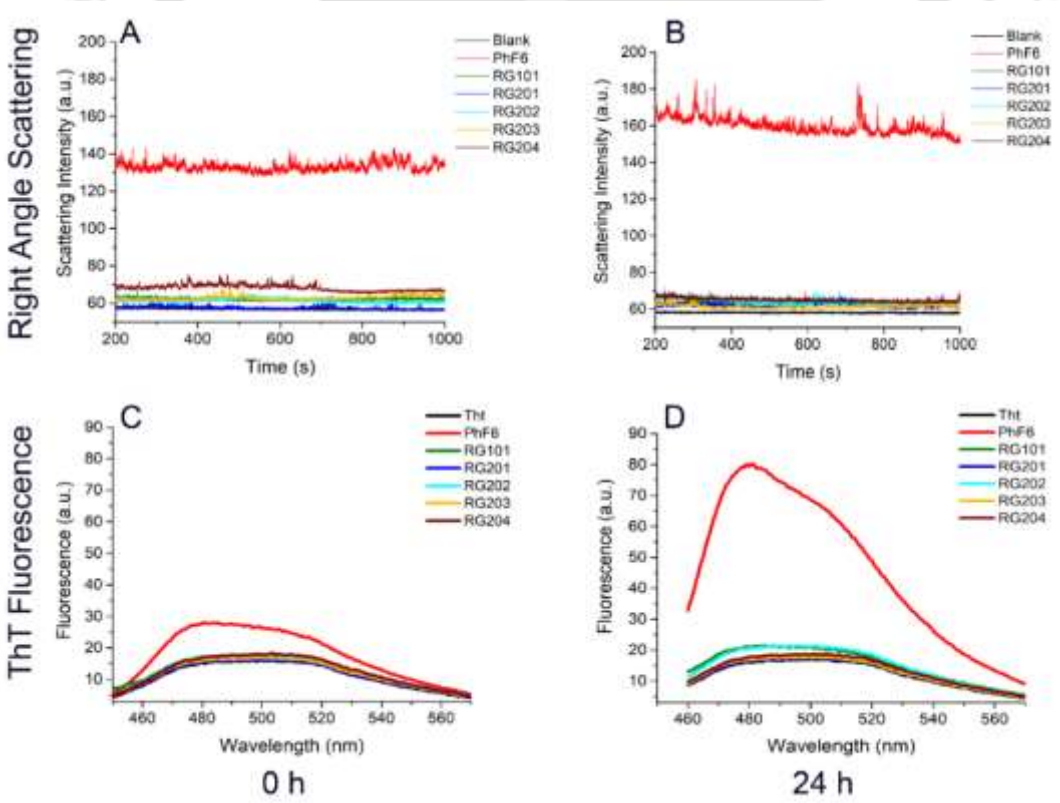

Figure 5.9. Verification of peptide self-assembly. *The self-assembly formation of peptides in solution was verified by Right Angle Scattering (A, B) and ThT Fluorescence Assay (C, D) at two time points 0 h (A, C) and 24 h (B, D).*

5.4. DISCUSSION

Tumor homing peptides have RGD/NGR trimers as common motifs with Glycine as the middle residue; without Glycine, motif generally loses its activity except in few cases such as RHD and RYD (*114, 115*). This observation compelled us to understand the specific selection of Glycine amino acid in these motifs. This study started with the hypothesis that Glycine occupies the ϕ,ψ dihedral angle combinations typical of a D-amino acid, to provide flexibility for recognition of cognate receptors of these motifs. To verify this, we mutated Glycine with D-Proline to fix the topology with clearly defined and constrained dihedral angles; and also verified that using Molecular Dynamics Simulation (Figure 5.10 A). We calculated the geometrical parameters like Euclidean distance and the angle between the terminal residues of homing domains to observe the effect of D-Proline mutation (Figure 5.10 B). We designed a second segment to the peptide, which is cationic or amphipathic, in its charge distribution (Figure 5.10 C-E). Our earlier studies on anti-microbial peptides and cell penetrating peptides have shown that the properties like amphipathicity and syndiotacticity add good value to overall penetrative ability (*17, 130*). It is also reported that the alternating LDLDLD stereochemical sequence has a natural tendency to form Gramicidin helix (*153, 154*).

Using this information, we designed a peptide system with a homing domain and a penetrating segment loaded with a typical anti-cancer drug molecule. The designed peptides were synthesized by solid-phase peptide synthesis using Fmoc chemistry, and N-terminally conjugated with fluorophore and anti-cancer drug for imaging and cytotoxicity studies. CD and FTIR spectroscopic studies provided the necessary information on the extended secondary structures of synthesized peptides.

The attempt of sequential addition of cationic and hydrophobic residues after the homing segment in the designed peptides alters their electrostatic potential and, consequently, functional properties like selectivity and penetrative ability. This has been verified by evaluating their preferential uptake, stability against serum, and selective toxicity against cancer cells. Flow cytometry experiments suggest the preferential cellular uptake or binding of peptides in breast cancer MDA-MB-231 and osteosarcoma U2-OS cells, compared to non-cancerous mammary epithelial MCF-10A cells. This observed preferential selectivity was further corroborated with

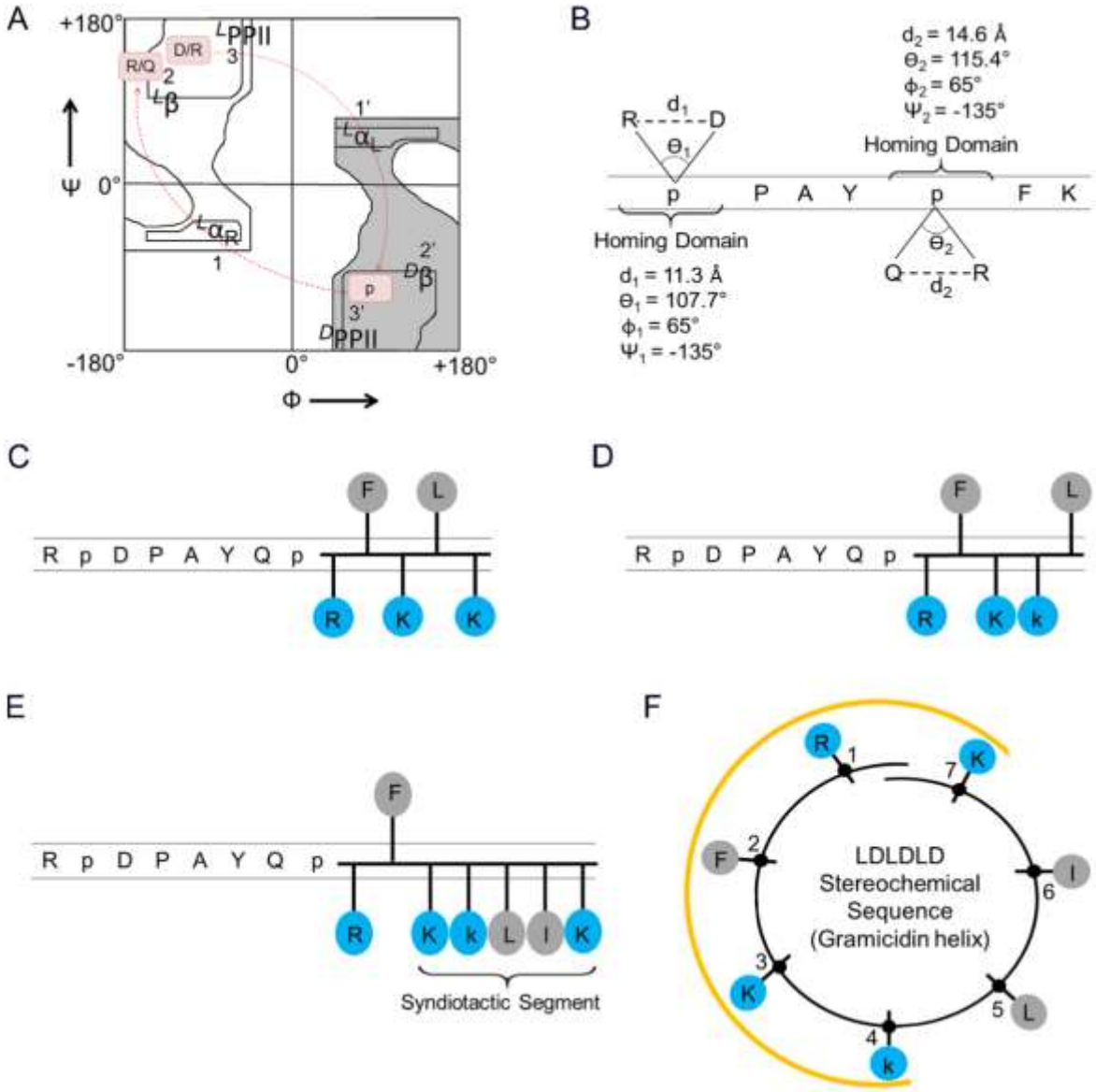

Figure 5.10. Schematic illustration of the evolved concept for vector design. *(A) Ramachandran Plot with the highlighted region to depict the fixed geometry of D-Proline in RGD and QGR motifs. (B) Geometrical parameters of D-Proline fixation showed in peptide RG201. (C, D, and E) The amino acid sequence of designed peptides RG202, RG203, and RG204, respectively, specifically indicating the tailed cationic (blue) and hydrophobic (grey) residues. (F) The syndiotactic segment of RG204 peptide forming a Gramicidin helix with a distinct cationic zone highlighted by the yellow arc. L- and D-amino acids are mentioned as upper case and lower case letters, respectively.*

confocal imaging and toxicity experiments. In confocal imaging, we observed that the cellular uptake of each peptide varies with cancer cell types. Peptide RG202 with poly-L tail penetrates in MDA-MB-231 cells and HeLa cells whereas, peptide RG203 and RG204 with syndiotactic (LDLD) extension penetrate only in MDA-MB-231 cells. We consider that the syndiotactic tail

of RG204 is forming the Gramicidin helix (Figure 5.10 F) and aids the penetration, whereas, the homing domain is providing selectivity.

The principal aim of any delivery vector is to enhance the therapeutic index. We observed a two-three folds difference in the cytotoxicity of conjugates compared to MTX alone. The selective toxicity to MDA-MB-231 cells by all peptides, compared to non-cancerous MCF-10A cells, points to the possibility of developing the designed molecular system as a specific vector for breast cancer. Furthermore, the ratiometric fluorescence assay of Caspase-3 activation confirms the apoptotic cell death, which is a preferred feature for any such lead candidates.

The designed molecules retained their activity after serum treatment indicating their stability against serum proteases, and their negligible toxicity against mammalian RBCs indicates their therapeutic safety. Taken together, our approach of vector design can be helpful in developing potential peptide-conjugated drug delivery vehicles for selective targeting of different cancer types.

5.5. CONCLUSION

The scope of peptide therapeutics is evident from their current status in the pharmaceutical industry. The synergism of peptide-cargo conjugations has offered better solutions to the present therapeutics. We have conceived this project with an aim to develop a comprehensive therapeutic agent with three distinct motifs; a tumor homing segment, a cell penetrating sequence, and a cytotoxic drug molecule. The conceptual development of tumor homing peptide designed by mutating Glycine of RGD and NGR motifs with D-Proline was found to be very effective in homing cancer cells preferentially, and to a greater extent introduce selectivity between cancer cell types. Incorporation of the amphipathic syndiotactic tail could translocate the cargo (MTX) into the cell, inducing apoptosis. The developed peptides offer selective membrane targeting or cellular penetration or both, depending on cell types. The two to three-fold difference observed in drug conjugates in cytotoxicity experiments clearly suggest the possibility of a corresponding difference in their therapeutic index. The strategy of encoding topology with RpD and QpR motifs, along with the amphipathic cell penetrating tail, worked well in inducing selectivity and penetration. The tuning of the structure by stereochemical sequence selection and tuning of electrostatics by chemical sequence selection were the guiding

principles for the design of these delivery vectors. This work will be further extended with in vivo and clinical studies to graduate from a proof of concept investigation to a therapeutic solution.

6

Generation of a Complete Tumor Targeting Molecular Construct

The selective targeting and poor penetration of small molecules in tumors limit the overall desirability of a chemotherapy medicine as a futuristic option. Tumor homing and cell penetrating peptides are known to recognize cancer cells specifically, and to translocate the cytotoxic molecule through the cellular membranes. In this study, we have integrated the previously designed tumor homing and cell penetrating peptide motifs in a single molecule for tumor targeting and penetration. A total of four molecules (RG301-RG304) with intended point mutations in the parent sequence were designed, synthesized, characterized, and tested on three different cell lines, including MDA-MB-231, HeLa and HEK-293, for cellular uptake and cytotoxicity evaluation. The peptide uptake experiments using flow cytometry and confocal imaging shows that the designed peptides have the variable potential for preferential penetration in cancerous cell types. The enhanced toxicity of peptide-methotrexate (MTX) conjugates compared to free drug or only peptides in MDA-MB-231 cells suggests the drug delivery potential of the designed peptides. Furthermore, the penetration of RG301 peptide in three-dimensional MDA-MB-231 tumorospheres confirms the utility of the peptide as a complete delivery vector.

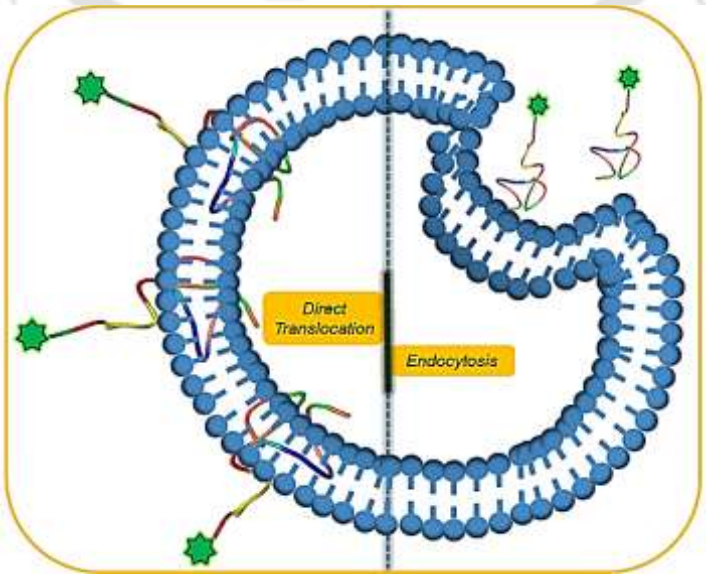

6.1. INTRODUCTION

A systemic disease demands a systemic cure. But what kind of systemic therapy could probably cure cancer? This question has begun the hunt for such specific, systemic cure for cancer (*4*). In an era obsessed with the development of cancer therapeutics, numerous chemo-agents have been introduced, including aminopterin, taxols, cisplatin, etc. The advancements in cancer research have led to the emergence of nanocarriers, hydrogels, radioconjugates, and peptide-based vectors for drug delivery applications. Peptide-based therapeutics is preferred due to their low toxicity, predictable metabolism, and reduced side-effects.

Peptide engineering provides a platform to design application-oriented peptides for their particular utility. It addresses structure-based peptide design, peptide-peptide, peptide-protein and peptide-membrane interactions, bioactive peptides, and peptide-based materials. In a few cases, peptides with superior properties are designed by incorporating D-amino acids and unnatural amino acids like aminobutyric acid. Several antimicrobial peptides like Gramicidin, Valinomycin, and others have D-amino acids in their sequence, which makes them resistant to proteases and metabolically more stable. Further, it is observed that the specific use of D-amino acids, unnatural amino acids, and dehydro amino acids in peptide design also favors a particular secondary structure (*16*). Studies are reported, where the use of L- and D- amino acids in different combinations and proportions yielded molecules with enhanced activities in polymer chemistry (*17*). The arrangement of L- and D- (R and S) monomers in a polymer chain is termed as tacticity. Based on tacticity, polymers can be isotactic, syndiotactic, or heterotactic. Isotactic polymers have either L- amino acids or D- amino acids in the peptide chain, whereas; an alternate arrangement of LDLD or DLDL amino acids forms syndiotactic peptides. Heterotactic proteins have completely random L- and D- amino acid combinations in their sequence (*18*).

Cell penetrating peptides (CPPs) or protein transduction domains (PTDs) is another class of peptides, which are 5-30 amino acids long amphipathic molecules efficient in translocating through the cell membranes. Historically, studies with TAT, an HIV transactivating factor, and Penetratin, a third helix homeodomain of Antennapedia transcription factor of Drosophila, opened up the possibilities of translocation across cell membranes with the desired payloads (*9-11*). Molecules acting as CPP possess specific characteristic features that make them distinguishable from other peptides. Firstly, they are rich in positively charged residues.

Secondly, they have optimal hydrophobicity, which leads to better uptake of CPPs inside cells. Apart from sequence polarity, the secondary structure of CPPs also plays an important role in their cellular uptake. Structures adopted after interaction with cell membrane contributes more to cell penetration, but their inability of binding specifically to particular cells is a major demerit for their clinical applications (*71*). However, due to their phenomenal ability to penetrate inside cells, CPPs are widely used with targeting moieties for applications in the delivery of drugs and nanoparticles.

In this chapter, we have used our previous tumor homing and syndiotactic cell penetrating peptide designs for selective cellular targeting and small molecule delivery. This series of peptide design has a total of four molecules, each with 19-amino acid residues in the peptide chain. Our hybrid approach of combining tumor homing peptide with the syndiotactic cell penetrating segment from our earlier designs has introduced superior molecules capable of penetrating tumor-like cellular architectures.

6.2. MATERIALS AND METHODS

Most methods used in this chapter are similar to the already described sections in Chapter 4, section 4.2. The additional details specific to this chapter are elaborated in this section.

6.2.1. Mechanism of uptake. The mechanism of peptide uptake is investigated for the designed tumor penetrating peptides (Series-3) using fluorescence spectroscopy. The dependency of cellular uptake on physicochemical factors like temperature and energy availability seems important to understand the mechanism of peptide uptake. For this experiment, 10,000 cells per well were seeded in 96 well black fluorescence plates. After 24 h, the cells were treated with different conditions. The effect of temperature was studied by comparing the peptide uptake at 4 °C and 37 °C. Prior to the treatment in 4 °C, cells and all reagents were incubated at 4 °C for 1 h as it slows down the metabolic activity of cells. After that, the cells were treated with peptides and again incubated at 4 °C for 1 h. Further, the energy requirement for driving peptide uptake was checked by pre-incubating the cells with 0.1% NaN_3 for 1 h before peptide treatment (*155, 156*). After treatment, cells were washed with PBS thrice and stained with Hoechst 33342 (0.005 mg/ml, 50 µl). After 5 min, cells were washed with PBS again and subjected to analysis using a multimode microplate reader (Tecan M200 Infinite Pro). The fluorescence was recorded for CF-tagged peptides (ex 489 nm / em 517 nm) and Hoechst 33342 (ex 346 nm / em 460 nm).

Post-treatment, the cells were treated with 0.04% Trypan blue solution to quench the extracellular fluorescence and washed again with PBS before recording fluorescence intensities. The cellular uptake corresponding to carboxyfluorescein intensity was corrected by dividing it with Hoechst fluorescence intensity and multiplying the obtained value by 1000 to get "corrected fluorescence units" *(157)*.

6.2.2. MTT Cell Viability assay. MDA-MB-231, HeLa, and HEK-293 cells were seeded in triplicate 96-well microtiter plate at a density of 10,000 cells per well. After overnight incubation, the cells were treated with different concentrations of peptides, free methotrexate drug (MTX), and peptide-methotrexate conjugates in serum-free media for 48 h at 37°C. Cells treated with the only medium were taken as the negative control. After 48 h, 50 µl of MTT was added, and cells were incubated at 37°C for 4 h. 100 µl Dimethyl sulfoxide (DMSO) was added to dissolve formazan crystals. The plates were incubated for ten minutes, and absorbance was recorded at 540 nm and 660 nm.

6.2.3. Annexin V- Propidium iodide (PI) staining. MDA-MB-231 cells were seeded ($5*10^4$ cells/well) in 24 well plates for overnight. The cells were washed with PBS, and the culture medium was replaced with serum-free media containing methotrexate drug and peptide-methotrexate conjugates at different concentrations. After incubation for 48 h, the cells were harvested by trypsinization. The collected cells were washed thrice with PBS and analyzed using flow cytometer (FACS Calibur, Becton-Dickinson) after staining with FITC-Annexin V and PI dyes, according to the manufacturer's instructions.

6.2.4. Penetration in 3D tumorospheres. To mimic the 3D spatial conformation, 3D in vitro cultures of breast cancer MDA-MB-231 cells were developed using CSC medium (Gibco, USA) in low attachment dishes. MDA-MB-231 cells grown in T-25 flasks were trypsinized and seeded in low density in low attachment plates using 40 µm cell strainer. The cells were allowed to grow for seven days at 37°C under the water-saturated environment with 5% CO_2. The numbers and morphology of tumorspheres were observed using a Nikon Eclipse light microscope. The formed tumorspheres were collected, followed by peptide treatment for 4 h in low attachment 96 well plates. After that, the spheroids were washed and subjected to confocal imaging (NikonA1R, Z-scan model) in glass-bottom plates.

6.3. RESULTS AND DISCUSSION

6.3.1. Design Strategy and Peptide Synthesis

Peptide engineering is a resourceful platform to design peptide molecules oriented for the particular application. In this chapter, we fused STRAP-3 peptide from our previously designed SyndioTactic Re-engineered Amphipathic Peptide (STRAP) (unpublished data) with the tumor homing peptide (Series-1, Chapter 4), in an attempt to generate tumor penetrating peptides. STRAP peptides are amphipathic, cationic and syndiotactic peptides designed to have left or right handed $\prod_{(L, D)}$ helix which eventually mediates the penetration in cells. This series of peptide design has a total of four molecules (RG301-RG304) each with 19 amino acids chain length. Our hybrid approach of combining tumor homing peptide with cell penetrating segment [STRAP-3] led to a new peptide (RG301) having both tumor homing and penetrating domains. We synthesized this peptide in a way to get the syndiotactic penetrating domain at the C-terminus and homing domain at N-terminus of the peptide. In the other peptide RG302, we reversed the segments to observe the directional-specific functional change of peptides. We also designed two more variants as RG303 and RG304 peptides by several point mutations in RG301 peptide at specific positions (Table 6.1). All peptides were synthesized by solid-phase peptide synthesis using Fmoc chemistry and conjugated with 5(6)- carboxyfluorescein (CF) and methotrexate (MTX) for cellular uptake and toxicity studies. All peptide conjugates were purified by semi-preparative RP-HPLC and characterized by MALDI-TOF MS or ESI-MS.

Table 6.1. Amino acid sequence of the designed peptides

Peptide Code	Amino acid Sequence
RG301	*R a D P A Y Q a R F L G K r K f I c L*
RG302	*K r K f I c L G R a D P A Y Q a R F L*
RG303	*R p D P A Y Q v R F L G K r K f I v L*
RG304	*R v D P A Y Q p R F L G K r K f I v L*

Note: *L- and D-amino acids are written as upper case and lower case characters, respectively.*

6.3.2. Electrostatic Fingerprinting

Electrostatic interactions are the most important operators at the interface of the interacting molecules. The deigned peptides are composed of RXD/QXR zwitterionic motifs, cationic

residues, hydrophobic residues, etc. playing a significant role in imparting homing and penetration properties to peptides. The electrostatic potential distribution maps were calculated for the designed peptides through Finite Difference Poisson Boltzmann (FDPB) equation using DelPhi software (*128*). The distinct regions of polarity in each peptide obtained after electrostatic fingerprinting suggest their unique electrostatic signatures, which influence functional properties (Figure 6.1).

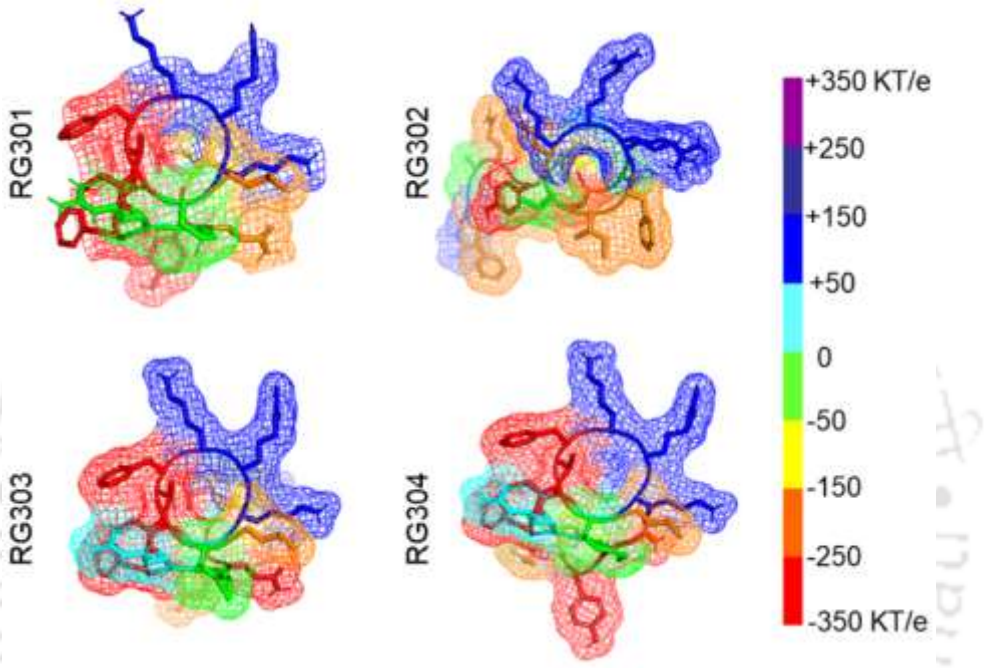

Figure 6.1. Electrostatic Mapping of the designed peptides. *Electrostatic potential distribution of the designed peptides representing the obtained potential value differences as the consequence of altered stereochemistry and amphipathicity.*

6.3.3. Secondary Structure Characterization

The structure of peptides is also get influenced by the microenvironment they are in like buffers, solvent, membranes, protein, etc. The hydrophobic interactions between the peptides and lipid molecules play an important role for direct penetration through cellular membranes. Studies have shown that the change in peptide-to-lipid molar ratios changes the conformation of peptides (*158*). In this study, the conformation of the designed peptides was evaluated using CD Spectroscopy. The peptides were dissolved at 10 µM concentration in water and analyzed by spectropolarimeter. Peptides RG301 and RG302 show the common peaks near 205 nm and 219 nm, whereas peptides RG303 and RG304 show a single major peak near 200 nm (Figure

6.2). The conformation of peptide RG301 and RG302 shows structural signatures similar to α-helix (208 nm and 222 nm), though this analysis will not be sufficient to conclusively prove that the amino acid constitution and stereochemistry of peptides pulls them to adopt helical structure. However, the principal aim of the design was to present distinct structural signatures and resultant, distinct electrostatic interaction profiles for differential efficacy and specificity.

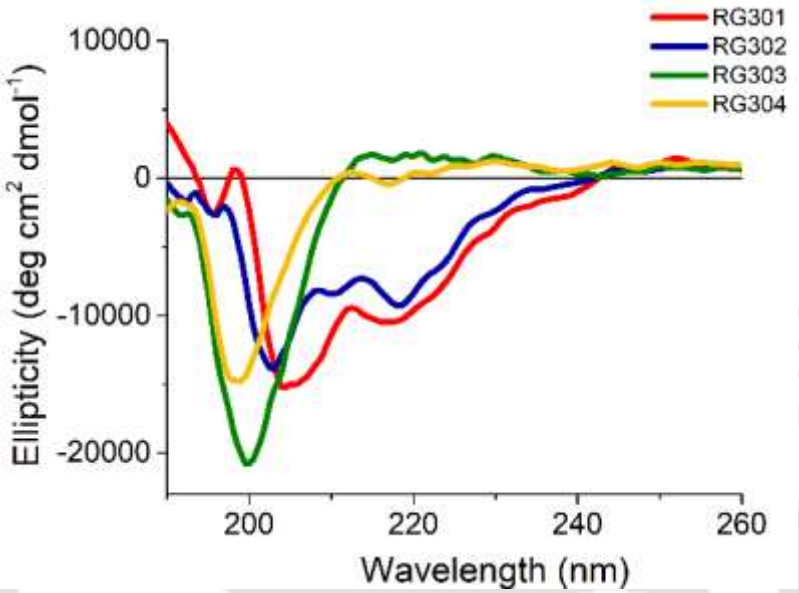

Figure 6.2. Circular Dichroism (CD) Spectroscopy. *CD Spectra of the designed peptides in water at 298 K.*

6.3.4. Cellular uptake of designed peptides

The comparative cellular uptake of the designed peptides was verified in MDA-MB-231, HeLa, and HEK-293 cells. All these cells were treated with 10 μM of CF-tagged peptides for 4 h at 37°C. TAT peptide was taken as a positive control. After treatment, the cells were washed, harvested, and analyzed using flow cytometry. A couple of candidates in the designed peptide series presented a significant difference in the peptide uptake compared to TAT peptide. We observed that the cellular uptake of peptide RG301 and RG302 is up to 10-fold more as compared to TAT, RG303, and RG304 peptides, in all cell lines (Figure 6.3). However, the uptake of the particular peptide is significantly different in different cell types. The cellular uptake of RG301 peptide was around two times more in breast cancer (MDA-MB-231) cells compared to cervical cancer (HeLa) and human embryonic kidney (HEK-293) cells.

Further, the cellular internalization of RG301 and RG302 peptides was confirmed by confocal laser scanning microscopy in MDA-MB-231 and HeLa cells. The cellular uptake of both peptides RG301 and RG302 was evident but, with diffused and vesicular patterns in the cytosol (Figure 6.4). This suggests that the peptides don't show any selectivity to a particular subcellular compartment, indicating a cellular uptake through a membrane-based mechanism (*159*). Thus, organelle-specific uptake studies were not undertaken further in the present work.

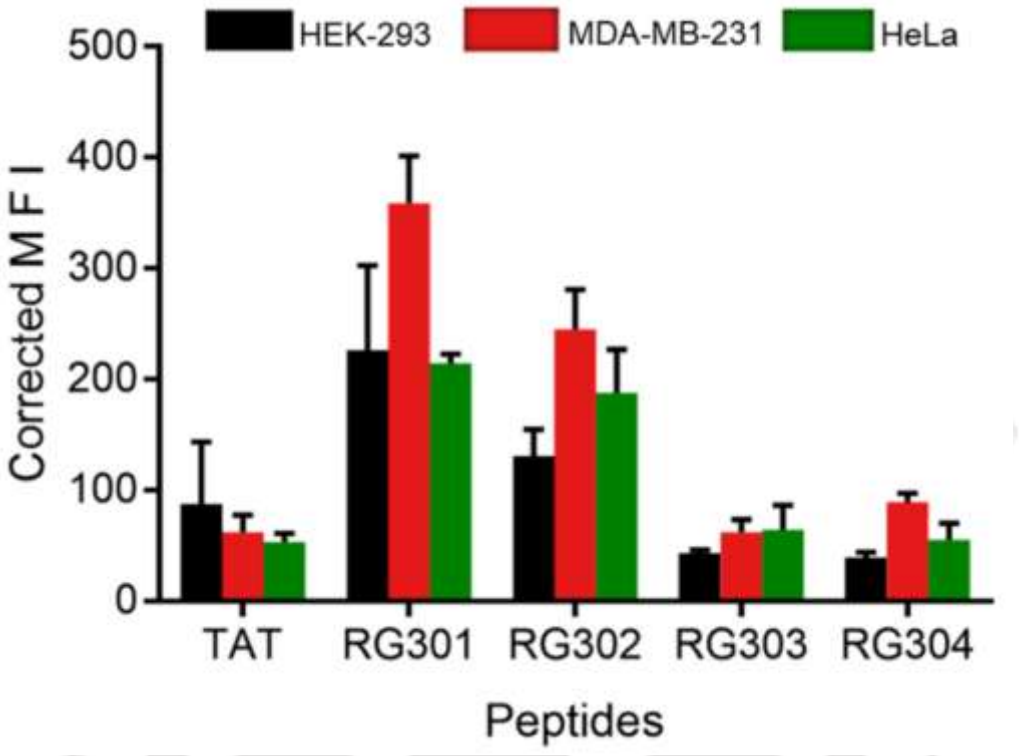

Figure 6.3. Cellular uptake of the designed peptides. *The comparative uptake of peptides in breast cancer (MDA-MB-231) cells, cervical cancer (HeLa) cells, and human embryonic kidney (HEK-293) cells using flow cytometry. All cells were incubated with 10 µM of CF-tagged peptides (TAT, RG301-RG304) in serum-free DMEM for 4 h at 37 °C and analyzed using flow cytometry. Corrected MFI represents Mean Fluorescence Intensity. Results are presented as mean ± SD of three independent experiments.*

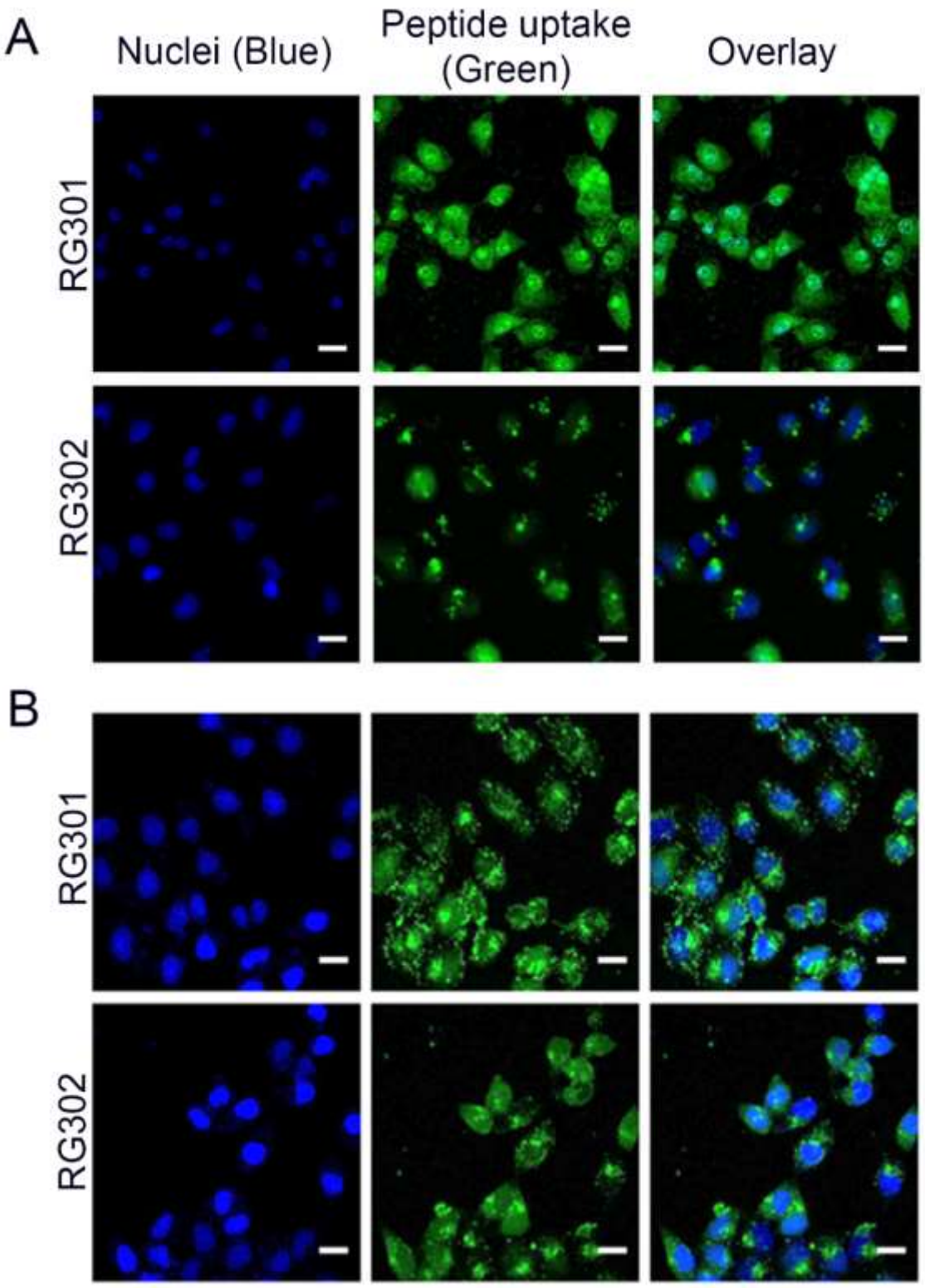

Figure 6.4. Cellular uptake of designed peptides. *The cellular internalization of designed peptides was observed in (A) MDA-MB-231 and (B) HeLa cells after treatment with 10 µM of peptides for four hours at 37°C. Scale bar corresponds to 20 µm.*

6.3.5. Mechanism of cellular uptake

Cell penetrating peptides are known to internalize majorly through two pathways, i.e., direct membrane translocation and/or endocytosis (*74, 160*). The mentioned uptake mechanisms are influenced by variables like temperature, size of cargo, available energy to cells, and cell types (*74*). Generally, the cellular uptake of peptides occurs by both membrane-mediated and endocytic mechanisms at physiological temperature (37°C), whereas, at low temperatures (<10°C), mostly membrane translocation is involved. Endocytosis is an energy-driven process but, in case of energy depleted conditions, the cellular uptake get switched to passive membrane translocation pathway. The blocking conditions for one particular pathway, forces the cells to continue peptide uptake through the active alternate pathway.

In our study, we tried to investigate the mechanism of cellular uptake of two best performing peptides (RG301 and RG302) by comparing their uptake in two cell lines MDA-MB-231 and HeLa, under different conditions of temperature and energy availability using fluorescence spectroscopy. Firstly, both the cell lines were treated with 5 µM of CF-tagged RG301 and RG302 peptides for 1 h at 4°C and 37°C. Secondly, we treated both cell lines with 0.1% sodium azide at 37°C for 1 h before peptide treatment. Sodium azide reduces the energy available to the cells (*161*). After sodium azide treatment, cells were treated with 5 µM of the same peptides for 1 h at 37°C. We compared the cellular uptake of test conditions with the untreated cells maintained at 37°C (control). A reduced cellular uptake was observed for both peptides in both treatment conditions (Figure 6.5). At 4°C, the uptake was reduced to nearly 50% in both cell types, whereas the cellular uptake of peptides gets reduced to only 25% in the sodium azide treated conditions. The reduced uptake at both treatment conditions of low temperature and energy availability suggests the following- (i) inhibition of energy-dependent endocytic pathway (*155*) and (ii) restriction in membrane dynamics affecting the permeation properties (*74, 156, 162*). The obtained results indicate that multiple paths of endocytosis and membrane translocation are involved in the uptake of designed peptides, and are similar to our earlier reports (*130*). These observations of involvement of multiple pathways for the peptide uptake in cells might be responsible for their diffused and vesicular patterns in cytosols, as observed by confocal imaging in section 6.3.4.

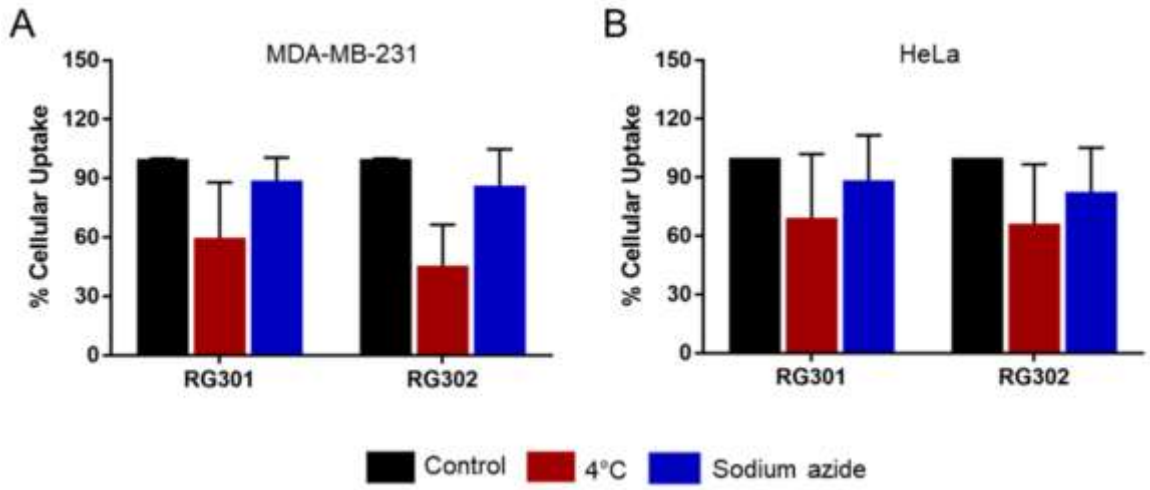

Figure 6.5. Cellular uptake of designed peptides. *(A) Breast (MDA-MB-231) and (B) cervical cancer (HeLa) cells were treated with 5 µM of CF-tagged designed peptides for one hour in different temperature condition and in the presence of sodium azide. The cellular uptake of designed peptides in both cell lines gets reduced to 40-50% at the low-temperature variable condition. However, the peptide uptake in the presence of sodium azide was just reduced to 70-80% of the control.*

6.3.6. Biocompatibility of designed peptides

The functional activity of peptides in the presence of serum is an important limitation for their development as drug delivery vectors. Keeping this in mind, we tested the peptide uptake after treating them with fetal bovine serum (FBS). MDA-MB-231, HeLa, and HEK-293 cells were treated with 10 µM of serum pre-treated and untreated peptides for four hours. We observed that the uptake of the peptide is similar in both conditions, indicating the biocompatibility of peptides in the serum. (Figure 6.6). In general, all peptides retained more than 90% functional activity after the serum treatment except in the case of RG301/RG302 peptides, where it varies between 60-90% for MDA-MB-231 and HeLa cells. This indicates that the serum components do not obstruct the cellular uptake of peptides completely, which suggests that the peptides can sustain the serum treatment without much compromising the functional properties.

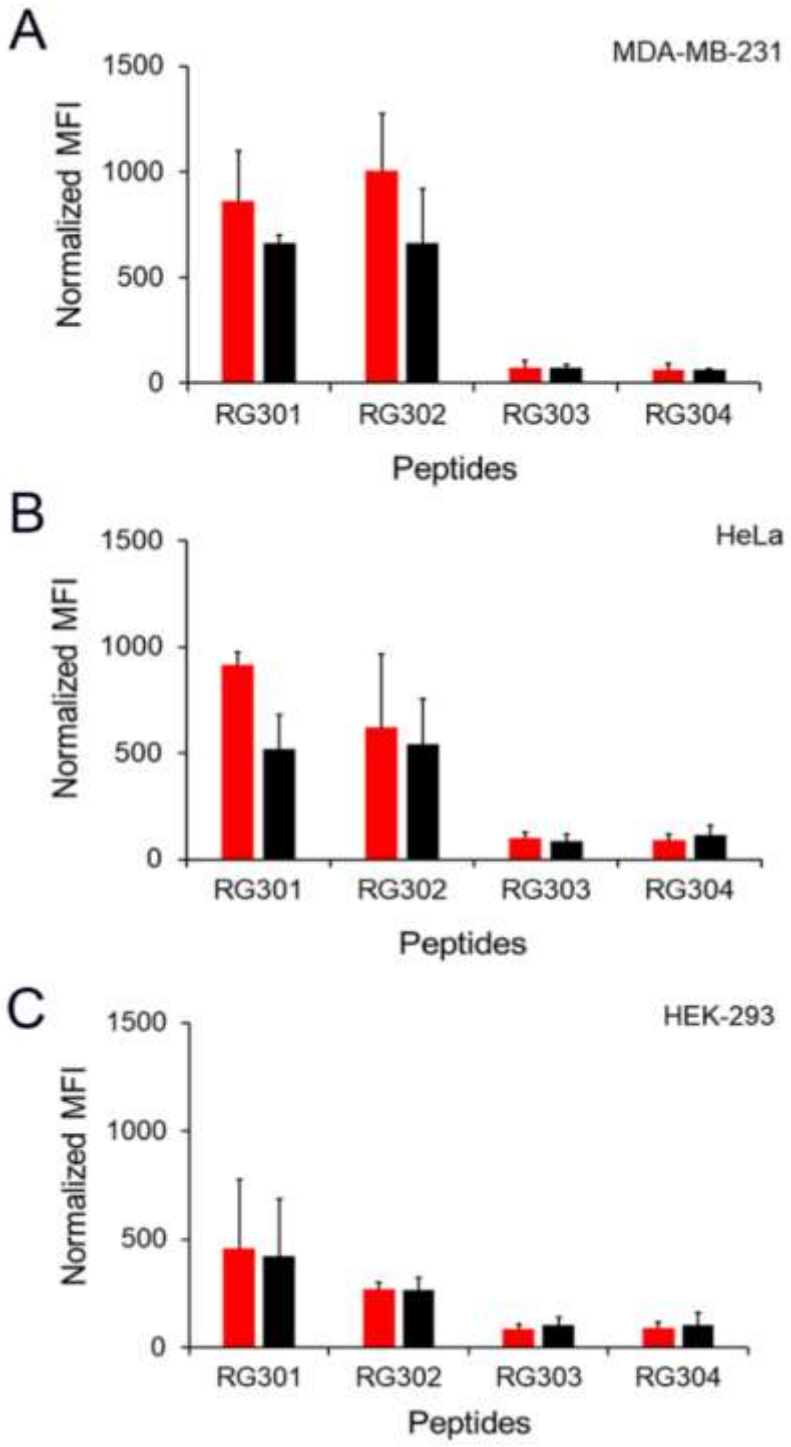

Figure 6.6. Biocompatibility of the designed peptides. *Cellular uptake of designed peptides in the presence of serum was verified in (A) MDA-MB-231, (B) HeLa and (C) HEK-293 cells after treatment with 10 µM of designed peptides in serum and serum-free conditions. The uptake by all peptides in both conditions suggests that the serum presence in the media doesn't hinder their activity.*

6.3.7. Cytotoxicity of the designed peptides

The toxicity of methotrexate, designed peptides, and peptide-methotrexate conjugates was tested with MDA-MB-231, HeLa, and HEK-293 cells. The reduced toxicity of peptide conjugates to HEK-293 cells compared to MDA-MB-231 cells suggest a selective uptake by MDA-MB-231 cells (Figure 6.7). In case of all four designed peptides, their peptide-MTX conjugates are more cytotoxic compared to MTX drug alone against MTX-resistant MDA-MB-231 cells (*132*). Even at 5 µM concentration of RG301-MTX and RG302-MTX conjugates, the cell viability of MDA-MB-231 cells gets reduced to around 50% compared to their respective peptides and MTX drug unlike in HeLa and HEK-293 cells. Also, at 50 µM concentration treatment of RG301-MTX peptide, there is only 3% MDA-MB-231 viable cells, unlike in HeLa and HEK-293 cells. This observation indicates that there is selective uptake of RG301 peptide by MDA-MB-231 cells. This also suggests that the peptides itself act as the vector to increase MTX bioavailability in MDA-MB-231 cells. Noticeably, among these four molecules of Series-3, RG301, and RG302 peptide conjugates showed more toxicity in cells compared to RG303 and RG304. (Figure 6.7).

As observed by MTT assay, there is around 97% cell death of MDA-MB-231 cells after 48 h treatment with 50 µM of RG301-MTX peptide conjugate. This impelled us to verify the apoptotic cellular toxicity of this peptide in MDA-MB-231 cells using Annexin V and Propidium Iodide (PI) staining. The results of Annexin V and PI staining showed around 81% late apoptotic cells after treatment of RG301-MTX peptide conjugate, which suggests that the peptide-MTX conjugates are able to induce apoptosis but also, disrupts the membrane integrity being penetrating peptides (Figure 6.8).

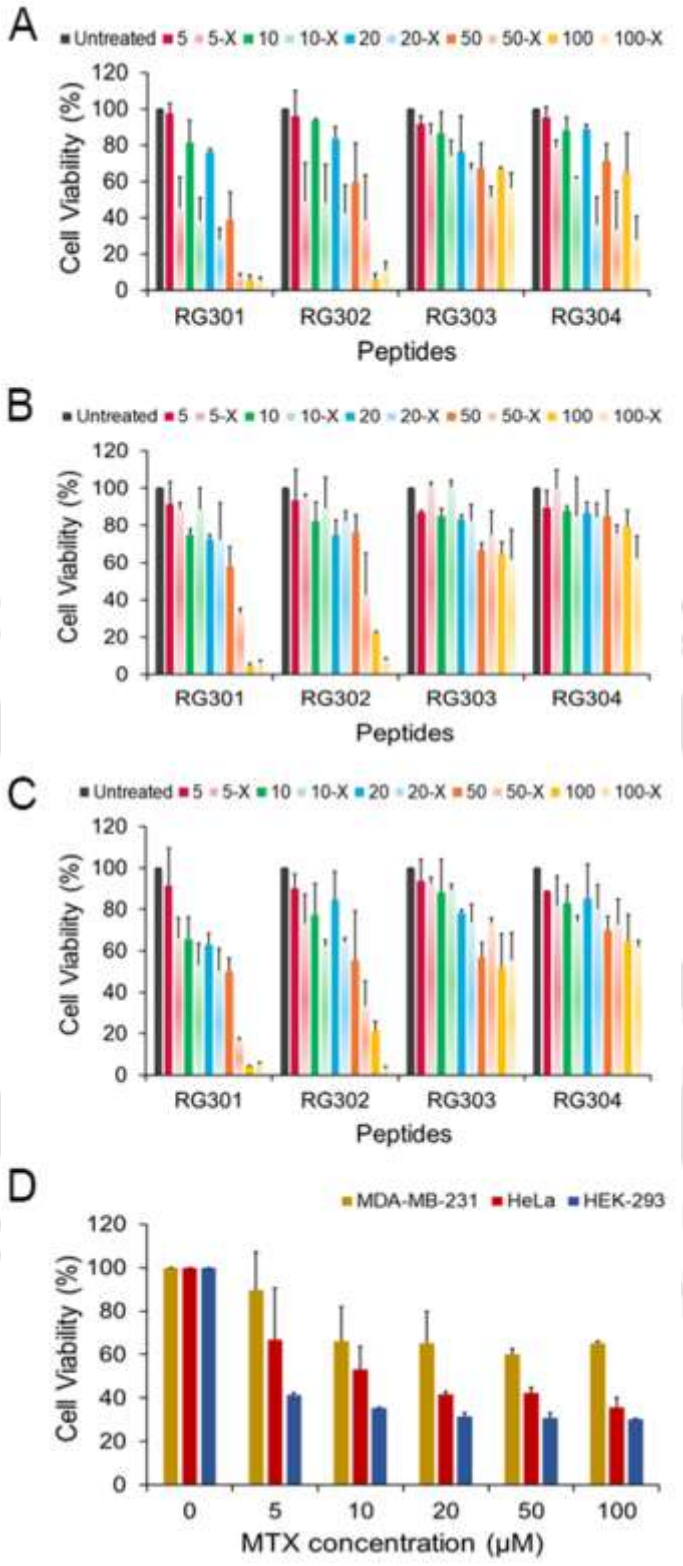

Figure 6.7. Cytotoxicity of designed peptides using MTT assay. *(A) MDA-MB-231, (B) HeLa and (C) HEK-293 cells were treated with varying concentrations of peptides (n) and peptide-methotrexate (n-X) conjugates for 48 h at 37°C in serum-free conditions. (D) Cell viability of all cell types after similar treatment to them by only standard drug methotrexate (MTX). (n = 5 μM, 10 μM 20 μM, 50 μM and 100 μM).*

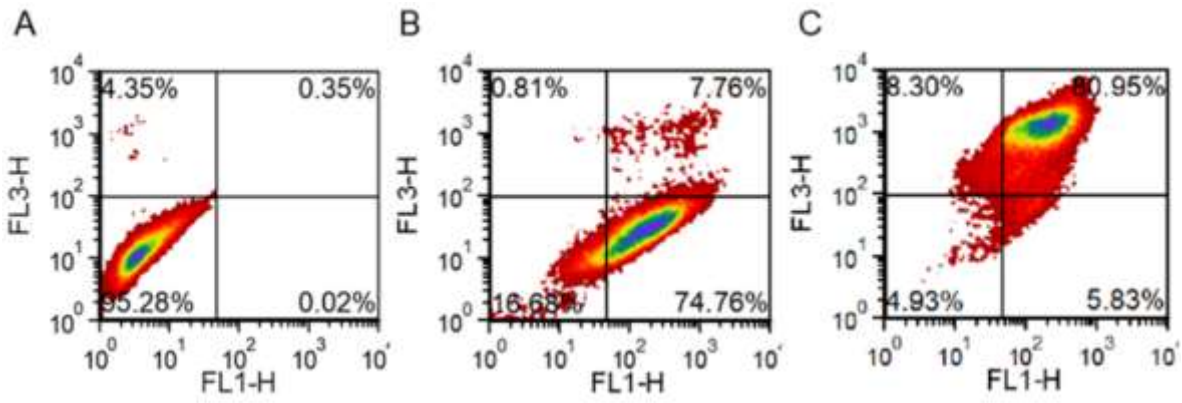

Figure 6.8. Annexin V-PI Cytotoxicity assay. *Flow cytometry analysis of Annexin-PI stained MDA-MB-231 cells after 48 h treatment with MTX drug and RG301-MTX conjugate at 50 µM concentration. (A) No treatment, (B) MTX treatment, and (C) RG301-MTX conjugate treated cells were harvested and stained with Annexin V and PI before analysis. FL1-H represents FITC labeled Annexin-V staining, and FL3-H represents PI staining.*

6.3.8. Hemotoxicity of designed peptides

The extent of hemotoxicity has been performed against human RBCs at 100 µM concentration of peptides and peptide-MTX conjugates. In our study, the heme release measured at 540 nm after treating human RBCs is less than 4% in all test molecules, indicating the non-hemolytic nature of the designed peptides and their peptide-MTX conjugates (Figure 6.9).

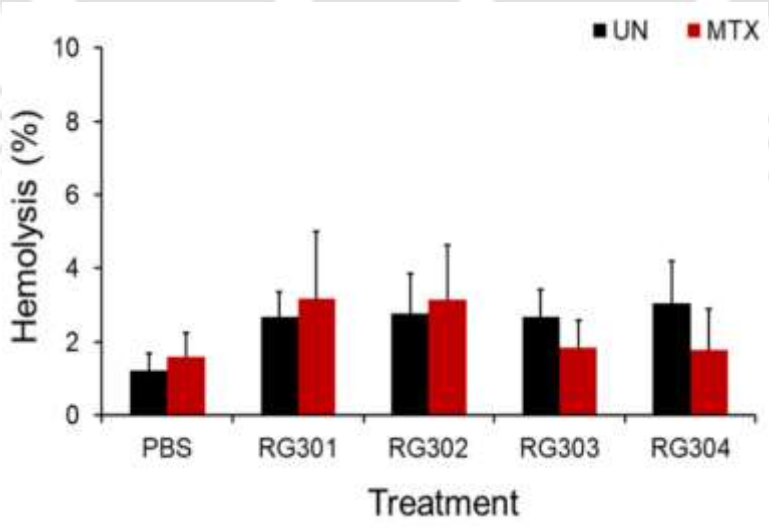

Figure 6.9. Hemotoxicity of peptides. *Hemolytic assay of the designed peptides (UN) and their MTX conjugates (MTX) at 100 µM for 2 h at 37°C against human red blood corpuscles (RBCs). The data was normalized by complete lysis with 0.5 % of Triton X-100. All results are presented as the mean ± SD of three independent experiments.*

6.3.9. Penetration in 3D tumorospheres

Inspired by the differential cellular uptake of the designed peptides, we further evaluated their ability to penetrate MDA-MB-231 tumorospheres. The three-dimensional growth of cells in tumorospheres resembles the tumor architecture and microenvironment heterogeneity. Tumorospheres were treated with CF-tagged RG301 peptide for four hours at 37°C and imaged by confocal microscopy using the Z-scan model. The obtained volume projections illustrate the peptide uptake in tumorospheres up to 50 μm depth from the surface, clearly indicating their ability to penetrate into 3D tumor-like architectures. This connotes their potential for targeting tumor vasculatures as such. The results of peptide penetration are also presented by the depth coded color, which corresponds to the depth of the obtained green fluorescence signal (Figure 6.10). This experiment prompted us to explore further their utility for developing them as a therapeutic option.

6.4. CONCLUSION

In the last three decades, the development of various chemotherapeutic agents for cancer diagnosis and treatment has accelerated as a result of the committed efforts from the scientific community. Tumor homing peptides (THPs) are receiving more attention due to the receptor-mediated specificity in recognition of cancer cells. In addition to this, cell penetrating peptides (CPPs) are regarded as the trojan horses for their ability to deliver large cargoes inside cells. In the present work, we attempted to create the fusion product of tumor homing and cell penetrating peptides with an aim to improve selective targeting and penetration in tumors. The addition of the cationic amphipathic syndiotactic segment in the tumor homing peptide has remarkably enhanced the penetrating properties of the parent peptide. Flow cytometry results clearly show around a 10-fold difference of RG301 and RG302 peptide uptake compared to the positive control TAT peptide and other two RG303 and RG304 designed peptides. The experiments related to cellular uptake, mechanism of uptake, and toxicity suggest the selective uptake of RG301 peptide in MDA-MB-231 cells. In addition to this, the minimal toxicity to RBCs confirms its therapeutic safety. The major limitation of any delivery vector is the penetration in tumor vasculatures. Confocal imaging in three-dimensional cultures of MDA-MB-231 cells confirms the penetrative ability of RG301 peptide, indicating that this could be

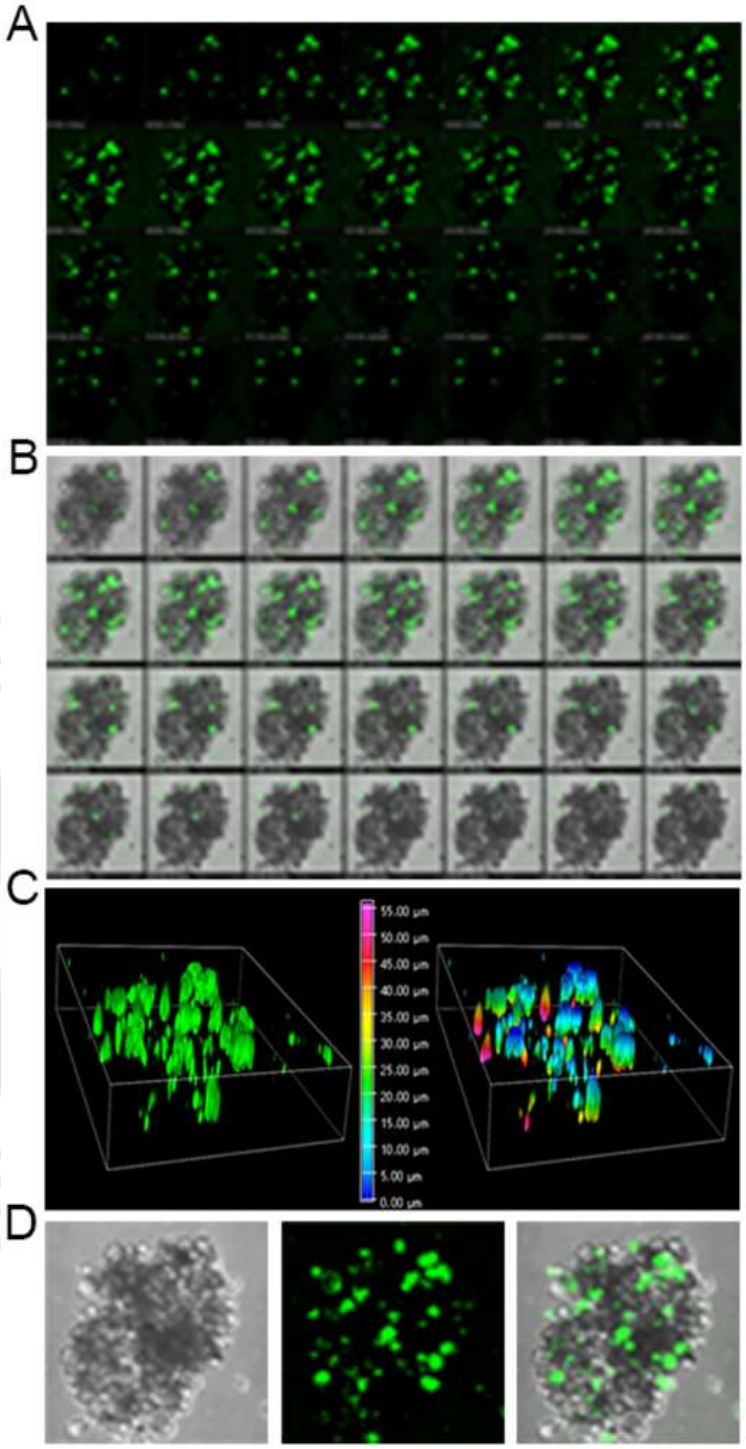

Figure 6.10. Peptide uptake in 3D cultures. *MDA-MB-231 tumorospheres were treated with CF-tagged RG301 peptide for 4 h at 37°C. After treatment, the tumorospheres were washed and imaged using a confocal microscope. (A) Peptide fluorescence acquired from different planes of the tumorosphere. (B) Peptide fluorescence merged with Bright field images of each plane to distinctly represent peptide uptake. (C) Three-dimensional view of peptide uptake in tumorosphere. (D) Maximum intensity projection images for the same tumorosphere to show the tumorosphere areas with peptide uptake.*

developed as a tumor penetrating peptide (TPP) as well. The experiments on tumorigenic animal models to verify the selective penetrating and anti-cancer nature of RG301 peptide are yet to be performed in the subsequent works. Taken together, this piece of work shows the importance of amino acid composition, stereochemistry, and amphipathicity in tuning the electrostatics of the delivery vectors for better selectivity and efficacy.

7

Conclusions and Future Directions

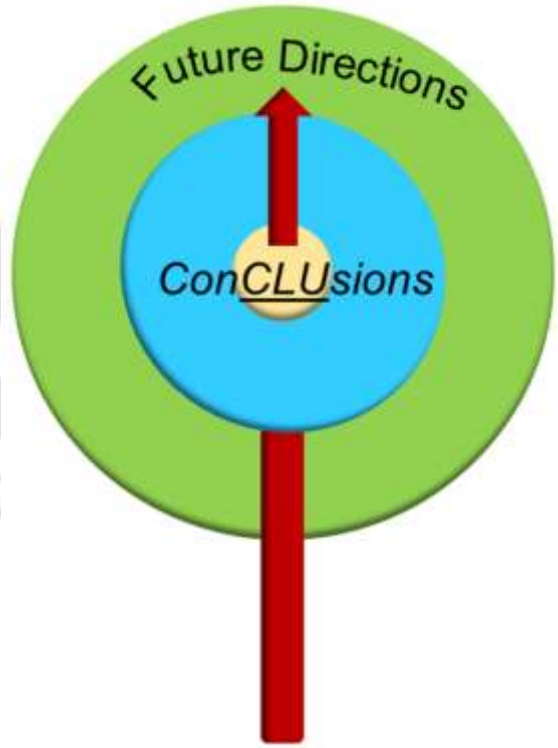

7.1. GEOMETRICALLY DIRECTED DELIVERY VECTORS

The drug delivery application of peptides facilitates the development of therapeutically safe molecules. In the present thesis, we rationally designed three peptide series having a total of sixteen peptide molecules, each encoded with distinct design ideas for targeted drug delivery. The systemic development of Series-1 to Series-2 to Series-3 peptides, underlines the story of a design evolution starting from structural engineering of a peptide molecule in a geometrical space, culminating in the generation of a complete drug delivery vector.

From the design perspective:

- The first series of peptides (chapter 4) reveals the possibility of an 'informed walk' across Ramachandran geometrical space in search of conformational lockers. This is the first attempt to make tumor homing 'programmable' by permuting and fixing the topology of RGD and QGR motifs through the extensive modeling of RXD/QXR trimers, as discussed in chapter 3. It offers a space for conceptual innovations in drug design at the conformational level.

- The second series of peptides (chapter 5) shows the development of initial designs through the incorporation of cationic amphipathic tails. The resultant electrostatic fingerprint of each molecule is different from the parent molecule, which, subsequently, is evident from the downstream experiments of cellular uptake and toxicity studies.

- The third series of peptides (chapter 6) is an attempt to construct the tumor penetrating peptides. In this series of peptide design, the homing peptides are linked with the previously designed syndiotactic penetrating domain (unpublished data). The guided integration of the cationic amphipathic domain to the homing segment enhanced the selective uptake in cancer cell types. Electrostatic profiling shows that there is a distinct distribution of cationic and hydrophobic zone in the designed peptides, which may help in interacting with the cellular membranes.

Further, secondary structure characterization routines suggest that the designed peptides of each series are distinctly different in their conformations, as envisaged by the design. The

experiments related to peptide uptake and toxicity showed that each designed peptide has its unique behavior for a particular cell type. For example, the poly-D peptides (RG103 and RG105) display the minimal cellular binding or uptake, indicating the stereochemistry influenced change in the functional behavior of peptides. The designed peptides displayed differential cellular uptake in cancerous cell types, revealing their potential for selective targeting. This corroborates our hypothesis that the topological specifications coded in the peptide design and the resulting electrostatic fingerprint play a critical role while interacting with the cell surface. All members in the designed peptide series retained their functional activity in serum, indicating their biocompatible nature and showed negligible toxicity to mammalian red blood corpuscles (RBCs). Improved cytotoxicity to MTX resistant breast cancer (MDA-MB-231) cells by peptide-MTX conjugates, compared to the free MTX or THPs, guarantees the enhanced drug accumulation in cells, leading to the effective delivery of the designed molecules. Further, ratiometric fluorescence-based assay and Annexin V-Propidium Iodide (PI) staining, confirms that the anticancer activity of peptides is induced by apoptosis, a desirable trait for a typical drug delivery vehicle. The study with the clinical isolates confirmed that the topological signatures encoded in the design of series-1 peptides have manifested as differential binding to normal and tumor tissues. In a nutshell, the topology and electrostatics of peptides were tuned by applying the knowledge of Ramachandran map, torsional angle modifications, and stereochemistry with an aim to design selective drug delivery vectors.

7.2. PHILOSOPHICAL OUTCOME (SIGNIFICANCE)

Targeted drug delivery in oncology research has offered plenty of space to develop new therapeutic agents for treating resistant cancers. The present study contributed to the development of topologically constrained tumor homing peptides for targeted delivery by an 'informed walk' across peptide geometrical space. This creates a scope for conceptual innovations in drug design at the conformational level. Validation of the engineered molecules employing biophysical techniques, mammalian cell culture routines, and clinical examination suggest that the designed peptides homes effectively to cancerous cells and possess a strong anti-cancer effect through apoptosis. Moreover, the differential binding of the designed molecules in clinical samples corroborates their selectivity towards cancer

tissues. This study unfolds the possibility of engineering biological molecules using geometrical directives for cellular targeting and drug delivery. The unique feature of this study is that it offers a new design protocol for the generation of delivery vectors encoded with 'cell type' specificity.

The underlying philosophy in encoding a three-bodied functionary as a homing domain, penetrating domain, and cytotoxic agent originated from the model of a chariot explained in kathopanishad (91.3.3-4) [v21]. The Upaniṣhads say: there is a chariot, having five horses pulling it; the horses have their respective reins in their mouths, which are in the hands of a charioteer. Then there is a passenger sitting at the seat of the chariot. The passenger instructs the charioteer, who controls the reins and guide the horses in the intended direction to the designed destination (*163, 164*). We have a homing domain (H) controlling the reins like a charioteer, a penetrating domain in a chariot (P), and a passenger drug molecule (D) (Figure 7.1).

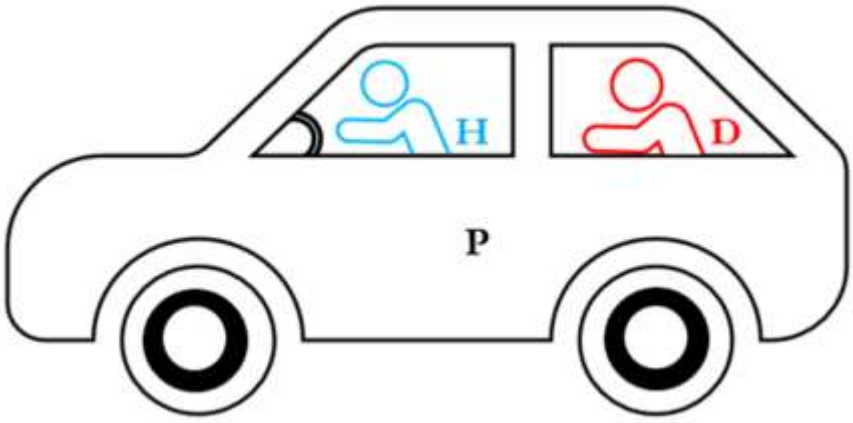

Figure 7.1. Schematic representation of overall philosophy. *H: Homing Domain, P: Penetrating Domain, and D: Drug molecule.*

7.3. FUTURE DIRECTIONS

Peptide therapies are already working well in the pharmaceutical market. This study presents the scope for the development of the designed peptide-based vectors as targeted therapies. The major future objectives include but are not limited to, the following:

- *In vivo* investigations on the bio-distribution and anti-cancer properties of the designed peptide-based vectors in cancer models.

- Development of peptide-based penetrating domains for solid and resistant tumors.
- Extension to clinical studies to graduate from a proof of concept investigation to a therapeutic solution.
- Translation of preclinical results to the pharmaceutical industry for clinical development.
- Conceptual emergence of a peptide design platform for therapeutic peptides.

REFERENCES

(1) Packer, L. (1968) Molecular Insights Into the Living Process. David E. Green , Robert F. Goldberger. *The Quarterly Review of Biology 43*, 70-71.

(2) Banting, F. G., Best, C. H., Collip, J. B., Campbell, W. R., and Fletcher, A. A. (1922) Pancreatic Extracts in the Treatment of Diabetes Mellitus. *Can Med Assoc J 12*, 141-146.

(3) Sawyer, T. K. (2017) Renaissance in peptide drug discovery: the third wave.

(4) Mukherjee, S. (2010) *The emperor of all maladies: a biography of cancer*, Simon and Schuster.

(5) Bray, F., Ferlay, J., Soerjomataram, I., Siegel, R. L., Torre, L. A., and Jemal, A. (2018) Global cancer statistics 2018: GLOBOCAN estimates of incidence and mortality worldwide for 36 cancers in 185 countries. *CA: A Cancer Journal for Clinicians 68*, 394-424.

(6) Le Joncour, V., and Laakkonen, P. (2018) Seek & Destroy, use of targeting peptides for cancer detection and drug delivery. *Bioorganic & medicinal chemistry 26*, 2797-2806.

(7) Gautam, A., Kapoor, P., Chaudhary, K., Kumar, R., and Raghava, G. P. (2014) Tumor homing peptides as molecular probes for cancer therapeutics, diagnostics and theranostics. *Current medicinal chemistry 21*, 2367-91.

(8) Hatley, R. J. D., Macdonald, S. J. F., Slack, R. J., Le, J., Ludbrook, S. B., and Lukey, P. T. (2018) An alphav-RGD Integrin Inhibitor Toolbox: Drug Discovery Insight, Challenges and Opportunities. *Angewandte Chemie (International ed. in English) 57*, 3298-3321.

(9) Green, M., and Loewenstein, P. M. (1988) Autonomous functional domains of chemically synthesized human immunodeficiency virus tat trans-activator protein. *Cell 55*, 1179-1188.

(10) Frankel, A. D., and Pabo, C. O. (1988) Cellular uptake of the tat protein from human immunodeficiency virus. *Cell 55*, 1189-1193.

(11) Derossi, D., Joliot, A. H., Chassaing, G., and Prochiantz, A. (1994) The third helix of the Antennapedia homeodomain translocates through biological membranes. *Journal of Biological Chemistry 269*, 10444-10450.

(12) Wang, Y., Cheetham, A. G., Angacian, G., Su, H., Xie, L., and Cui, H. (2017) Peptide-drug conjugates as effective prodrug strategies for targeted delivery. *Advanced drug delivery reviews 110-111*, 112-126.

(13) Craik, D. J., Fairlie, D. P., Liras, S., and Price, D. (2013) The future of peptide-based drugs. *Chem Biol Drug Des 81*, 136-47.

(14) Mas-Moruno, C., Rechenmacher, F., and Kessler, H. (2010) Cilengitide: the first anti-angiogenic small molecule drug candidate design, synthesis and clinical evaluation. *Anti-cancer agents in medicinal chemistry 10*, 753-68.

(15) Abdel-Rahman, H. M., Al-karamany, G. S., El-Koussi, N. A., Youssef, A. F., and Kiso, Y. (2002) HIV protease inhibitors: peptidomimetic drugs and future perspectives. *Current medicinal chemistry 9*, 1905-22.

(16) Kumar, A., and Ramakrishnan, V. (2010) Creating novel protein scripts beyond natural alphabets. *Systems and synthetic biology 4*, 247-56.

(17) Hazam, P. K., Jerath, G., Kumar, A., Chaudhary, N., and Ramakrishnan, V. (2017) Effect of tacticity-derived topological constraints in bactericidal peptides. *Biochim Biophys Acta Biomembr 1859*, 1388-1395.

(18) Hazam, P. K., Jerath, G., Chaudhary, N., and Ramakrishnan, V. (2018) Peptido-mimetic approach in the design of syndiotactic antimicrobial peptides. *International Journal of Peptide Research and Therapeutics 24*, 299-307.

(19) Handschumacher, R. E., Harding, M. W., Rice, J., Drugge, R. J., and Speicher, D. W. (1984) Cyclophilin: a specific cytosolic binding protein for cyclosporin A. *Science 226*, 544-547.

(20) Chang, Y. S., Graves, B., Guerlavais, V., Tovar, C., Packman, K., To, K.-H., Olson, K. A., Kesavan, K., Gangurde, P., and Mukherjee, A. (2013) Stapled α– helical peptide drug development: A potent dual inhibitor of MDM2 and MDMX for p53-dependent cancer therapy. *Proceedings of the National Academy of Sciences 110*, E3445-E3454.

(21) McCauley, J. A., and Rudd, M. T. (2016) Hepatitis C virus NS3/4a protease inhibitors. *Current opinion in pharmacology 30*, 84-92.

(22) Upadhyaya, P., Qian, Z., Selner, N. G., Clippinger, S. R., Wu, Z., Briesewitz, R., and Pei, D. (2015) Inhibition of Ras signaling by blocking Ras–effector interactions with cyclic peptides. *Angewandte Chemie International Edition 54*, 7602-7606.

(23) Koo, O. M., Rubinstein, I., and Onyuksel, H. (2005) Role of nanotechnology in targeted drug delivery and imaging: a concise review. *Nanomedicine: Nanotechnology, Biology and Medicine 1*, 193-212.

(24) Del Pozo, E., Schluter, K., and Neufeld, M. (1986) Endocrine profile and pharmacokinetics of the new somatostatin analog SMS 201-995. *Acta Endocrinol (Copenh)*.

(25) Begum, A. A., Moyle, P. M., and Toth, I. (2016) Investigation of bombesin peptide as a targeting ligand for the gastrin releasing peptide (GRP) receptor. *Bioorganic & medicinal chemistry 24*, 5834-5841.

(26) Mansi, R., Wang, X., Forrer, F., Kneifel, S., Tamma, M.-L., Waser, B., Cescato, R., Reubi, J. C., and Maecke, H. R. (2009) Evaluation of a 1, 4, 7, 10-Tetraazacyclododecane-1, 4, 7, 10-Tetraacetic acid–conjugated bombesin-based radioantagonist for the labeling with single-photon emission computed tomography, positron emission tomography, and therapeutic radionuclides. *Clinical cancer research 15*, 5240-5249.

(27) Parry, J. J., Andrews, R., and Rogers, B. E. (2007) MicroPET imaging of breast cancer using radiolabeled bombesin analogs targeting the gastrin-releasing peptide receptor. *Breast cancer research and treatment 101*, 175-183.

(28) Yang, Q., Zhang, F., Ding, Y., Huang, J., Chen, S., Wu, Q., Wang, Z., and Chen, C. (2014) Antitumour activity of the recombination polypeptide GST-NT21MP is mediated by inhibition of CXCR4 pathway in breast cancer. *British journal of cancer 110*, 1288.

(29) Bumpers, H., Huang, M.-B., Katkoori, V., Manne, U., and Bond, V. (2013) Nef-M1, a CXCR4 peptide antagonist, enhances apoptosis and inhibits primary tumor growth and metastasis in Breast Cancer. *Journal of cancer therapy 4*, 898.

(30) Katkoori, V. R., Basson, M. D., Bond, V. C., Manne, U., and Bumpers, H. L. (2015) Nef-M1, a peptide antagonist of CXCR4, inhibits tumor angiogenesis and epithelial-to-mesenchymal transition in colon and breast cancers. *Oncotarget 6*, 27763.

(31) Mercurio, L., Ajmone-Cat, M. A., Cecchetti, S., Ricci, A., Bozzuto, G., Molinari, A., Manni, I., Pollo, B., Scala, S., and Carpinelli, G. (2016) Targeting CXCR4 by a selective peptide antagonist modulates tumor microenvironment and microglia reactivity in a human glioblastoma model. *Journal of experimental & clinical cancer research 35*, 55.

(32) Hunt, J. F., Rath, P., Rothschild, K. J., and Engelman, D. M. (1997) Spontaneous, pH-dependent membrane insertion of a transbilayer α-helix. *Biochemistry 36*, 15177-15192.

(33) Al-Ahmady, Z. S., Al-Jamal, W. T., Bossche, J. V., Bui, T. T., Drake, A. F., Mason, A. J., and Kostarelos, K. (2012) Lipid–peptide vesicle nanoscale hybrids for triggered drug release by mild hyperthermia in vitro and in vivo. *ACS nano 6*, 9335-9346.

(34) Na, K., Jung, J., Lee, J., and Hyun, J. (2010) Thermoresponsive pore structure of biopolymer microspheres for a smart drug carrier. *Langmuir 26*, 11165-11169.

(35) Eberle, A. N., Bapst, J.-P., Calame, M., Tanner, H., and Froidevaux, S. (2010) MSH radiopeptides for targeting melanoma metastases, in *Melanocortins: Multiple Actions and Therapeutic Potential* pp 133-142, Springer.

(36) Ren, G., Liu, Z., Miao, Z., Liu, H., Subbarayan, M., Chin, F. T., Zhang, L., Gambhir, S. S., and Cheng, Z. (2009) PET of malignant melanoma using 18F-labeled metallopeptides. *Journal of Nuclear Medicine 50*, 1865-1872.

(37) Koivunen, E., Wang, B., and Ruoslahti, E. (1995) Phage libraries displaying cyclic peptides with different ring sizes: ligand specificities of the RGD-directed integrins. *Bio/technology 13*, 265.

(38) Varner, J. A., and Cheresh, D. A. (1996) Integrins and cancer. *Current opinion in cell biology 8*, 724-730.

(39) Askoxylakis, V., Zitzmann, S., Mier, W., Graham, K., Krämer, S., von Wegner, F., Fink, R. H., Schwab, M., Eisenhut, M., and Haberkorn, U. (2005) Preclinical evaluation of the breast cancer cell-binding peptide, p160. *Clinical cancer research 11*, 6705-6712.

(40) Sugahara, K. N., Teesalu, T., Karmali, P. P., Kotamraju, V. R., Agemy, L., Girard, O. M., Hanahan, D., Mattrey, R. F., and Ruoslahti, E. (2009) Tissue-penetrating delivery of compounds and nanoparticles into tumors. *Cancer cell 16*, 510-520.

(41) Liu, C., Yang, Y., Chen, L., Lin, Y.-L., and Li, F. (2014) A unified mechanism for aminopeptidase N-based tumor cell motility and tumor-homing therapy. *Journal of Biological Chemistry 289*, 34520-34529.

(42) Pasqualini, R., Koivunen, E., Kain, R., Lahdenranta, J., Sakamoto, M., Stryhn, A., Ashmun, R. A., Shapiro, L. H., Arap, W., and Ruoslahti, E. (2000) Aminopeptidase N is a receptor for tumor-homing peptides and a target for inhibiting angiogenesis. *Cancer research 60*, 722-727.

(43) Corti, A., and Curnis, F. (2011) Tumor vasculature targeting through NGR peptide-based drug delivery systems. *Current pharmaceutical biotechnology 12*, 1128-1134.

(44) Corti, A., Gasparri, A. M., Ghitti, M., Sacchi, A., Sudati, F., Fiocchi, M., Buttiglione, V., Perani, L., Gori, A., Valtorta, S., Moresco, R. M., Pastorino, F., Ponzoni, M., Musco, G., and Curnis, F. (2017) Glycine N-Methylation in NGR-Tagged Nanocarriers Prevents Isoaspartate Formation and Integrin Binding without Impairing CD13 Recognition and Tumor Homing. *Advanced Functional Materials 27*, 1701245.

(45) Enyedi, K. N., Tóth, S., Szakács, G., and Mező, G. (2017) NGR-peptide–drug conjugates with dual targeting properties. *PLOS ONE 12*, e0178632.

(46) Qiu, L., Hu, Q., Cheng, L., Li, L., Tian, C., Chen, W., Chen, Q., Hu, W., Xu, L., Yang, J., Cheng, L., and Chen, D. (2016) cRGDyK modified pH responsive nanoparticles for specific intracellular delivery of doxorubicin. *Acta Biomater 30*, 285-298.

(47) Zhang, L., Giraudo, E., Hoffman, J. A., Hanahan, D., and Ruoslahti, E. (2006) Lymphatic zip codes in premalignant lesions and tumors. *Cancer research 66*, 5696-5706.

(48) Laakkonen, P., Porkka, K., Hoffman, J. A., and Ruoslahti, E. (2002) A tumor-homing peptide with a targeting specificity related to lymphatic vessels. *Nature medicine 8*, 751.

(49) Laakkonen, P., Åkerman, M. E., Biliran, H., Yang, M., Ferrer, F., Karpanen, T., Hoffman, R. M., and Ruoslahti, E. (2004) Antitumor activity of a homing peptide that targets tumor lymphatics and tumor cells. *Proceedings of the National Academy of Sciences 101*, 9381-9386.

(50) Yao, V. J., Ozawa, M. G., Trepel, M., Arap, W., McDonald, D. M., and Pasqualini, R. (2005) Targeting pancreatic islets with phage display assisted by laser pressure catapult microdissection. *The American journal of pathology 166*, 625-636.

(51) Fukumura, D., and Jain, R. K. (2007) Tumor microvasculature and microenvironment: targets for anti-angiogenesis and normalization. *Microvascular research 74*, 72-84.

(52) Christian, S., Pilch, J., Akerman, M. E., Porkka, K., Laakkonen, P., and Ruoslahti, E. (2003) Nucleolin expressed at the cell surface is a marker of endothelial cells in angiogenic blood vessels. *The Journal of cell biology 163*, 871-878.

(53) Shibata, Y., Muramatsu, T., Hirai, M., Inui, T., Kimura, T., Saito, H., McCormick, L. M., Bu, G., and Kadomatsu, K. (2002) Nuclear targeting by the growth factor midkine. *Molecular and cellular biology 22*, 6788-6796.

(54) Said, E. A., Krust, B., Nisole, S., Svab, J., Briand, J.-P., and Hovanessian, A. G. (2002) The anti-HIV cytokine midkine binds the cell surface-expressed nucleolin as a low affinity receptor. *Journal of Biological Chemistry 277*, 37492-37502.

(55) Cherukuri, S., Hock, R., Ueda, T., Catez, F., Rochman, M., and Bustin, M. (2008) Cell cycle-dependent binding of HMGN proteins to chromatin. *Molecular biology of the cell 19*, 1816-1824.

(56) Drecoll, E., Gaertner, F. C., Miederer, M., Blechert, B., Vallon, M., Müller, J. M., Alke, A., Seidl, C., Bruchertseifer, F., and Morgenstern, A. (2009) Treatment of peritoneal carcinomatosis by targeted delivery of the radio-labeled tumor homing peptide 213Bi-DTPA-[F3] 2 into the nucleus of tumor cells. *PLoS One 4*, e5715.

(57) Numata, K., Mieszawska-Czajkowska, A. J., Kvenvold, L. A., and Kaplan, D. L. (2012) Silk-based nanocomplexes with tumor-homing peptides for tumor-specific gene delivery. *Macromolecular bioscience 12*, 75-82.

(58) Kumar, A., Ma, H., Zhang, X., Huang, K., Jin, S., Liu, J., Wei, T., Cao, W., Zou, G., and Liang, X.-J. (2012) Gold nanoparticles functionalized with therapeutic and targeted peptides for cancer treatment. *Biomaterials 33*, 1180-1189.

(59) Lan, L., and Hin, C. C. (2013), Federation of American Societies for Experimental Biology.

(60) Lu, L., Li, Z. J., Li, L. F., Wu, W. K. K., Shen, J., Zhang, L., Chan, R. L. Y., Yu, L., Liu, Y. W., and Ren, S. X. (2015) Vascular-targeted TNFα improves tumor blood vessel function and enhances antitumor immunity and chemotherapy in colorectal cancer. *Journal of Controlled Release 210*, 134-146.

(61) Li, Z. J., Wu, W. K. K., Ng, S. S. M., Yu, L., Li, H. T., Wong, C. C. M., Wu, Y. C., Zhang, L., Ren, S. X., and Sun, X. G. (2010) A novel peptide specifically targeting the vasculature of orthotopic colorectal cancer for imaging detection and drug delivery. *Journal of Controlled Release 148*, 292-302.

(62) Wischnjow, A., Sarko, D., Janzer, M., Kaufman, C., Beijer, B., Brings, S., Haberkorn, U., Larbig, G., Kubelbeck, A., and Mier, W. (2016) Renal Targeting: Peptide-Based Drug Delivery to Proximal Tubule Cells. *Bioconjug Chem 27*, 1050-7.

(63) Zhao, J., Zhang, B., Shen, S., Chen, J., Zhang, Q., Jiang, X., and Pang, Z. (2015) CREKA peptide-conjugated dendrimer nanoparticles for glioblastoma multiforme delivery. *Journal of colloid and interface science 450*, 396-403.

(64) Okur, A. C., Erkoc, P., and Kizilel, S. (2016) Targeting cancer cells via tumor-homing peptide CREKA functional PEG nanoparticles. *Colloids and Surfaces B: Biointerfaces 147*, 191-200.

(65) Park, J. H., von Maltzahn, G., Zhang, L., Derfus, A. M., Simberg, D., Harris, T. J., Ruoslahti, E., Bhatia, S. N., and Sailor, M. J. (2009) Systematic surface engineering of magnetic nanoworms for in vivo tumor targeting. *Small (Weinheim an der Bergstrasse, Germany) 5*, 694-700.

(66) Guan, Y.-Y., Luan, X., Xu, J.-R., Liu, Y.-R., Lu, Q., Wang, C., Liu, H.-J., Gao, Y.-G., Chen, H.-Z., and Fang, C. (2014) Selective eradication of tumor vascular pericytes by peptide-conjugated nanoparticles for antiangiogenic therapy of melanoma lung metastasis. *Biomaterials 35*, 3060-3070.

(67) Lee, T.-Y., Lin, C.-T., Kuo, S.-Y., Chang, D.-K., and Wu, H.-C. (2007) Peptide-mediated targeting to tumor blood vessels of lung cancer for drug delivery. *Cancer research 67*, 10958-10965.

(68) He, X., Na, M.-H., Kim, J.-S., Lee, G.-Y., Park, J. Y., Hoffman, A. S., Nam, J.-O., Han, S.-E., Sim, G. Y., and Oh, Y.-K. (2011) A novel peptide probe for imaging and targeted delivery of liposomal doxorubicin to lung tumor. *Molecular pharmaceutics 8*, 430-438.

(69) Ho, I. A., Lam, P. Y., and Hui, K. M. (2004) Identification and characterization of novel human glioma-specific peptides to potentiate tumor-specific gene delivery. *Human gene therapy 15*, 719-732.

(70) Ho, I. A., Hui, K. M., and Lam, P. Y. (2010) Isolation of peptide ligands that interact specifically with human glioma cells. *Peptides 31*, 644-650.

(71) Vivès, E., Schmidt, J., and Pèlegrin, A. Cell Penetrating and Cell Targeting Peptides in Drug Delivery (revised version).

(72) Cheng, H., Zhu, J. Y., Xu, X. D., Qiu, W. X., Lei, Q., Han, K., Cheng, Y. J., and Zhang, X. Z. (2015) Activable Cell-Penetrating Peptide Conjugated Prodrug for Tumor Targeted Drug Delivery. *ACS applied materials & interfaces 7*, 16061-9.

(73) Jin, Y., Huang, Y., Yang, H., Liu, G., and Zhao, R. (2015) A peptide-based pH-sensitive drug delivery system for targeted ablation of cancer cells. *Chemical Communications 51*, 14454-14457.

(74) Copolovici, D. M., Langel, K., Eriste, E., and Langel, U. (2014) Cell-penetrating peptides: design, synthesis, and applications. *ACS nano 8*, 1972-1994.

(75) Harada, H., Hiraoka, M., and Kizaka-Kondoh, S. (2002) Antitumor effect of TAT-oxygen-dependent degradation-caspase-3 fusion protein specifically stabilized and activated in hypoxic tumor cells. *Cancer research 62*, 2013-2018.

(76) Snyder, E. L., and Dowdy, S. F. (2004) Cell penetrating peptides in drug delivery. *Pharmaceutical research 21*, 389-93.

(77) Snyder, E. L., Saenz, C. C., Denicourt, C., Meade, B. R., Cui, X. S., Kaplan, I. M., and Dowdy, S. F. (2005) Enhanced targeting and killing of tumor cells expressing the CXC chemokine receptor 4 by transducible anticancer peptides. *Cancer Res 65*, 10646-50.

(78) Patel, L. N., Zaro, J. L., and Shen, W.-C. (2007) Cell Penetrating Peptides: Intracellular Pathways and Pharmaceutical Perspectives. *Pharmaceutical research 24*, 1977-1992.

(79) Cordova, A., Woodrick, J., Grindrod, S., Zhang, L., Saygideger-Kont, Y., Wang, K., DeVito, S., Daniele, S. G., Paige, M., and Brown, M. L. (2016) Aminopeptidase P Mediated Targeting for Breast Tissue Specific Conjugate Delivery. *Bioconjugate Chemistry 27*, 1981-1990.

(80) Myrberg, H., Zhang, L., Mae, M., and Langel, U. (2008) Design of a tumor-homing cell-penetrating peptide. *Bioconjug Chem 19*, 70-5.

(81) Kersemans, V., and Cornelissen, B. (2010) Targeting the Tumour: Cell Penetrating Peptides for Molecular Imaging and Radiotherapy. *Pharmaceuticals (Basel) 3*, 600-620.

(82) Bolhassani, A. (2011) Potential efficacy of cell-penetrating peptides for nucleic acid and drug delivery in cancer. *Biochimica et biophysica acta 1816*, 232-46.

(83) Jiang, Q. Y., Lai, L. H., Shen, J., Wang, Q. Q., Xu, F. J., and Tang, G. P. (2011) Gene delivery to tumor cells by cationic polymeric nanovectors coupled to folic acid and the cell-penetrating peptide octaarginine. *Biomaterials 32*, 7253-62.

(84) Crombez, L., Morris, M. C., Heitz, F., and Divita, G. (2011) A non-covalent peptide-based strategy for ex vivo and in vivo oligonucleotide delivery. *Methods Mol Biol 764*, 59-73.

(85) Shi, N. Q., Gao, W., Xiang, B., and Qi, X. R. (2012) Enhancing cellular uptake of activable cell-penetrating peptide-doxorubicin conjugate by enzymatic cleavage. *International journal of nanomedicine 7*, 1613-21.

(86) Ding, J., Yao, J., Xue, J., Li, R., Bao, B., Jiang, L., Zhu, J. J., and He, Z. (2015) Tumor-Homing Cell-Penetrating Peptide Linked to Colloidal Mesoporous Silica Encapsulated (-)-Epigallocatechin-3-gallate as Drug Delivery System for Breast Cancer Therapy in Vivo. *ACS applied materials & interfaces 7*, 18145-55.

(87) Lin, Y.-C., Lim, Y. F., Russo, E., Schneider, P., Bolliger, L., Edenharter, A., Altmann, K.-H., Halin, C., Hiss, J. A., and Schneider, G. (2015) Multidimensional Design of Anticancer Peptides. *Angewandte Chemie International Edition 54*, 10370-10374.

(88) Pfaff, M., Tangemann, K., Muller, B., Gurrath, M., Muller, G., Kessler, H., Timpl, R., and Engel, J. (1994) Selective recognition of cyclic RGD peptides of NMR defined conformation by alpha IIb beta 3, alpha V beta 3, and alpha 5 beta 1 integrins. *The Journal of biological chemistry 269*, 20233-8.

(89) Ramachandran, G. N., Ramakrishnan, C., and Sasisekharan, V. (1963) Stereochemistry of polypeptide chain configurations. *Journal of molecular biology 7*, 95-9.

(90) Towse, C. L., Hopping, G., Vulovic, I., and Daggett, V. (2014) Nature versus design: the conformational propensities of D-amino acids and the importance of side chain chirality. *Protein engineering, design & selection : PEDS 27*, 447-55.

(91) Ahmed, S., Mathews, A. S., Byeon, N., Lavasanifar, A., and Kaur, K. (2010) Peptide Arrays for Screening Cancer Specific Peptides. *Analytical Chemistry 82*, 7533-7541.

(92) Mathews, A. S., Ahmed, S., Shahin, M., Lavasanifar, A., and Kaur, K. (2013) Peptide modified polymeric micelles specific for breast cancer cells. *Bioconjug Chem 24*, 560-70.

(93) Ngandeu Neubi, G. M., Opoku-Damoah, Y., Gu, X., Han, Y., Zhou, J., and Ding, Y. (2018) Bio-inspired drug delivery systems: an emerging platform for targeted cancer therapy. *Biomaterials science 6*, 958-973.

(94) Qiao, Z.-Y., Zhao, W.-J., Gao, Y.-J., Cong, Y., Zhao, L., Hu, Z., and Wang, H. (2017) Reconfigurable Peptide Nanotherapeutics at Tumor Microenvironmental pH. *ACS applied materials & interfaces 9*, 30426-30436.

(95) Jiang, Z., Guan, J., Qian, J., and Zhan, C. (2019) Peptide ligand-mediated targeted drug delivery of nanomedicines. *Biomaterials science 7*, 461-471.

(96) Goyal, R., and Ramakrishnan, V. (2019) Chapter 2 - Peptide-Based Drug Delivery Systems, in *Characterization and Biology of Nanomaterials for Drug Delivery* (Mohapatra, S. S., Ranjan, S., Dasgupta, N., Mishra, R. K., and Thomas, S., Eds.) pp 25-45, Elsevier.

(97) Hu, C., Yang, X., Liu, R., Ruan, S., Zhou, Y., Xiao, W., Yu, W., Yang, C., and Gao, H. (2018) Coadministration of iRGD with Multistage Responsive Nanoparticles Enhanced Tumor Targeting and Penetration Abilities for Breast Cancer Therapy. *ACS Appl. Mater. Interfaces 10*, 22571-22579.

(98) Kondo, E., Saito, K., Tashiro, Y., Kamide, K., Uno, S., Furuya, T., Mashita, M., Nakajima, K., Tsumuraya, T., Kobayashi, N., Nishibori, M., Tanimoto, M., and Matsushita, M. (2012) Tumour lineage-homing cell-penetrating peptides as anticancer molecular delivery systems. *Nature communications 3*, 951.

(99) Tesei, G., Vazdar, M., Jensen, M. R., Cragnell, C., Mason, P. E., Heyda, J., Skepö, M., Jungwirth, P., and Lund, M. (2017) Self-association of a highly charged arginine-rich cell-penetrating peptide. *Proceedings of the National Academy of Sciences 114*, 11428.

(100) Tang, F. H. F., Staquicini, F. I., Teixeira, A. A. R., Michaloski, J. S., Namiyama, G. M., Taniwaki, N. N., Setubal, J. C., da Silva, A. M., Sidman, R. L., Pasqualini, R., Arap, W., and Giordano, R. J. (2019) A ligand motif enables differential vascular targeting of endothelial junctions between brain and retina. *Proceedings of the National Academy of Sciences 116*, 2300.

(101) Nischan, N., Herce, H. D., Natale, F., Bohlke, N., Budisa, N., Cardoso, M. C., and Hackenberger, C. P. R. (2015) Covalent Attachment of Cyclic TAT Peptides to GFP Results in Protein Delivery into Live Cells with Immediate Bioavailability. *Angewandte Chemie International Edition 54*, 1950-1953.

(102) Lundberg, P., and Langel, Ü. (2003) A brief introduction to cell-penetrating peptides. *Journal of Molecular Recognition 16*, 227-233.

(103) Litvinov, R. I., Mravic, M., Zhu, H., Weisel, J. W., DeGrado, W. F., and Bennett, J. S. (2019) Unique transmembrane domain interactions differentially modulate integrin αvβ3 and αIIbβ3 function. *Proceedings of the National Academy of Sciences 116*, 12295.

(104) Ruoslahti, E. (2003) The RGD story: a personal account. *Matrix biology : journal of the International Society for Matrix Biology 22*, 459-65.

(105) Pierschbacher, M. D., and Ruoslahti, E. (1984) Cell attachment activity of fibronectin can be duplicated by small synthetic fragments of the molecule. *Nature 309*, 30-3.

(106) Hood, J. D., and Cheresh, D. A. (2002) Role of integrins in cell invasion and migration. *Nature Reviews Cancer 2*, 91-100.

(107) Lark, M. W., Stroup, G. B., Hwang, S. M., James, I. E., Rieman, D. J., Drake, F. H., Bradbeer, J. N., Mathur, A., Erhard, K. F., and Newlander, K. A. (1999) Design and characterization of orally active Arg-Gly-Asp peptidomimetic vitronectin receptor antagonist SB 265123 for prevention of bone loss in osteoporosis. *Journal of Pharmacology and Experimental Therapeutics 291*, 612-617.

(108) Storgard, C. M., Stupack, D. G., Jonczyk, A., Goodman, S. L., Fox, R. I., and Cheresh, D. A. (1999) Decreased angiogenesis and arthritic disease in rabbits treated with an αvβ3 antagonist. *The Journal of clinical investigation 103*, 47-54.

(109) Hu, C., Chen, X., Huang, Y., and Chen, Y. (2018) Co-administration of iRGD with peptide HPRP-A1 to improve anticancer activity and membrane penetrability. *Scientific Reports 8*, 2274.

(110) Yu, X., Song, Y., Di, Y., He, H., Fu, D., and Jin, C. (2016) Enhanced tumor targeting of cRGD peptide-conjugated albumin nanoparticles in the BxPC-3 cell line. *Scientific Reports 6*, 31539.

(111) Dou, X., Nomoto, T., Takemoto, H., Matsui, M., Tomoda, K., and Nishiyama, N. (2018) Effect of multiple cyclic RGD peptides on tumor accumulation and intratumoral distribution of IRDye 700DX-conjugated polymers. *Scientific Reports 8*, 8126.

(112) Sugahara, K. N., Teesalu, T., Karmali, P. P., Kotamraju, V. R., Agemy, L., Girard, O. M., Hanahan, D., Mattrey, R. F., and Ruoslahti, E. (2009) Tissue-penetrating delivery of compounds and nanoparticles into tumors. *Cancer cell 16*, 510-20.

(113) Scarborough, R. M., Rose, J. W., Hsu, M. A., Phillips, D., Fried, V., Campbell, A., Nannizzi, L., and Charo, I. (1991) Barbourin. A GPIIb-IIIa-specific integrin antagonist from the venom of Sistrurus m. barbouri. *Journal of Biological Chemistry 266*, 9359-9362.

(114) Kodandapani, R., Veerapandian, B., Kunicki, T. J., and Ely, K. R. (1995) Crystal Structure of the OPG2 Fab AN ANTIRECEPTOR ANTIBODY THAT MIMICS AN RGD CELL ADHESION SITE. *Journal of Biological Chemistry 270*, 2268-2273.

(115) Ghiso, J., Rostagno, A., Gardella, J., Liem, L., Gorevic, P., and Frangione, B. (1992) A 109-amino-acid C-terminal fragment of Alzheimer's-disease amyloid precursor protein contains a sequence,-RHDS-, that promotes cell adhesion. *Biochemical Journal 288*, 1053-1059.

(116) Henry, C., Moitessier, N., and Chapleur, Y. (2002) Vitronectin receptor alpha(V)beta(3) integrin antagonists: chemical and structural requirements for activity and selectivity. *Mini Rev Med Chem 2*, 531-542.

(117) Gentilucci, L., Cardillo, G., Squassabia, F., Tolomelli, A., Spampinato, S., Sparta, A., and Baiula, M. (2007) Inhibition of cancer cell adhesion by heterochiral Pro-containing RGD mimetics. *Bioorganic & medicinal chemistry letters 17*, 2329-33.

(118) Marinelli, L., Lavecchia, A., Gottschalk, K.-E., Novellino, E., and Kessler, H. (2003) Docking Studies on αvβ3 Integrin Ligands: Pharmacophore Refinement and Implications for Drug Design. *Journal of Medicinal Chemistry 46*, 4393-4404.

(119) Coleman, P. J., Askew, B. C., Hutchinson, J. H., Whitman, D. B., Perkins, J. J., Hartman, G. D., Rodan, G. A., Leu, C. T., Prueksaritanont, T., Fernandez-Metzler, C., Merkle, K. M., Lynch, R., Lynch, J. J., Rodan, S. B., and Duggan, M. E. (2002) Non-peptide alpha(v)beta(3) antagonists. Part 4: potent and orally bioavailable chain-shortened RGD mimetics. *Bioorganic & medicinal chemistry letters 12*, 2463-5.

(120) Xiong, J.-P., Stehle, T., Zhang, R., Joachimiak, A., Frech, M., Goodman, S. L., and Arnaout, M. A. (2002) Crystal structure of the extracellular segment of integrin αVβ3 in complex with an Arg-Gly-Asp ligand. *Science 296*, 151-155.

(121) Haubner, R., Finsinger, D., and Kessler, H. (1997) Stereoisomeric Peptide Libraries and Peptidomimetics for Designing Selective Inhibitors of the αvβ3 Integrin for a New Cancer Therapy. *Angewandte Chemie International Edition in English 36*, 1374-1389.

(122) Haubner, R., Gratias, R., Diefenbach, B., Goodman, S. L., Jonczyk, A., and Kessler, H. (1996) Structural and Functional Aspects of RGD-Containing Cyclic Pentapeptides as Highly Potent and Selective Integrin αVβ3 Antagonists. *Journal of the American Chemical Society 118*, 7461-7472.

(123) Royo, M., Van Den Nest, W., del Fresno, M., Frieden, A., Yahalom, D., Rosenblatt, M., Chorev, M., and Albericio, F. (2001) Solid-phase syntheses of constrained RGD scaffolds and their binding to the αvβ3 integrin receptor. *Tetrahedron Letters 42*, 7387-7391.

(124) Belvisi, L., Bernardi, A., Colombo, M., Manzoni, L., Potenza, D., Scolastico, C., Giannini, G., Marcellini, M., Riccioni, T., Castorina, M., LoGiudice, P., and Pisano, C. (2006) Targeting integrins: insights into structure and activity of cyclic RGD pentapeptide mimics containing azabicycloalkane amino acids. *Bioorganic & medicinal chemistry 14*, 169-80.

(125) Perdih, A., and Dolenc, M. S. (2010) Small molecule antagonists of integrin receptors. *Current medicinal chemistry 17*, 2371-92.

(126) Rose, G. D., Glerasch, L. M., and Smith, J. A. (1985) Turns in Peptides and Proteins, in *Advances in Protein Chemistry* (Anfinsen, C. B., Edsall, J. T., and Richards, F. M., Eds.) pp 1-109, Academic Press.

(127) Rizo, J., and Gierasch, L. M. (1992) Constrained Peptides: Models of Bioactive Peptides and Protein Substructures. *Annual Review of Biochemistry 61*, 387-416.

(128) Li, L., Li, C., Sarkar, S., Zhang, J., Witham, S., Zhang, Z., Wang, L., Smith, N., Petukh, M., and Alexov, E. (2012) DelPhi: a comprehensive suite for DelPhi software and associated resources. *BMC biophysics 5*, 9.

(129) Fischer, R., Mader, O., Jung, G., and Brock, R. (2003) Extending the Applicability of Carboxyfluorescein in Solid-Phase Synthesis. *Bioconjugate Chemistry 14*, 653-660.

(130) Jerath, G., Goyal, R., Trivedi, V., Santhoshkumar, T. R., and Ramakrishnan, V. (2019) Syndiotactic peptides for targeted delivery. *Acta Biomaterialia 87*, 130-139.

(131) Haris, P. I., and Chapman, D. (1995) The conformational analysis of peptides using Fourier transform IR spectroscopy. *Biopolymers 37*, 251-63.

(132) Lindgren, M., Rosenthal-Aizman, K., Saar, K., Eiríksdóttir, E., Jiang, Y., Sassian, M., Östlund, P., Hällbrink, M., and Langel, Ü. (2006) Overcoming methotrexate resistance in breast cancer tumour cells by the use of a new cell-penetrating peptide. *Biochemical Pharmacology 71*, 416-425.

(133) Scaduto, R. C., Jr., and Grotyohann, L. W. (1999) Measurement of mitochondrial membrane potential using fluorescent rhodamine derivatives. *Biophys J 76*, 469-477.

(134) Budd, S. L., Tenneti, L., Lishnak, T., and Lipton, S. A. (2000) Mitochondrial and extramitochondrial apoptotic signaling pathways in cerebrocortical neurons. *Proceedings of the National Academy of Sciences 97*, 6161.

(135) Elmore, S. (2007) Apoptosis: a review of programmed cell death. *Toxicol Pathol 35*, 495-516.

(136) Jones, S., Holm, T., Mäger, I., Langel, Ü., and Howl, J. (2010) Characterization of Bioactive Cell Penetrating Peptides from Human Cytochrome c: Protein Mimicry and the Development of a Novel Apoptogenic Agent. *Chemistry & Biology 17*, 735-744.

(137) Buckley, C. D., Pilling, D., Henriquez, N. V., Parsonage, G., Threlfall, K., Scheel-Toellner, D., Simmons, D. L., Akbar, A. N., Lord, J. M., and Salmon, M. (1999) RGD peptides induce apoptosis by direct caspase-3 activation. *Nature 397*, 534-9.

(138) Joseph, J., Seervi, M., Sobhan, P. K., and Retnabai, S. T. (2011) High Throughput Ratio Imaging to Profile Caspase Activity: Potential Application in Multiparameter High Content Apoptosis Analysis and Drug Screening. *PLOS ONE 6*, e20114.

(139) Kim, H., Jang, J. H., Kim, S. C., and Cho, J. H. (2014) De novo generation of short antimicrobial peptides with enhanced stability and cell specificity. *The Journal of antimicrobial chemotherapy 69*, 121-32.

(140) Inwald, E. C., Klinkhammer-Schalke, M., Hofstadter, F., Zeman, F., Koller, M., Gerstenhauer, M., and Ortmann, O. (2013) Ki-67 is a prognostic parameter in breast cancer patients: results of a large population-based cohort of a cancer registry. *Breast cancer research and treatment 139*, 539-52.

(141) Lau, J. L., and Dunn, M. K. (2018) Therapeutic peptides: Historical perspectives, current development trends, and future directions. *Bioorganic & medicinal chemistry 26*, 2700-2707.

(142) Craik, D. J., Fairlie, D. P., Liras, S., and Price, D. (2013) The Future of Peptide-based Drugs. *Chemical Biology & Drug Design 81*, 136-147.

(143) Mullard, A. (2014) Once-yearly device takes on daily and weekly diabetes drugs. *Nature Biotechnology 32*, 1178-1178.

(144) Camacho, P. M., Petak, S. M., Binkley, N., Clarke, B. L., Harris, S. T., Hurley, D. L., Kleerekoper, M., Lewiecki, E. M., Miller, P. D., Narula, H. S., Pessah-Pollack, R., Tangpricha, V., Wimalawansa, S. J., and Watts, N. B. (2016) American Association of Clinical Endocrinologists and American College Of Endocrinology Clinical Practice Guidelines for the Diagnosis and Treatment of Postmenopausal Osteoporosis — 2016. *Endocrine Practice 22*, 1-42.

(145) Sun, J., Wei, Q., Zhou, Y., Wang, J., Liu, Q., and Xu, H. (2017) A systematic analysis of FDA-approved anticancer drugs. *BMC Syst Biol 11*, 87-87.

(146) Divita, G. (2010) Bioactive Cell-Penetrating Peptides: Kill Two Birds with One Stone. *Chemistry & Biology 17*, 679-680.

(147) Klein, M. J., Schmidt, S., and Wadhwani, P. (2017) Lactam-Stapled Cell-Penetrating Peptides: Cell Uptake and Membrane Binding Properties. *60*, 8071-8082.

(148) Verdurmen, Wouter P. R., Bovee-Geurts, Petra H., Wadhwani, P., Ulrich, Anne S., Hällbrink, M., van Kuppevelt, Toin H., and Brock, R. (2011) Preferential Uptake of L- versus D-Amino Acid Cell-Penetrating Peptides in a Cell Type-Dependent Manner. *Chemistry & Biology 18*, 1000-1010.

(149) Zou, Q., Abbas, M., Zhao, L., Li, S., Shen, G., and Yan, X. (2017) Biological Photothermal Nanodots Based on Self-Assembly of Peptide–Porphyrin Conjugates for Antitumor Therapy. *Journal of the American Chemical Society 139*, 1921-1927.

(150) Li, S., Zhao, L., Chang, R., Xing, R., and Yan, X. (2019) Spatiotemporally Coupled Photoactivity of Phthalocyanine–Peptide Conjugate Self-Assemblies for Adaptive Tumor Theranostics. *Chemistry – A European Journal 25*, 13429-13435.

(151) Li, Y., Zou, Q., Yuan, C., Li, S., Xing, R., and Yan, X. (2018) Amino Acid Coordination Driven Self-Assembly for Enhancing both the Biological Stability and Tumor Accumulation of Curcumin. *Angewandte Chemie International Edition 57*, 17084-17088.

(152) Pandey, G., Morla, S., Nemade, H. B., Kumar, S., and Ramakrishnan, V. (2019) Modulation of aggregation with an electric field; scientific roadmap for a potential non-invasive therapy against tauopathies. *RSC Advances 9*, 4744-4750.

(153) Wang, C. K., King, G. J., Conibear, A. C., Ramos, M. C., Chaousis, S., Henriques, S. T., and Craik, D. J. (2016) Mirror Images of Antimicrobial Peptides Provide Reflections on Their Functions and Amyloidogenic Properties. *Journal of the American Chemical Society 138*, 5706-5713.

(154) Kumar, A., Ranbhor, R., Patel, K., Ramakrishnan, V., and Durani, S. (2017) Automated protein design: Landmarks and operational principles. *Progress in biophysics and molecular biology 125*, 24-35.

(155) Cascales, L., Henriques, S. T., Kerr, M. C., Huang, Y.-H., Sweet, M. J., Daly, N. L., and Craik, D. J. (2011) Identification and characterization of a new family of cell-penetrating peptides cyclic cell-penetrating peptides. *Journal of Biological Chemistry 286*, 36932-36943.

(156) Drin, G., Cottin, S., Blanc, E., Rees, A. R., and Temsamani, J. (2003) Studies on the internalization mechanism of cationic cell-penetrating peptides. *Journal of Biological Chemistry 278*, 31192-31201.

(157) Jha, D., Mishra, R., Gottschalk, S., Wiesmüller, K.-H., Ugurbil, K., Maier, M. E., and Engelmann, J. r. (2011) CyLoP-1: a novel cysteine-rich cell-penetrating peptide for cytosolic delivery of cargoes. *Bioconjugate chemistry 22*, 319-328.

(158) Mühlhäuser, P., Wadhwani, P., Strandberg, E., Bürck, J., and Ulrich, A. S. (2017) Structure analysis of the membrane-bound dermcidin-derived peptide SSL-25 from human sweat. *Biochimica et Biophysica Acta (BBA) - Biomembranes 1859*, 2308-2318.

(159) Medina, S. H., Miller, S. E., Keim, A. I., Gorka, A. P., Schnermann, M. J., and Schneider, J. P. (2016) An Intrinsically Disordered Peptide Facilitates Non-Endosomal Cell Entry. *Angewandte Chemie International Edition 55*, 3369-3372.

(160) Heitz, F., Morris, M. C., and Divita, G. (2009) Twenty years of cell-penetrating peptides: from molecular mechanisms to therapeutics. *British journal of pharmacology 157*, 195-206.

(161) Mäger, I., Eiríksdóttir, E., Langel, K., Andaloussi, S. E., and Langel, Ü. (2010) Assessing the uptake kinetics and internalization mechanisms of cell-penetrating peptides using a quenched fluorescence assay. *Biochimica et Biophysica Acta (BBA)-Biomembranes 1798*, 338-343.

(162) Lewis, H. D., Husain, A., Donnelly, R. J., Barlos, D., Riaz, S., Ginjupalli, K., Shodeinde, A., and Barton, B. E. (2010) Creation of a novel peptide with enhanced nuclear localization in prostate and pancreatic cancer cell lines. *BMC biotechnology 10*, 79.

(163) Whitney, W. D. (1890) Translation of the Katha-Upanishad. *Transactions of the American Philological Association (1869-1896) 21*, 88-112.

(164) Gambhirananda, S. *Katha Upanishad: With the Commentary of Shankaracharya*, Advaita Ashrama (A Publication House of Ramakrishna Math, Belur Math).

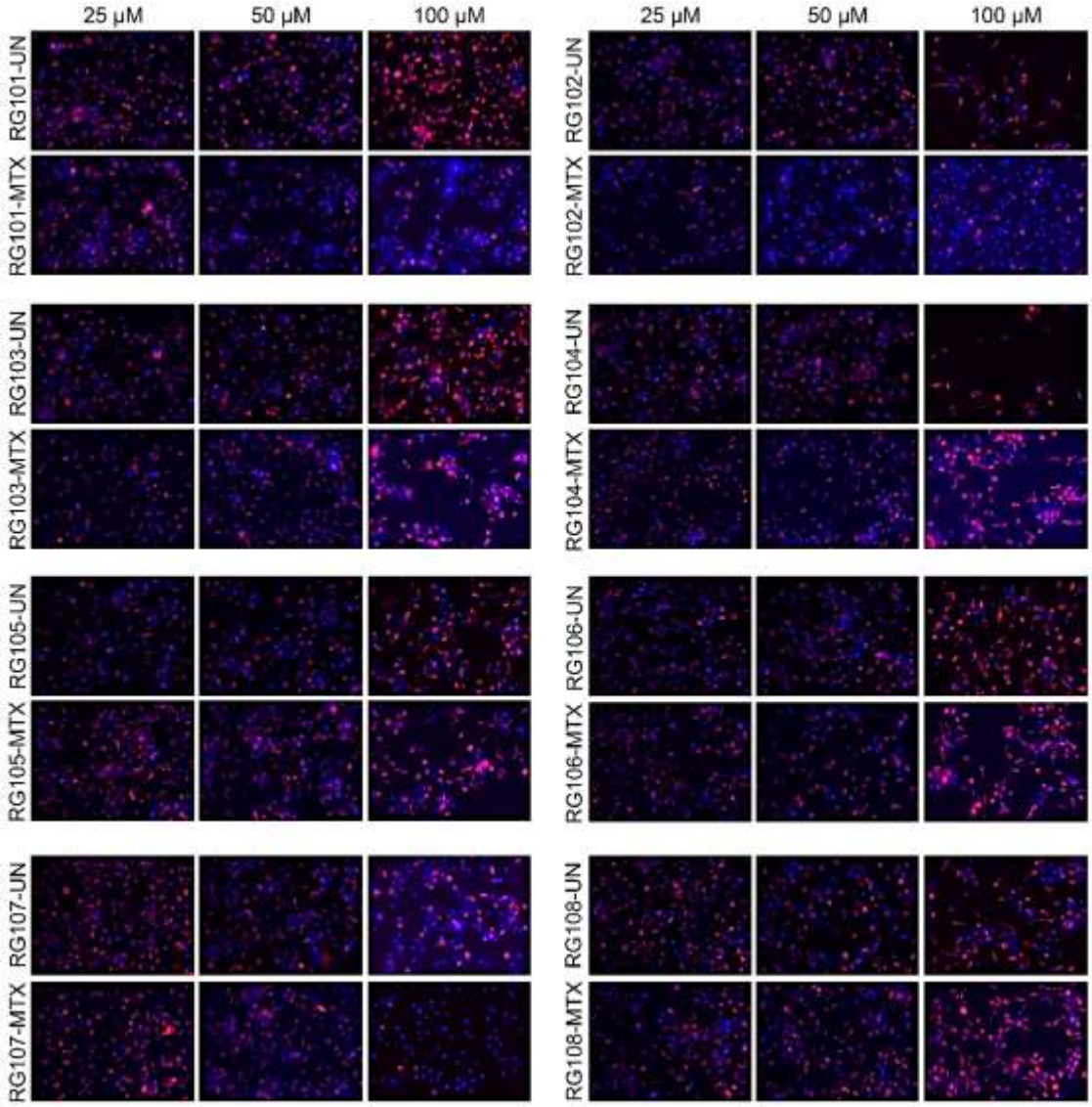

Figure A1. TMRM Cytotoxicity assessment in MDA-MB-231 cells. *Cytotoxicity of designed peptides (RG101-RG108) and their MTX conjugates to MTX resistant breast cancer MDA-MB-231 cells after 48 h at varying concentrations. The panel shows the representative images of the treated cells. The cells with TMRM loss and nuclear condensation were considered undergoing apoptosis and hence, taken for cell death analysis. The images were acquired as 2x2 montages, which later stitched as a single image for each well (n=4). Here, RG10X-UN denotes free peptides whereas, RG10X-MTX denotes their MTX conjugates.*

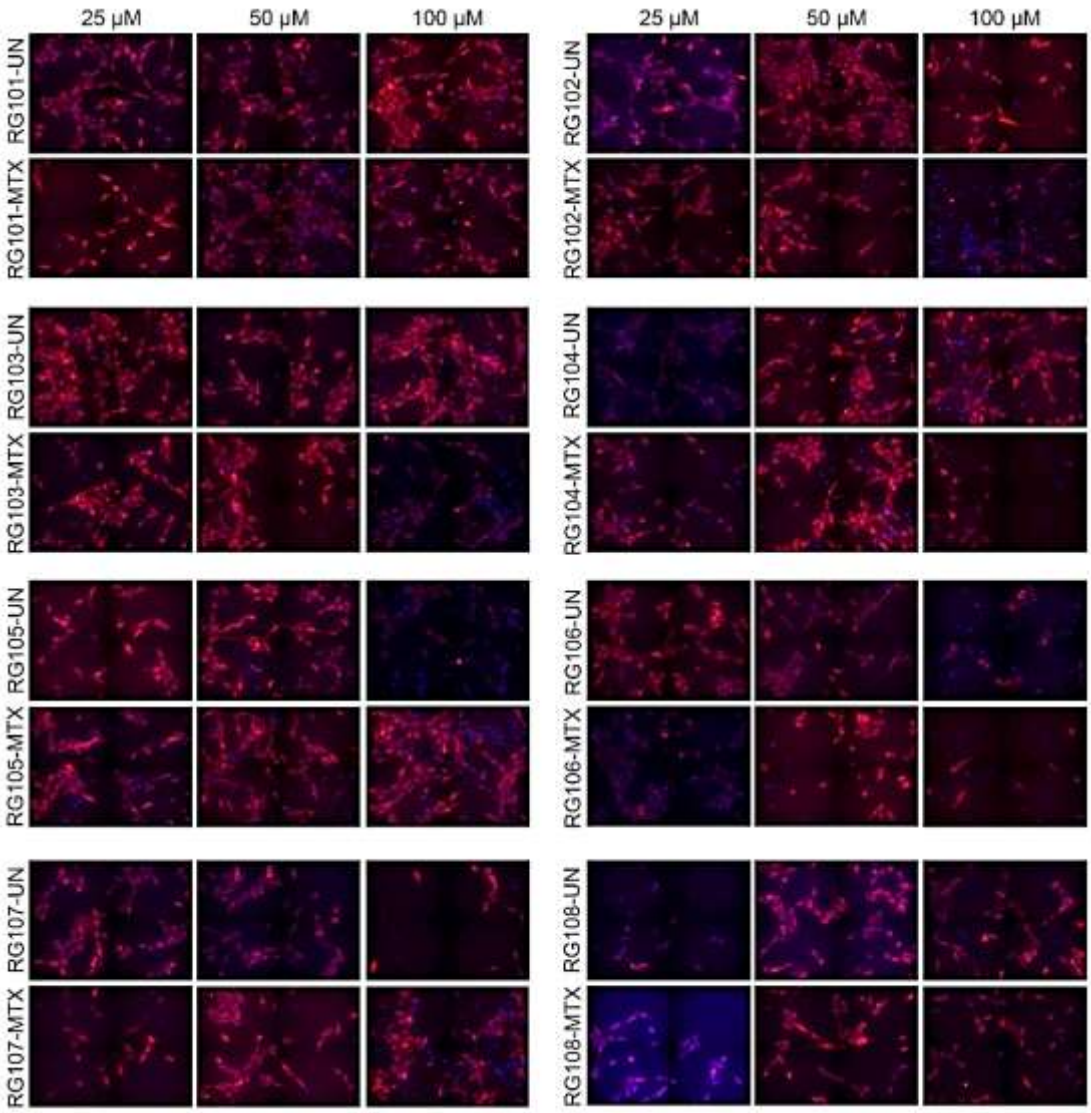

Figure A2. TMRM Cytotoxicity assessment in MCF-10A cells. *Cytotoxicity of the designed peptides and their MTX conjugates on non-cancerous mammary epithelial cells (MCF-10A) cells after 48 h at different concentrations. The panel shows the representative images of treated MCF-10A cells. The cells with TMRM loss and nuclear condensation were considered undergoing apoptosis and hence, taken for cell death analysis. The images were acquired as 2x2 montages, which later stitched as a single image for each well (n=4). Here, RG10X-UN shows free peptides, whereas, RG10X-MTX represents their MTX conjugates.*

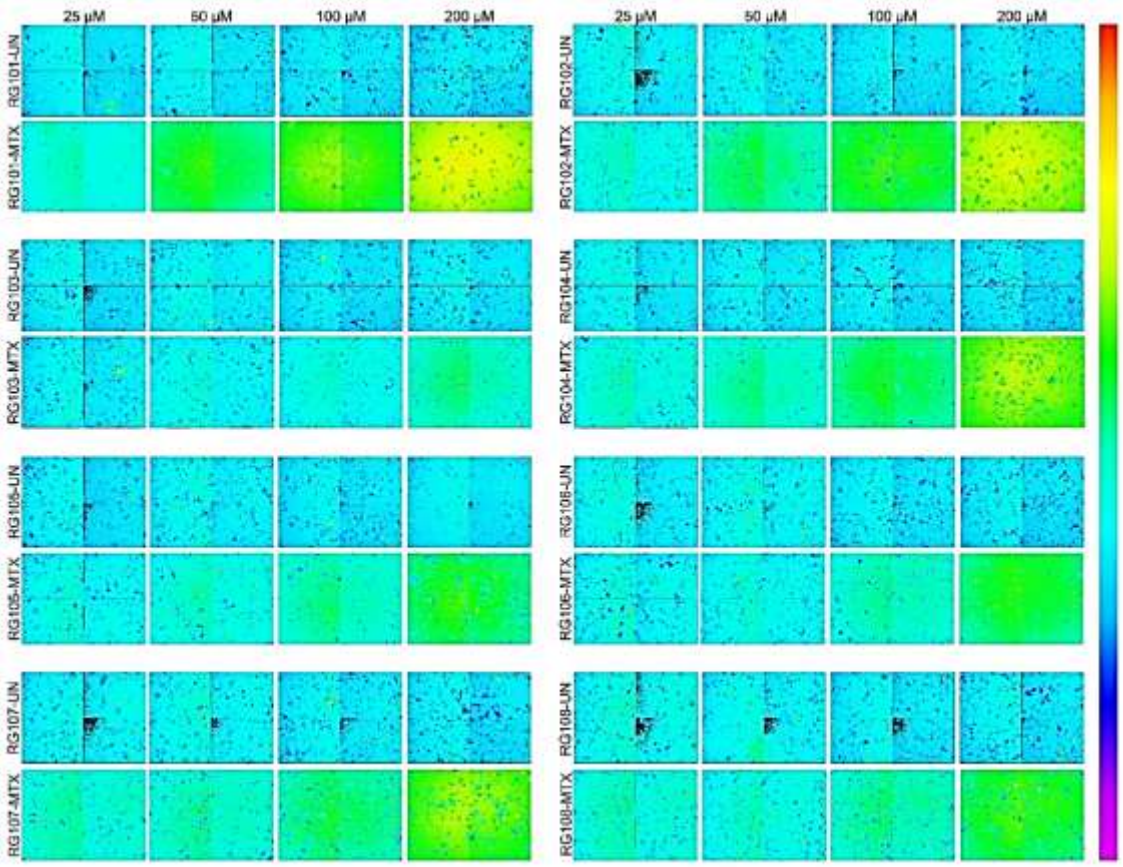

Figure A3. FRET-based Caspase-3 activation assay. *Detection of Caspase-3 activation by ratiometric fluorescence-based assay in MDA-MB-231 cells having a stable expression of CFP-YFP FRET-based caspase sensor, DEVD. These cells were treated with peptides and peptide-methotrexate conjugates for 48 h at 25 µM, 50 µM, and 100 µM concentrations. The loss of FRET in cells was measured in terms of an increase in the CFP-YFP ratio, which corresponds to color change from purple towards red on the ratio scale. The images were acquired as 2x2 montages, which later stitched as a single image for each well (n=4).*

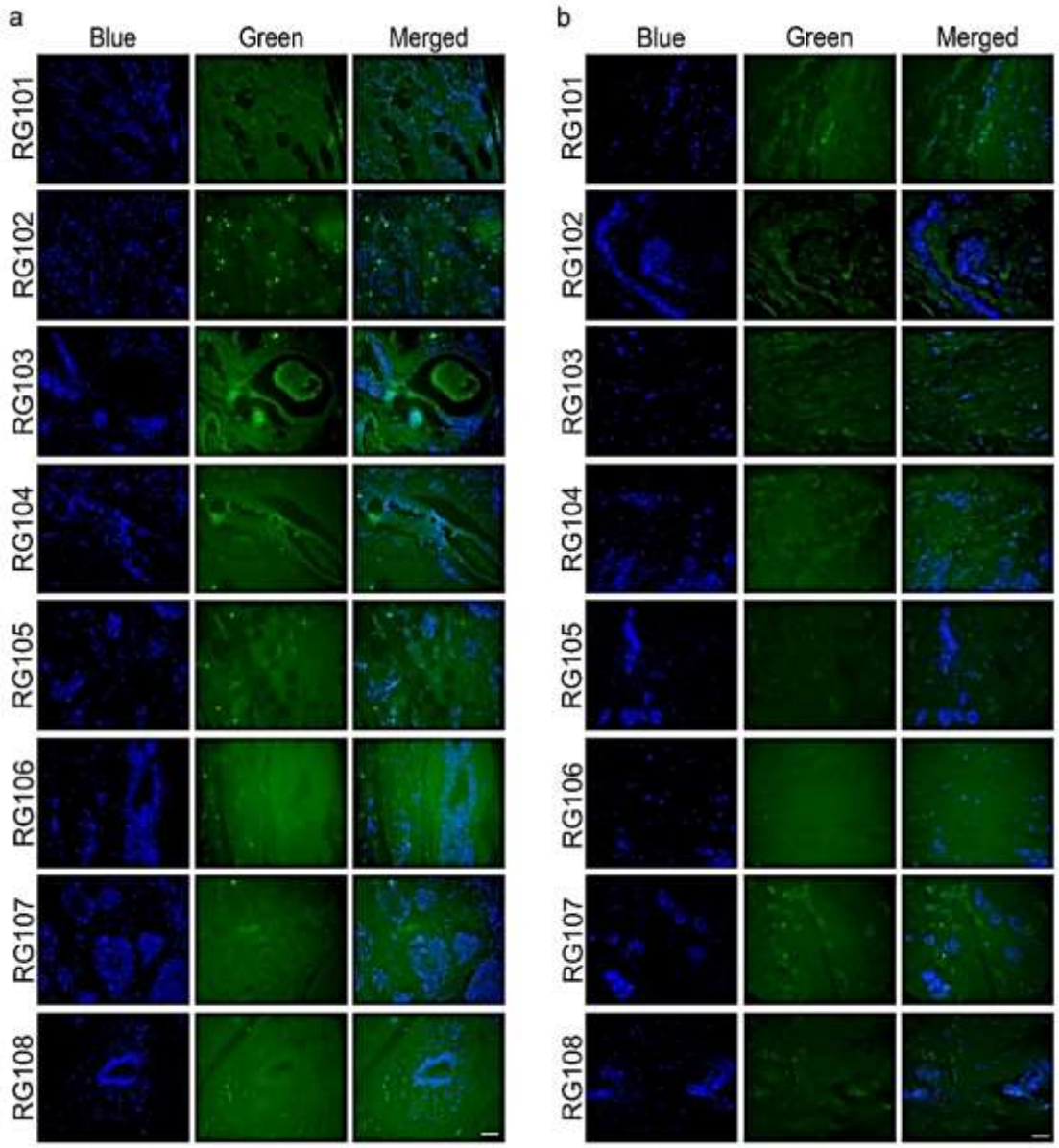

Figure A4. Comparative histopathological peptide staining in clinical samples. *Representative fluorescence microscopic images of selected tissue slices of (a) invasive ductal breast carcinoma and (b) adjacent normal tissues stained with 50 µM of CF-tagged peptides (RG101-RG108) for 6 h. Blue color represents nuclei staining with DAPI, and green color denotes CF-tagged peptides. Magnification: 200 X; Scale bar: 50 µm.*

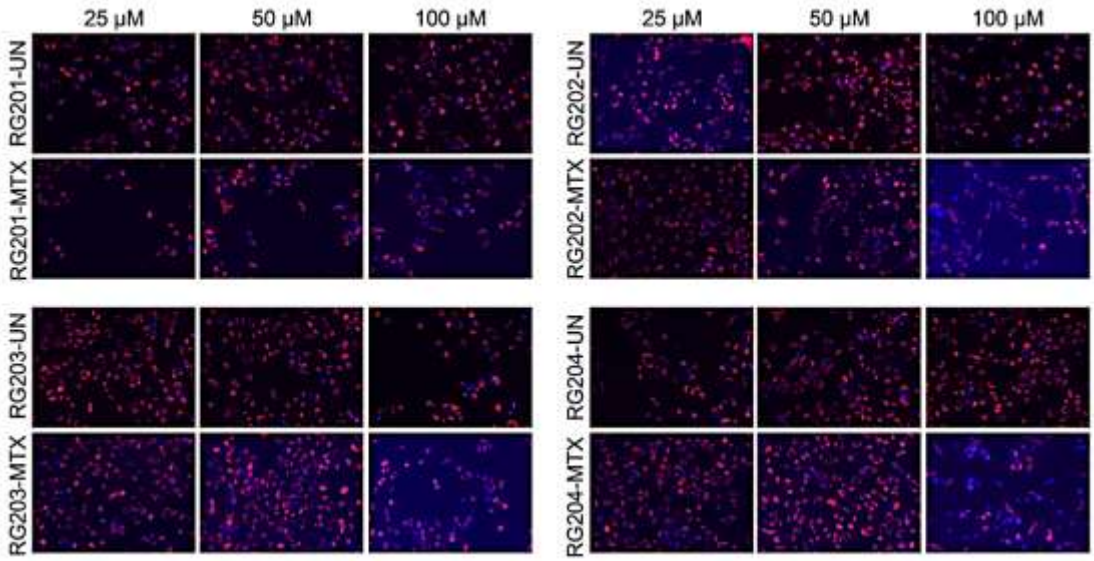

Figure A5. TMRM cytotoxicity assay. *Representative images of cytotoxicity of designed peptides and their MTX conjugates on breast cancer MDA-MB-231 cells after 48 h at 25 µM, 50 µM, and 100 µM concentrations. The cells with TMRM loss and chromatin condensation were considered undergoing apoptosis and hence, taken for cell death analysis.*

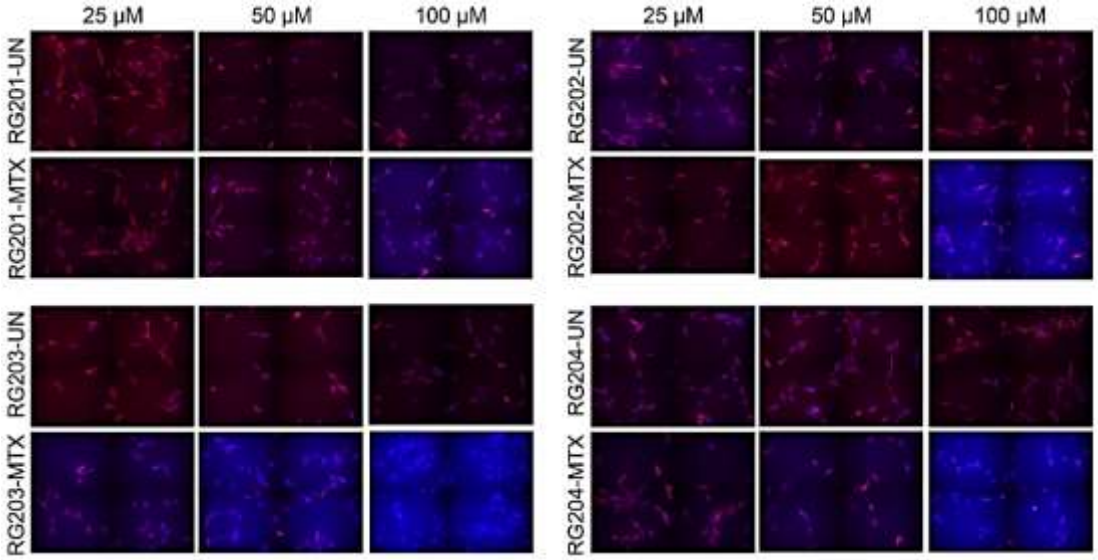

Figure A6. TMRM cytotoxicity assay. *Representative images of cytotoxicity of designed peptides and their MTX conjugates on mammary epithelial MCF-10A cells after 48 h at 25 µM, 50 µM, and 100 µM concentrations. The cells with TMRM loss and chromatin condensation were considered undergoing apoptosis and hence, taken for cell death analysis.*

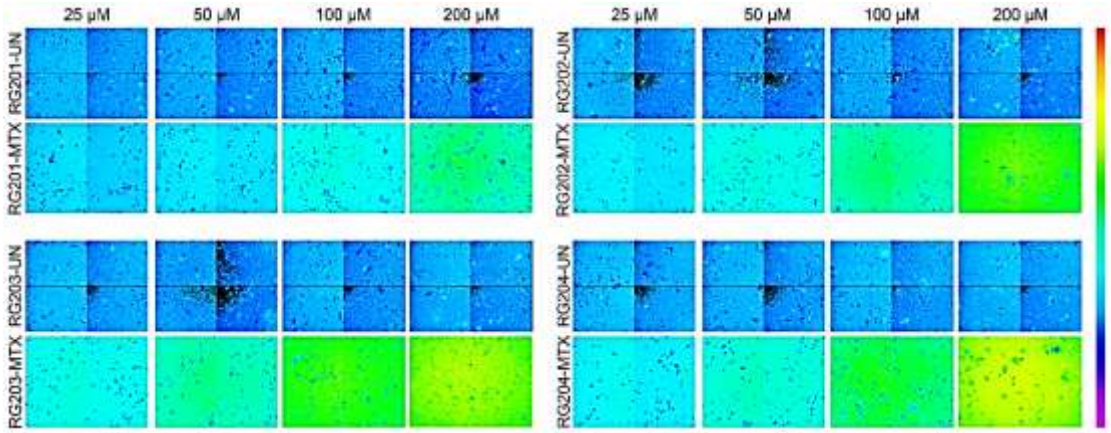

Figure A7. Representative images to show apoptotic cell death. *To confirm the cell death by apoptosis, MDA-MB-231 cells having a stable expression of CFP-YFP FRET-based caspase sensor, DEVD, were treated with peptides and peptide-methotrexate conjugates for 48 h at 25 µM, 50 µM, and 100 µM concentrations. The loss of FRET in cells was measured in terms of an increase in the CFP-YFP ratio, which corresponds to color change from purple to red on the ratio scale. The images were acquired as 2x2 montages, which later stitched as a single image for each well (n=4).*

Table A1. Summary of obtained RXD distances through a modeling study

S. No.	Sequence	Distance >=10	Distance =10	Distance =11	Distance =12	Distance =13	Distance =14
1	RGD (486 files)	278	74	84	73	31	16
	Percentage	57.20%	15.22%	17.28%	15.02%	6.37%	3.29%
2	rGd (486 files)	264	64	75	72	40	13
	Percentage	54.32%	13.16%	15.43%	14.81%	8.23%	2.67%
3	rQd (81 files)	39	15	14	10	0	0
	Percentage	48.14%	18.51%	17.28%	12.34%	0	0
4	RqD (81 files)	42	17	16	9	0	0
	Percentage	51.85%	20.98%	19.75%	11.11%	0	0
5	rAd (81 files)	39	15	14	10	0	0
	Percentage	48.14%	18.51%	17.28%	12.34%	0	0
6	RaD(81 files)	42	17	16	9	0	0
	Percentage	51.85%	20.98%	19.75%	11.11%	0	0
7	rVd (81 files)	64	12	14	21	11	6
	Percentage	79.01%	14.81%	17.28%	25.92%	13.58%	7.40%
8	RvD (81 files)	63	12	11	19	15	6
	Percentage	77.77%	14.81%	13.58%	23.45%	18.51%	7.40%
9	rPd (81 files)	55	13	10	12	17	3
	Percentage	67.90%	16.04%	12.34%	14.81%	20.98%	3.70%
10	RpD (81 files)	57	10	19	11	11	6
	Percentage	70.37%	12.34%	23.45%	13.58%	13.58%	7.40%
11	rBd (81 files)	39	15	14	10	0	0
	Percentage	48.14%	18.51%	17.28%	12.34%	0	0
12	RPD (81 files)	41	7	14	12	6	2
	Percentage	50.61%	8.64%	17.28%	14.81%	7.40%	2.46%
13	rpd (81 files)	42	10	15	8	7	2
	Percentage	51.85%	12.34%	18.51%	9.87%	8.64%	2.46%
14	RVD (81 files)	48	16	16	11	3	2
	Percentage	59.25%	19.75%	19.75%	13.58%	3.70%	2.46%
15	rvd (81 files)	42	11	10	13	6	2
	Percentage	51.85%	13.58%	12.34%	16.04%	7.40%	2.46%
16	RBD (81 files)	27	10	9	7	1	0
	Percentage	33.34%	12.34%	11.12%	8.64%	1.23%	0

LIST OF PUBLICATIONS

Patent

I. Ruchika Goyal, Gaurav Jerath, and Vibin Ramakrishnan. Peptide-based Molecular Constructs for Tumor Homing and Cell Penetration. Patent number TEMP/E 1/36087/2019-KOL; 2019 (Filed).

Publications

I. Ruchika Goyal, Gaurav Jerath, Aneesh Chandrasekharan, T. R. Santhosh Kumar, and Vibin Ramakrishnan. Peptide-Based Delivery Vectors with Pre-defined Geometrical Locks. RSC Medicinal Chemistry. 2020 (DOI: 10.1039/D0MD00229A).

II. Ruchika Goyal and Vibin Ramakrishnan. Peptide-based Drug Delivery Systems. Characterization and Biology of Nanomaterials for Drug Delivery. 2018, ISBN: 978-0-12-814031-4. Elsevier.

III. Prakash Kishore Hazam*, Ruchika Goyal*, and Vibin Ramakrishnan. Peptide-based Antimicrobials: Design Strategies and Therapeutic Potential. Progress in Biophysics and Molecular Biology. 2019, 142: 10-22. Elsevier. (*equal contribution)

IV. Gaurav Jerath, Ruchika Goyal, Vishal Trivedi, T.R. Santhoshkumar, and Vibin Ramakrishnan. Syndiotactic peptides for targeted delivery. Acta Biomaterialia. 2019, 87: 130–139. Elsevier.

V. Gaurav Jerath, Ruchika Goyal, Vishal Trivedi, T. R. Santhosh Kumar, and Vibin Ramakrishnan. Conformationally Constrained Peptides for Drug Delivery. Journal of Peptide Science. 2020, Wiley (DOI: 10.1002/psc.3244).

Current Status of other Manuscripts

I. Ruchika Goyal, Gaurav Jerath, Akhil R., Aneesh Chandrasekharan, Anupam Sarma, T. R. Santhosh Kumar, and Vibin Ramakrishnan. Geometry Encoded Functional Programming of Drug Delivery Vehicles. 2020. (Under Review).

II. Ruchika Goyal, Gaurav Jerath, Aneesh Chandrasekharan, T. R. Santhosh Kumar, and Vibin

Ramakrishnan. Generation of a Complete Tumor Targeting Molecular Construct. 2020. (Under Preparation).

Conferences

- Ruchika Goyal, Gaurav Jerath, T. R. Santhosh Kumar, Vishal Trivedi, and Vibin Ramakrishnan. Design, Synthesis, and Rationale of short Tumor Homing Peptides for Targeted Delivery in 20th Indo-US Flow Cytometry Symposium cum Workshop on 'Applications of Flow Cytometry in Biotechnology,' Indian Institute of Technology Guwahati, Assam, 13th to 16th March 2019 (Best Poster Award).
- Ruchika Goyal, Gaurav Jerath, T. R. Santhosh Kumar, Vishal Trivedi, and Vibin Ramakrishnan. Peptide-Based Molecular Constructs for Cellular Targeting and Small Molecule Delivery in International Symposium on Tumor Microenvironment and Cancer Prevention & Therapeutics, School of Life Sciences, Jawaharlal Nehru University, New Delhi, 8th to 9th February 2019.
- Ruchika Goyal, Gaurav Jerath, Vishal Trivedi, and Vibin Ramakrishnan. Design, Synthesis, and Characterisation of short Tumor Homing Peptides for their Potential as Targeted Drug Delivery System in National Workshop on Fluorescence and Raman Spectroscopy: FCS 2017, Indian Institute of Technology Guwahati, 17th to 21st December 2017.
- Ruchika Goyal, Gaurav Jerath, Vishal Trivedi & Vibin Ramakrishnan. Design, Synthesis, and Characterisation of short Tumor Homing Peptides for their Potential as Targeted Drug Delivery System in 9th TCS Annual Event on Flow Applications in Basics, Applied and Clinical Biology (FABACTCS 2016), Indian Institute of Technology Guwahati, 3rd to 5th November 2016 (2nd Best Poster Award).
- Ruchika Goyal, Anjali Singh, Prakash Kishore Hazam, Gaurav Jerath, and V.Ramakrishnan. Peptide-Based Molecular Constructs as Theranostic Agents in Research Conclave, Indian Institute of Technology Guwahati, 18th to 20th March 2016.